JRC Scientific and Technical Reports

ASTEC V1.3rev2 Code Application on Medium Cold Leg Break Accident for a reference PWR 1000 Reactor

(Source Term Evaluation)

A. Bujan [1], L. Ammirabile [2]
J. Slaby [1], A. Bieliauskas [2]

[1] **VUJE Institute**
Slovakia
[2] **European Commission, Joint Research Centre**
Institute for Energy, The Netherlands

EUR 23797 EN - 2008

JRC
EUROPEAN COMMISSION

ie
Institute for Energy

The Institute for Energy provides scientific and technical support for the conception, development, implementation and monitoring of community policies related to energy. Special emphasis is given to the security of energy supply and to sustainable and safe energy production.

European Commission
Joint Research Centre
Institute for Energy

Contact information
Address: Westerduinweg 3
E-mail: jrc-ie-info@ec.europa.eu
Tel.: +31 (0)224 565656
Fax: +31 (0)224 565600

http://ie.jrc.ec.europa.eu/
http://www.jrc.ec.europa.eu/

JRC 50206

EUR 23797 EN
ISSN 1018-5593

Luxembourg: Office for Official Publications of the European Communities

Printed in Luxembourg

Executive Summary

During a hypothetical severe accident in a nuclear reactor most of the radioactivity would be released from the damaged core and the broken primary circuit in form of aerosols and chemical vapours and gases. However the radio-toxicity of released materials depends both on the released mass and on the chemical form as well. The fission products release and transport in the circuit has been analysed for a Medium Break cold leg Loss Of Coolant Accident (MBLOCA) for a reference PWR 1000 reactor using the severe accident integral code ASTECV1.2 rev2. A detailed description of the reactor model is given.

Sensitivity analyses were performed in terms of break location and accumulator availability.

The break location has an impact on the carrier gas temperature and in turn on the chemical speciation of the fission products. Also retention is influenced by the different flow pathways establishing in the circuit.

The accumulator availability extends the duration of the core degradation process affecting the total production of hydrogen and the cumulated released mass of low, semi and highly volatile fission products.

In agreement with the ASTEC equilibrium chemistry model, the Mo/Cs (Rb) molar ratio has the most influence on the fraction of Iodine which can reach the containment in the gaseous or highly volatile form. Due to the surplus of Cs, the predicted dominant Iodine species to the containment are CsI and its dimmer.

A 3-4% of Iodine which reaches the break exists in gaseous (HI) and highly volatile metal-iodides (I2MoO2, SnI2, SnI4) species.

CONTENTS

Figures

Tables

1 Introduction

Safety analysis is performed on Nuclear Reactor power plants to ensure the health and safety of the public, for accidents that are postulated to occur. Accidents are analysed which are anticipated to occur over the life time of the plant as well as hypothetical accidents which are not expected to occur but are acknowledged as highly improbable events. One of the aims of such analysis is to determine the mitigating features of the particular reactor design. Each reactor design has a strong Containment and Engineered Safeguard Systems, which are safety systems designed to mitigate accident scenarios. Despite low probability frequencies, some severe accident sequences can lead to core melting and plant damage causing the dispersal of radioactive material into the environment and thus constituting a health hazard to the public.

Risk-oriented safety assessment and severe accident management (SAM) measures are currently developed and implemented at NPPs to prevent or to mitigate severe accidents. Such activities are only possible if there is a deep understanding of processes leading to severe accidents and of phenomena related to them.

Validations of codes and uncertainties evaluation are consequently needed to take account of severe accident measures in the regulation of plants.

To accomplish this, systems of so-called 'integral' computer codes, are being developed and assessed to simulate the scenario of a hypothetical sever accident in a nuclear reactor, from the initial event until the possible radiological release of fission products (FPs) out of the containment. They must include the relevant physical phenomena that occur in the different reactor zones (core, primary loop, containment) and simulate the actuation of safety systems by procedures and by operators. Also, a compromise must be found between the accuracy of models and calculation time in order to study a great number of scenarios. Such codes have first been developed in the United States (MAAP4 [1], MELCOR [2]) and are now used worldwide. In Europe, the experimental and analytical work in the field of severe accidents was mainly performed in France and Germany, albeit in a distinct manner. Consequently, the French IRSN and the German GRS decided to co-operate in the development and validation of a new integral code ASTEC that would contain the best available modelling.

Its application range would cover:

- Evaluation of possible radiological release out of the containment;
- Accident management studies, concerning the measures of prevention and mitigation of severe accidents;
- PSA level 2 studies, including the determination of uncertainties;
- Physical analyses of scenarios to improve the understanding of the phenomenology, including support to experimental programs.

Learning from MELCOR experience, where a great number of users have greatly increased the level of code performance, IRSN and GRS opened the ASTEC use for extended validation and generic application to a wide number of European organizations. ASTEC code has progressively reached a larger European dimension through the European Commission Framework Programme projects: VASA [3] (FP4), EVITA [4] (FP5) and more recently through the SARNET [5] (Severe Accident Research Network of Excellence) (FP6). Within these projects and integrated in a series of other severe accident activities, the code has been validated over a large number of experimental programs performed in in-pile and out-of-pile facilities, at various scales. These included analytical experiments, coupled-effect tests and integral experiments (e.g. PHEBUS-FP, PACTEL, CORA-13) mostly belonging to the list of ISP OECD exercises. Besides the experiment selected, the ASTEC modules were also applied in several benchmarks on plant applications with other codes such as MELCOR and MAAP4. As a common conclusion is that the level of ASTEC models is near the state of the art in

most domains, it has only been recently acknowledged the capability to perform a full realistic integral calculation with regard to integral tests (Phebus-FP) and more to plant applications.
The JRC-IE has greatly contributed to the validation of the ASTEC code (ELSA/DIVA, SOPHAEROS, CPA modules), mainly in fission product release and transport in the circuits and containment (PHEBUS-FP, STORM). This activity led, in particular, to the full integral analysis of the FPT-2 PHEBUS experiment which allowed confirming the consistency between the main modules of the code.
The aim of this report is to move, in co-operation with the VUJE Institute, the expertise acquired on fission product release and transport in the circuits (with the analysis of the Phebus experiments) towards the main application of ASTEC code, the evaluation of the source term and its chemical forms in plant severe accident analysis. Indeed, the radio-toxicity of released FPs depends not only from their mass but also on the chemical forms as well. In particular gaseous iodine release is a main concern. So far the chemical form of gaseous iodine was identified as I_2 and/or HI. However, this needs confirmation and recently some preliminary calculations showed that gaseous iodine can release in form of metal-iodides as well. The confirmation of conservative forms and the identification of new metallic forms can lead to novel approaches in the management and mitigation of consequences of iodine release.
As plant a reference 3-loop PWR 1000 MWe has been chosen, based mainly on the public data available and the diffusion of this type of reactor in Europe. But most of the conclusions derived can be easily extended to other type of plants.
Based on the NUREG-1150 [6] and NUREG/CR-5750 [7] LOCA size classification a severe Medium Break LOCA accident study on the cold leg , combined with the total loss of electric power supply (Black-Out), has been performed using the last version of the integral code ASTEC V1.3 rev2.

Chapter Two briefly introduces the ASTEC code and gives a short description of its different modules. In Chapter Three the ASTEC model for the reference 3-loop PWR plant is described. The core, the primary and secondary circuit features are given together with the different options for the modules involved. The severe accident sequences and analysed cases are presented in Chapter Four. The analysis of the results begins in Chapter Five and includes the thermal-hydraulic behaviour, the fission products and structural material release from the core and their transport in the circuit. A summary of the results is subject of Chapter Six. In Chapter Seven the final conclusions are given.

2 Short Description of the ASTEC V1.3rev2 Integral Code

The **ASTEC V1.3 Rev.2** [8, 9] code system was distributed in December 2007 and consists of the following modules, which can be used, either in stand-alone mode or in integral mode:

- **CESAR** [10]: It is the module in charge of the primary and secondary circuits two-phase thermal-hydraulics in case of a nuclear reactor accident, both during the front-end and during the degradation phases of an accident up to the reactor vessel lower head failure;

- **DIVA** [11]: Calculation of the core degradation and thermal hydraulic in the reactor vessel. In previous versions of ASTEC, DIVA was automatically stopped after the vessel lower head failure. It is now possible to continue DIVA calculation after the vessel rupture and then to feed MEDICIS with additional corium masses in the cavity;

- **ELSA 2.1** [12]: The module of fission products and structural materials release during core heat-up and degradation, from intact rods, debris beds and molten pools;

- **SOPHAEROS** [13]: The module of fission product and structural materials transport and deposition in the circuits during severe accidents. It presents vapour phase (equilibrium chemistry, homogenous nucleation etc.), vapour interactions with structures (condensation, sorption), aerosol deposition and agglomeration mechanisms. This version is able to compute chemical equilibrium of species in the gas phase and uses new model for aerosols mechanical resuspension;

- **RUPUICUV 1.2** [14]: The module is designed to compute the ex-vessel corium discharge occurring after the lower head vessel failure and the corium entrainment to the containment due to primary circuit gas blow-down into the cavity. Entrained corium might be oxidized, releasing a large amount of energy in the containment building;

- **CORIUM** [15]: This module models the behaviour of the corium present in the containment, after its entrainment. Important phenomenon is the Direct Containment Heating (DCH), i.e. the heating of the containment atmosphere by the corium gas mixture coming from the RCS after the vessel rupture;

- **WEX 3.1** [16]: A new version of the WECHSL module for calculation of the molten corium - concrete interaction (MCCI) in the cavity during ex-vessel phase. The module assumes either a mixed corium or a stratified one (oxide, metal). It computes the concrete ablation, corium oxidation and production of the non-condensable gases (CO_2, CO, H_2) and H_2O steam;

- **MEDICIS** [17]: The scope of this module is the same as of WEX 3.1, i.e. simulation of the MCCI in cavity (selection of the module is user input). The corium pool may be constituted of one homogeneous single oxide layer or of several layers. The last situation corresponds to a stratification of oxide and metal species or to the growth of an upper crust at the corium - water-pool interface;

- **CPA** [18] – Containment Part of ASTEC, which consists of the following sub-modules:
  - Thermal-hydraulic main module (**CPA-THY**) – modelling of the containment t-h phenomena: gas distribution, pressure built-up, hydrogen combustion, spray system operation and others;
  - FIPHOST [19] module (**CPA-AFP**) – calculation of the FP transport in the containment. This module uses the results of CPA-THY (flow rates at junctions) to transport gas species and to study condensed FP (they form a part of aerosols), in particular the various depletion rates. The

results of FIPHOST are mainly the distribution of FP in the containment (on walls, in sumps and in the gas). CPA- THY uses them to compute precisely the local decay heat;

- **IODE** [20]: The purpose of this module is to model the iodine and ruthenium chemistry in the reactor containment in a situation of severe accident (i.e. creation and destruction of highly volatile organic and molecular iodine and ruthenium tetraoxide). In a coupled mode of the calculation the CPA module provides the thermal-hydraulic boundary conditions. The module now covers above 40 possible chemical reactions in the gas and liquid phases;

- **ISODOP** [21]: FP and actinide isotopes under natural disintegration. It starts the computation using an initial isotope inventory, and allows a better estimation of decay heat and activity in the core, in the RCS, in the containment and in the environment (more than 700 isotopes);

- **SYSINT** [22]: management of the operation of safety systems (containment spray system, opening–closing of relief valves, safety injection to RCS etc.) according to pre-defined criteria;

3 Description of the reference PWR 1000 Computational Model

In the following paragraphs the ASTEC modelling of the reference PWR 1000 plant is discussed. This includes the model for the modules actually used in the current analysis (CESAR, DIVA and SOPHAEROS)

3.1 Core and Reactor Vessel

DIVA module: Core and Lower Reactor Vessel

As shown on Figure 3.1 the reactor vessel below the top of active core (elevation +3.6576 m) consists of the following components (note that these macro-structures are defined in VESSEL_D data for DIVA module):

VESSEL: Reactor vessel side wall between elevations +0.0 m to +3.6576 m with thickness 300 mm made from the stainless steel AISI-304. It is ASTEC default STEEL material with the following properties:
- composition: 68% of Fe, 12% of Ni and 20% of Cr,
- solidus temperature: 1398 ºC,
- liquidus temperature: 1454 ºC.

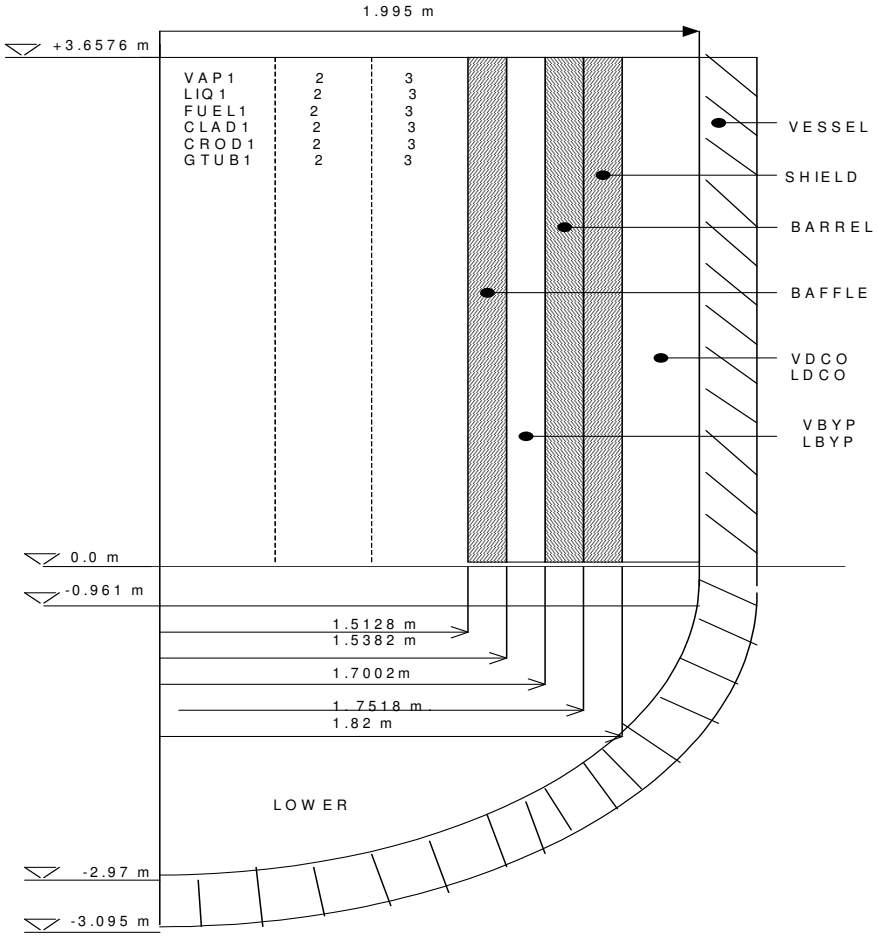

Figure 3.1: Reactor vessel and active core components (DIVA module)

SHIELD: Annular shroud made from ASTEC default STEEL material representing shielding of the reactor vessel side wall (thickness 68.2 mm).

LDCO, VDCO: Annular liquid and gas channels between vessel side wall and shielding.

BARREL: Annular shroud made from ASTEC default STEEL material representing core barrel (thickness 51.6 mm).

LBYP, VBYP: Annular liquid and gas channels between core baffle and core barrel representing coolant flow by-passing active core.

BAFFLE: Annular shroud made from ASTEC default STEEL material representing core baffle (thickness 25.4 mm).

The **active core volume** is divided into **3** radial rings with associated liquid (**LIQ1 – 3**) and gas (**VAP1 – 3**) channels, which contain fuel rods (**FUEL1 – 3**) with claddings (**CLAD1 – 3**) and control rods (**CROD1 – 3**) with guide tubes (**GTUB1 – 3**). The main characteristics of these components are given in Table 3.1 and main characteristics of the core rings in Table 3.2. The total number of the fuel rods (FR) is 41448 and 3768 of the control rods (CR).

Table 3.1: Main characteristics of initially solid core components

Input parameter	Fuel	Cladding	Control rod	Guide tube
Name	**FUEL1**	**CLAD1**	**CROD1**	**GTUB1**
Radial position, [m] [1)]	0.405 m	0.405 m	0.405 m	0.405 m
Internal diameter, [m]	0.0	0.008358	0.0	0.01164
External diameter, [m]	0.008191	0.0095	0.00859	0.01204
Material composition [2)]	UO2	ZR	SIC	ZR
Solidus temperature	2400 K	2098 K	1050 K	2098 K
Liquidus temperature	2500 K	2099 K	1100 K	2099 K

[1)] Radial positions of the 2nd and 3rd rings are defined at 0.9995 m and 1.3509 m.

[2)] The used solidus and liquidus temperatures of the materials UO2, ZR (Zircaloy alloy: Zr – 98.3%, Fe – 0.2%, Sn – 1.4% and Cr – 0.1%) and SIC (neutron absorber: Ag – 80%, In – 15% and Cd – 5%) are the ASTEC default values.

Table 3.2: Main characteristics of the core rings

Core ring No.	**1**	**2**	**3**
Radial power peaking factor	1.2207	1.183	0.662
Volume fraction (fuel)	0.2866	0.3312	0.3822
Number of FR	11879	13728	15841
Number of CR	1080	1248	1440

All components between the elevations from +0.0 m to +3.6576 m are divided into **10** uniform axial meshes.

LOWER PLENUM: Lower plenum represents the volume below bottom of active core (elevation +0.0 m) including spherical bottom head. The wall of lower plenum is divided into 5 radial meshes. The number of axial meshes in the spherical part is 8 and 1 axial mesh is used for cylindrical part

(length 0.961 m). Internal structures (50 tubes - STEEL) are also modelled in the lower plenum with a total mass equal to 624.1 kg.

Core decay heat model

The core decay heat is modelled under assumption that all decay heat is generated inside the uranium, i.e. transport of decay heat with the fission products released from the core into the RCS volumes and to containment is not taken into account. It should be noted that such approach leads on one hand to an overestimation of the decay heat in the core region and RV lower plenum (speed-up of the degradation process) and on the other hand to an underestimation of the dose rate in the water of containment sump and intensity of the chemical reactions (creation of I_2 and CH_3I). The time history of the core decay power is presented on Figure 3.2 (note that reactor scram is supposed 100 s from the start of transient calculation – see also Chapter 3.5).

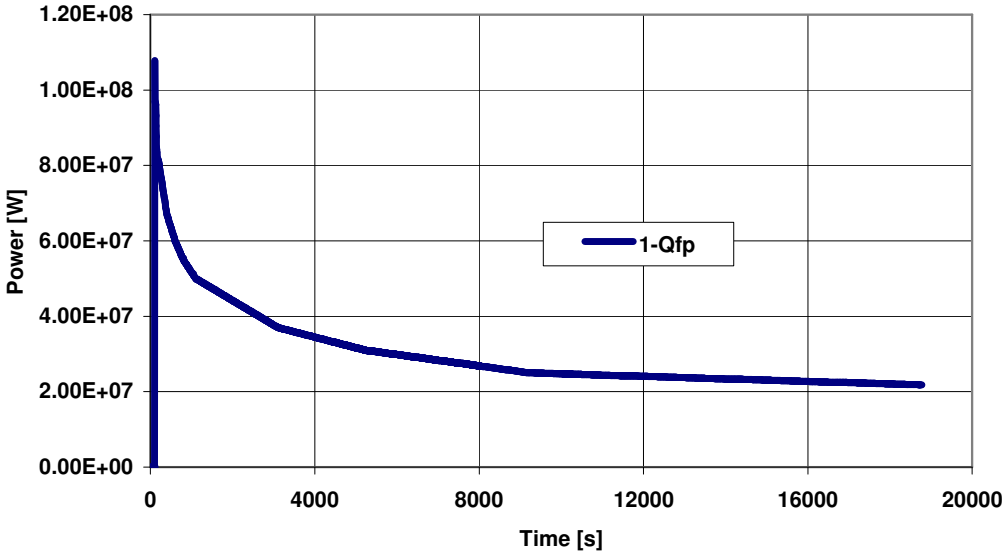

Figure 3.2: Core decay heat

The skewed cosine axial power profile is defined for **11** axial meshes with the maximum value in the centre of the core as is given in the Table 3.3. Note that this axial power profile is automatically recalculated by the code for 10 uniform meshes used for axial splitting of the core component between the elevations from +0.0 m to +3.6576 m as mentioned earlier.

Table 3.3: Axial power peaking factors

No.	Elevation: from – to, [m]	Peaking factor, [-]
1.	0.000 - 0.528	0.53
2.	0.528 - 0.788	0.69
3.	0.788 - 1.048	0.96
4.	1.048 - 1.308	1.23
5.	1.308 - 1.568	1.48
6.	1.568 - 2.088	**1.6**
7.	2.088 - 2.348	1.48
8.	2.348 - 2.608	1.23

9.	2.608 - 2.868	0.96
10.	2.868 - 3.128	0.69
11.	3.128 - 3.657	0.53

Thermal exchanges

The module COND is used for calculating the axial conduction (using the simple determination of the conductivity) in each component, i.e. representative fuel rod, representative control rod, baffle etc. The convective heat exchange of each channel with all components is calculated by means of the module CONV. The module RADC is used for the calculation of the radiative heat exchange between a representative fuel rod and the representative control rod and core baffle.
Radial conduction and radiation between fuel and cladding of the representative fuel rods and between the control rod and guide tube is calculated by means of the module GAP. In the case of contact between neighbouring elements due to the thermal expansion, the DIVA module automatically suppresses radiative exchange in the closed gap.

Chemical interactions

Oxidation kinetics of the fuel rod claddings and guide tubes is performed by means of the module ZROX. The value of MMIX (allowing to limit the oxidation area for relocated mixtures) is supposed equal to 1.0 (no limitation, default) and the URBANIC correlation is used. Double side oxidation could occur after destruction (cracking) of the fuel rod cladding in a given cell.
The oxidation kinetics of core baffle, barrel, RV shield and side wall is not calculated by means of the module FEOX.
The module UZRL (activation of the convective Kim-Olander correlation) is used for calculation of UO_2 and ZrO_2 dissolution by liquid Zr.

Mechanical behaviour

The module CCYL is used to avoid possible overlapping, due to thermal expansion, between cladding and fuel, control rod and guide tube and between core baffle, barrel and reactor vessel shield.
The fuel rod cladding stress-strain analysis may be performed by DIVA module. However, the rupture of cladding is not computed by the mechanistic model (module CREE), but simply simulated by a threshold temperature equal to 1173 K in the module INTE. Thus, the oxidation of cladding internal surface is initiated at the same temperature.
Melt of fuel (fuel relocation temperature) is simulated by change of the state from compact to dislocated at temperature equal to 2400 K (start of UO2 melting - see also Table 3.1).

Movement of materials

The module DECA is used to deal with the movement of molten fuel in the radial direction (onto the cladding surface).
Candling of molten fuel rods, on the external face of the fuel rod cladding, is calculated by means of the module CAND. The velocity of the flowing mixtures is reduced to 0.01 m/s (default = 0.6 m/s) and the blockage factor is considered 100% (default = 90%, i.e. percent of volume involving a flow blockage). A very low velocity value of 0.01 m/s is recommended [8] to simulate with 1D CAND model the very low downward progression of a molten pool (the lesson drawn from the Phébus FP tests interpretation). Note that this very low candling velocity has to be combined with the lowering of the UO_2 (ZrO_2) solidus temperatures to roughly account for the early fuel liquefaction process as observed in the Phébus FP tests ([23], [24]). All the other parameters of the 1D CAND model have

default values. The candling of SIC control rods and guide tubes is taken into account in the same way as for fuel rods.

It should be noted that in the current model of the reference PWR 1000 reactor the candling of the core baffle is not taken into account, but this is not crucial for the accident scenarios analysed in the report.

The module (structure) DEBR devoted to the management of debris bed and magma in the core (2D approach) has not been used, since it is not recommended in the version used of the ASTEC code [8].

Initial Inventory of the Fission Products in the Core

The representative initial inventory of the fission products is presented in the Table 3.4 and corresponds to the standard pressurized water reactor with the nominal thermal power ~3000 MWt at the end of equilibrium fuel cycle. This is the complete list of the nuclides (42 FP and 5 actinides), which are considered by the ELSA module [12], since a complete inventory has to be defined in the code input.

Table 3.4: Initial inventory of the fission products and actinides

Nuclide	Mass [kg]	Nuclide	Mass [kg]	Nuclide	Mass [kg]	Nuclide	Mass [kg]
Xe [1)]	265.7	**Ru** [1)]	108.55	**Pu**	675.14	**Cm**	0.992
Kr [1)]	20.85	**Sr**	54.28	**Nd**	185.69	**Sm**	38.28
I [1)]	11.14	**La**	62.85	**Pm**	8.284	**U**	65455.7
Br [1)]	1.2	**Eu**	10.47	**Gd**	2.521	**Zn**	1.22e-6
Cs [1)]	139.98	**Ce**	151.41	**Tb**	0.0	**As**	6.57e-3
Rb [1)]	19.71	**Mo**	162.83	**Dy**	0.0	**Cd**	3.246
Cu	1.2e-11	**Rh** [1)]	19.71	**Ho**	0.0	**Sn**	2.228
Se	3.142	**Pd**	48.56	**Er**	0.0	**Ga**	1.38e-4
Te [1)]	22.0	**Tc**	42.85	**Tm**	0.0	**Ge**	1.8e-4
Sb	0.8284	**Nb**	2.857	**Yb**	0.0	**In**	6.33e-2
Ag	2.514	**Zr**	191.4	**Pr**	57.13	**Y**	27.424
Ba [1)]	71.417	**Np**	25.14	**Am**	3.894	**-**	-

[1)] Fractions supposed to be in the fuel-to-clad gap: 0.01 (Xe, Kr), 0.005 (I, Br, Cs), 1.E-4 (Te, Ba) and 1.E-5 (Ru, Rh).

CESAR Module: Upper Reactor Vessel

The upper region of the reactor vessel is modelled in the CESAR module and includes the Upper Plenum, the Cold Leg Collector, the By-Pass and the Dome.

As shown on Figure 3.3 there are defined altogether three connections between VESSEL_D structure (part of DIVA module) and PRIMARY (part of CESAR and SOPHAEROS modules):

- *CORE_UPP*: It is connection of type FLOW between the channels of active core (including annular liquid and gas channels between core baffle and core barrel – core by-pass, se also Figure 3.1) and volume representing the RV upper plenum;
- *DC_VOLD*: It is also connection of type FLOW between the downcomer (DIVA channels LDCO and VDCO, see also Figure 3.1) and RV cold collector;
- *CORE_FP*: It is connection of type SOURCE for transport of FP (SM) released in the core region to RV upper plenum. It should be pointed out that in the used version of the ASTEC

code only one connection for FP transport from DIVA module to CESAR (SOPHAEROS) module is allowed;

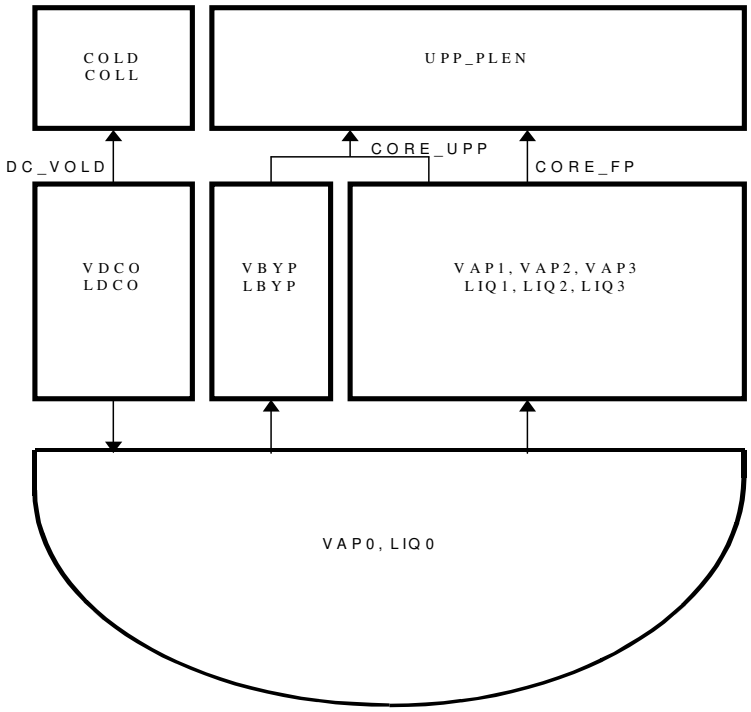

Figure 3.3: Connections from VESSEL_D (DIVA) to PRIMARY (CESAR and SOPHAEROS modules)

3.2 Primary Circuit

The computational model of the primary circuit consists of the three loops. In Figure 3.4 the nodalization scheme used for CESAR module is only shown for the loop containing the pressurizer. It should be noted that the RV control volumes "core", "lat1", "lat2" and "volinf" are created automatically from the data defined for DIVA module as described in the previous paragraph (§3.1). The main characteristics of the primary circuit volumes are described in Table 3.5.

Table 3.5: Main parameters of the primary circuit control volumes

No.	Name	TYPE [1)]	Volume, [m^3]	Elevation, [m]	Dh, [m]	VERT [2)]
1	Volinf	0	27.337	-1.485	3.0225	1
2	Core [3)]	-1	13.982	+1.8288	0.011	1
3	Lat1	0	6.029	+1.8288	0.2523	1
4	Lat2	0	7.645	+1.8288	0.1054	1
5	UPP_PLEN	1	20.25	+4.7	3.0	1
6	DOME	0	19.0	+7.75	3.2	1
7	CCBYPASS	0	3.0	+6.4	0.5	1
8	COLDCOLL	1	4.7	+4.3	0.45	1
9	HOL1	0	3.65	+5.0	0.735	0
10	PRESSLIN	0	1.45	+8.15	0.3	1
11	PRESSU	1	38.0	+17.0	1.15	1
12	HOTBOX1	0	4.0	+6.65	2.1	1

13	TUBES1 [4]	-1	23.4	+12.45	0.018	0
14	COLDBOX1	0	4.0	+6.65	2.1	1
15	ULEGA1	0	2.15	+4.35	0.8	1
16	ULEGAB1	0	0.95	+2.5	0.8	0
17	ULEGB1	0	1.85	+3.85	0.8	1
18	COL1	0	7.0	+5.0	0.7	0

[1] Type of the volume (0 – standard 2-phase volume, 1 – volume with a swollen level)
[2] Verticality of the volume (0 – horizontal, 1 – ascending, -1 – descending flow)
[3] Core volume is split into 10 uniform axial meshes.
[4] SG tubes (4520 in one SG) are split into 12 non-uniform axial meshes (see chapter 3.4).

Each loop is equipped with a primary circulation pump with a reference volumetric flow rate of 5.1 m^3/s.

The Pressurizer is modelled as one cylindrical volume (see PRESSU in Table 3.5) with an inner diameter of 1.15 m and with a total volume of 38 m^3. There are 2 valves connected to the Pressurizer (see Figure 3.4):

- Pressurizer **Relief Valve** (PRZ_PORV) with the following characteristics:
  - opening pressure: 16.259 MPa
  - closing pressure: 15.946 MPa
  - flow area : 1.1165E-3 m^2 (equivalent inner diameter = 37.71 mm)

- Pressurizer **Safety Valve** (PRZ_SRV) with the following characteristics:
  - opening pressure: 17.3 MPa
  - closing pressure: 16.97 MPa
  - flow area : 2.7746E-3 m^2 (equivalent inner diameter = 59.44 mm)

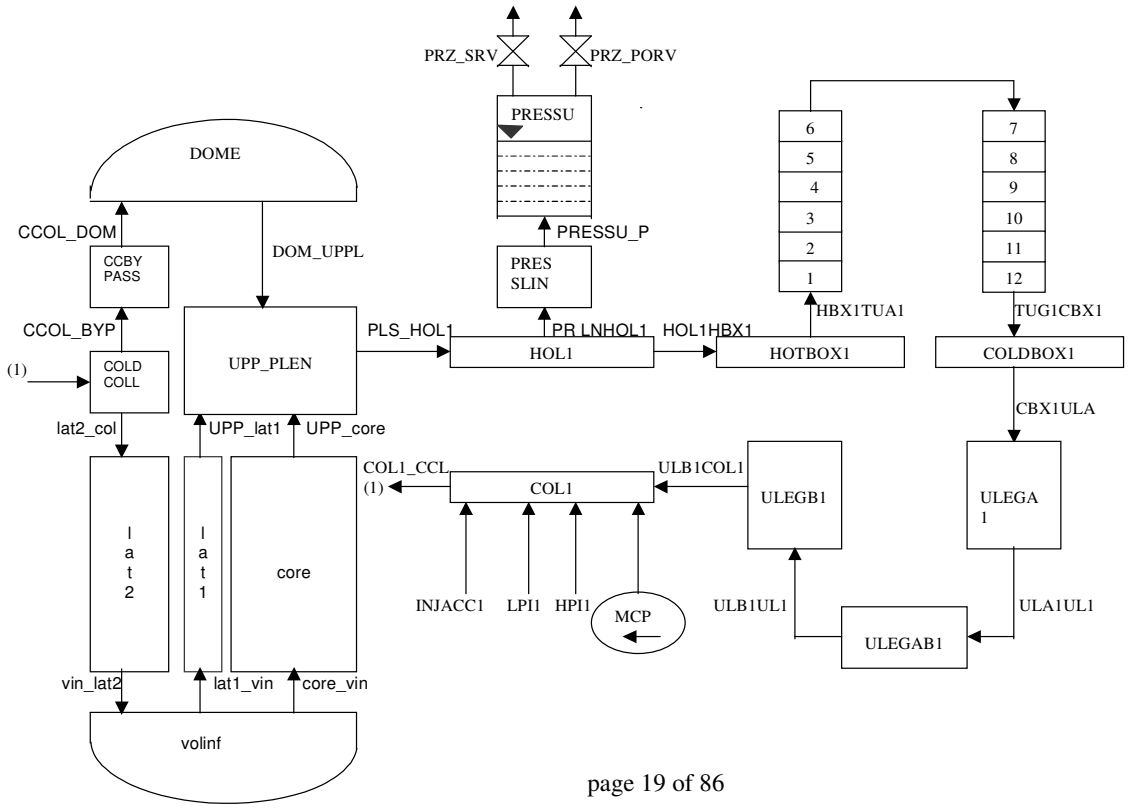

Figure 3.4: Primary circuit nodalization scheme for CESAR module (3-loop model)

There are 3 identical accumulators as passive emergency injection system (INJACC1, 2, 3), one for each loop, connected to the cold leg volumes (volumes COL1, 2 and 3) of the corresponding primary circuit loop. To the same volumes are connected three trains of high pressure (HPI1, 2, 3) and low pressure (LPI1, 2, 3) emergency core cooling systems (not used in this study).

The main characteristics of the reference accumulator are as follows:

- threshold pressure: 4.525 MPa,
- total free volume: 42.0 m^3
- initial water mass in one accumulator: 28907 kg
- cross section of the accumulator: 4.2424 m^2 (d_e = 2.324 m)
- liquid enthalpy in the accumulator: 1.73115E+5 J/kg (temperature ~40 °C)
- absolute elevation of the accumulator: +5.0 m

3.3 Secondary Circuit

The computational model of the secondary circuit consists of three identical steam generators connected to a common steam header (volume GVCOL). The nodalization scheme used for CESAR module is shown on Figure 3.5 for one steam generator. The main characteristics of the secondary circuit volumes are described in the Table 3.6.

Table 3.6: Main parameters of the secondary circuit control volumes

No.	Name	TYPE [1)]	Volume, [m^3]	Elevation, [m]	Dh, [m]	VERT [2)]
1	GWDOWNB1	0	21.0	+17.7	0.7	-1
2	GWDOWNA1	0	7.6	+11.25	0.2	-1
3	GWBUND11	0	3.05	+8.2	0.02	1
4	GWBUND21	0	7.9	+9.5	0.02	1
5	GWBUND31	0	9.0	+11.5	0.02	1
6	GWBUND41	0	8.5	+13.5	0.02	1
7	GWBUND51	0	7.1	+15.425	0.02	1
8	GWBUND61	0	11.4	+16.925	0.02	1
9	GWRISER1	0	13.5	+19.5	0.46	1
10	GWDOME1	1	71.0	+23.0	2.0	1
11	GVVAP1	0	44.1	16.8	0.75	1
12	GVCOL	0	81.5	12.3	0.95	0

[1)] Type of the volume (0 – standard 2-phase volume, 1 – volume with a swollen level)
[2)] Verticality of the volume (0 – horizontal, 1 – ascending, -1 – descending flow)

There are 3 main feedwater pumps in the secondary circuit (one for SG) with a nominal mass flow rate of 560 kg/s. The feedwater temperature is equal to 490 K (217 °C). There are also 3 auxiliary feedwater pumps with a nominal mass flow rate of 25 kg/s (the feedwater temperature is equal to 305 K (32 °C).

Each SG is equipped with 2 regulation valves with the following main characteristics:

• SG **Relief Valve** (VSG1PORV) with the following characteristics:
- opening pressure: 7.68 MPa
- closing pressure: 7.513 MPa
- flow area : 2.6E-3 m^2 (equivalent inner diameter = 37.71 mm)

• SG **Safety Valve** (VSG1SRV) with the following characteristics:
- opening pressure: 8.433 MPa
- closing pressure: 8.06 MPa
- flow area : 2.8067E-2 m^2 (equivalent inner diameter = 189.1 mm)

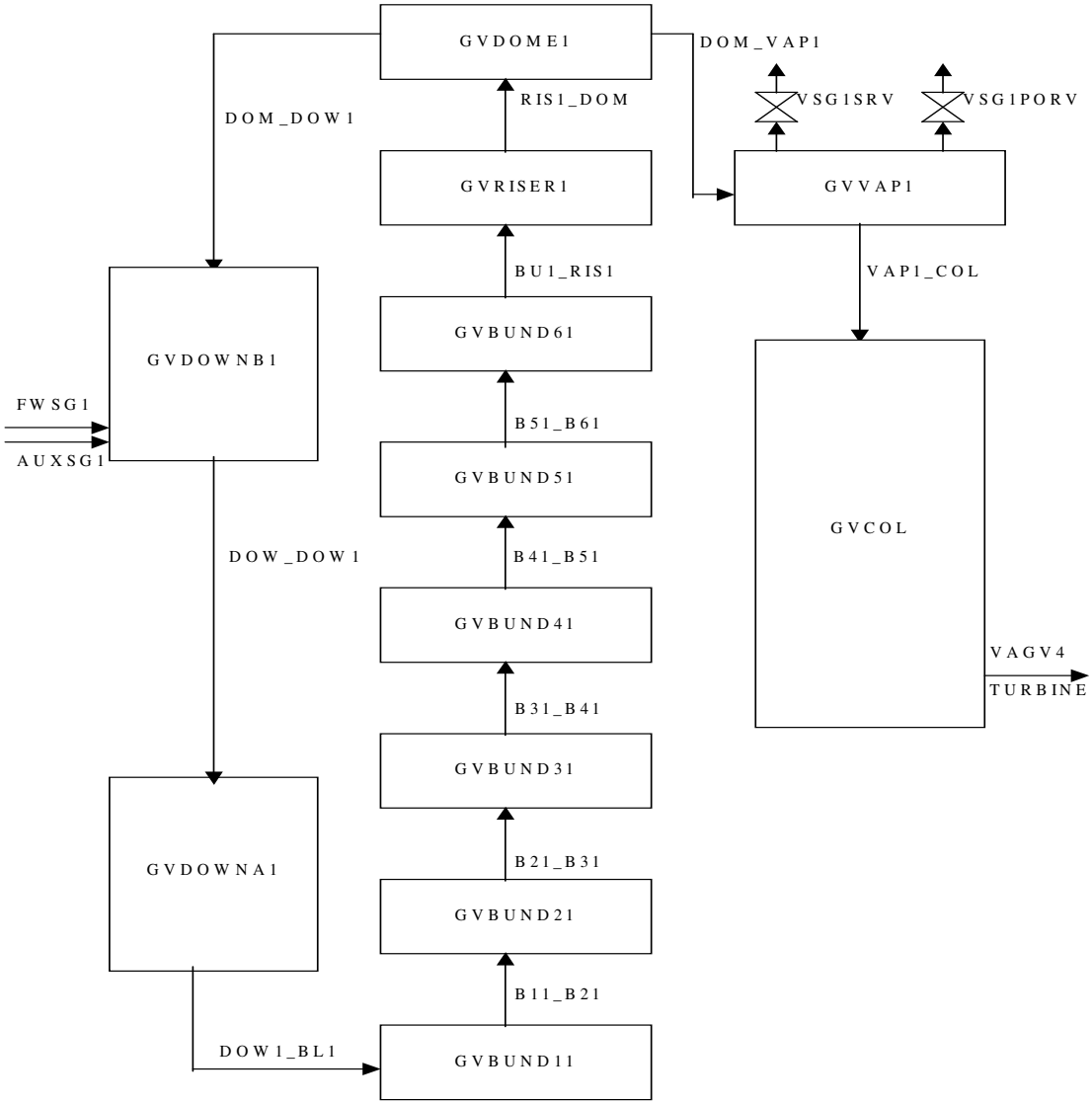

Figure 3.5: Secondary circuit nodalization scheme for CESAR module (3 – loop model)

3.4 Primary Circuit – Secondary Circuit Interface

The interface (thermal exchange) between primary and secondary circuits is realized through vertical SG tubes, which are divided altogether into 12 non-uniform axial meshes (6 ascending and 6 descending cells) in accordance with the splitting of the SG secondary side bundle region into 6 control volumes from GVBUND11 to GVBUND61 (see Figure 3.5). The model is based on a connection structure between two walls of the U-tubes (on the primary and secondary side respectively). The heat transfer is defined through the input parameter

$$lambda\_1 = lambda \bullet \frac{S}{e} \text{ [W/K]}$$

where:
lambda [W/mK] is wall thermal conductivity,
S [m^2] is wall exchange surface
e [m] is wall thickness.

The values of the "lambda_1" parameter are given in the Table 3.7.

Table 3.7: Definition of the parameter "lambda_1" for thermal Exchange in the SG

No.	SG tube mesh [1)]	lambda_1, [W/K]	SG secondary volume [1)]
1	CELL01	3620	GVBUND11
2	CELL02	9400	GVBUND21
3	CELL03	10500	GVBUND31
4	CELL04	10200	GVBUND41
5	CELL05	8400	GVBUND51
6	CELL06	7050	GVBUND61
7	CELL07	7050	GVBUND61
8	CELL08	8400	GVBUND51
9	CELL09	10200	GVBUND41
10	CELL10	10500	GVBUND31
11	CELL11	9400	GVBUND21
12	CELL12	3620	GVBUND11

[1)] It means that the corresponding wall belongs to this volume (cell).

3.5 Fission Products Transport and Deposition in the Primary Circuit

Fission products and structural materials (vapours, aerosols) transport and deposition in the primary circuit calculated by SOPHAEROS module depend on the release kinetics from the fuel and control rods (modules ELSA/DIVA), leakage pathway from the core volume to the break and on the boundary conditions calculated by CESAR module (carrier gas mass flow rates, gas and wall temperatures). The surfaces for gravitational settling and for all other deposition processes (lateral surfaces) are for the primary circuit control volumes (see also Figure 3.4) summarized in the Table 3.8.

It should be pointed out that in the ASTEC code version used here [9] only one connection with transport of FP/SM from DIVA to CESAR/SOPHAEROS is allowed (see connection CORE_FP on the Figure 3.3). As a rule this connection is defined from the core region to the upper plenum (Figure 3.3) and is located above the core. During the transient (e.g. LOCA on cold leg) a reverse gas flow can

be established for a limited time period. In such a case, the FP/SM released from the fuel and control rods during this time period and transported through the RV downcomer (channels LDCO and VDCO on Figure 3.3) to the RV cold collector (volume COLDCOLL) are not taken into account for the source term.

All physical processes simulated in the SOPHAEROS module:
- homogeneous and heterogeneous nucleation of vapours,
- condensation and re-evaporation of vapours on (from) the wall surfaces,
- aerosols gravitational settling, thermo-phoresis, turbulent-eddy impaction, resuspension,
were taken into account in the analyses, using the default options including the "vapour chemistry" model.

Table 3.8: Settling and lateral surfaces for the primary control volumes

VOLUME	Surf_set [m^2]	Surf_lat [m^2]	VOLUME	Surf_set [m^2]	Surf_lat [m^2]
UPP_PLEN	0.0	600.0 [1)]	CELL9	0.0	522.2
HOL1	6.323	19.86	CELL10	0.0	544.4
PRESSLIN	0.0	19.33	CELL11	0.0	477.8
PRESSU	0.0	132.2	CELL12	0.0	344.4
HOTBOX1	0.0	7.62	COLDBOX1	0.0	7.62
CELL1	0.0	344.4	ULEGA1	0.0	10.75
CELL2	0.0	477.8	ULEGAB1	1.512	4.75
CELL3	0.0	544.4	ULEGB1	0.0	9.25
CELL4	0.0	522.2	COL1	12.73	40.0
CELL5	0.0	433.3	COLDCOLL	0.0	38.5
CELL6	0.0	366.7	CCBYPASS	0.0	24.0
CELL7	0.0	366.7	DOME	0.0	23.75
CELL8	0.0	433.3	-	-	-

[1)] *This value is set by the user in accordance with heat transfer area of the corresponding wall for UPP_PLEN volume. All other values of "surf_set" and "surf_lat" parameters are automatically calculated by the code from input data for control volumes (see Table 3.5).*

The size distribution of aerosols particles entering the circuit was defined as a mono-modal log-normal distribution and only one distribution function was used. This distribution has 20 bin classes, the minimum radius of particles was set to 0.001 µm (default) and the maximum radius to 10.0 µm (default is 20 µm). The initial geometric mean radius is 0.1 µm (default) and the geometric standard deviation of 1.5 (default). The particles are assumed to be spherical with default values of uniform bulk density (3000 kg/m^3) and thermal conductivity (3.5 W/m/K).

3.6 Steady-state Calculation Results

The following initial conditions and controllers have been used to reach acceptable steady-state results:

- Start time of the steady-state calculation: -2500.0 s
- Stop of the regulation: -1000.0 s
- End of steady-state: 0.0 s
- Regulation of the water mass in the PRZ to reach the expected value: 18000.0 kg.

- Regulation of the pressure in the pressurizer to reach the expected value: 15.515 MPa.
- Regulation of feedwater (steam) mass flow rate to (from) the three Steam Generators.

The stabilization of the main plant parameters with this regulation is reached during the first 200 – 400 s and the parameters remain stable also after all the regulations are switched off 1000 seconds before the end of the steady-state calculation. The main plant parameters at the end of the steady-state calculation are presented in the Table 3.9.

Table 3.9: Calculated steady-state values

Parameter	Value	Unit
Reactor thermal power	2998	MW
Pressurizer pressure	15.47	MPa
Average temperature at core inlet	285.1	°C
Average temperature at core outlet	323.8	°C
Average coolant heating in core	38.7	°C
Total mass of water in primary circuit	198655.0	kg
Water mass in the pressurizer	18000.0	kg
Coolant flow through 1 MCP	4542.0	$kg.s^{-1}$
Total mass of water in secondary circuit	183768.0	kg
Pressure in the SG	6.136	MPa
Steam temperature in SG	277.0	°C
Steam mass flow from one SG	536.6	$kg.s^{-1}$
Feedwater temperature	216.9	°C

4 Selected Severe Accident Sequence and Analysed Cases

The transient phase begins with 100 seconds in steady-state conditions, without regulators to verify the stable conditions of the plant. The accident is assumed to be initiated (t_b=98 s) by the creation of a Medium size Break (MBLOCA, d_e = 51.6 mm) on the cold leg of one primary loop (the loop connected with the pressurizer – Figure 3.4), combined with the total loss of electric power supply (blackout). As definition of Medium Break, the three categories of NUREG-1150 and NUREG/CR-5750 in LOCA size classification were considered, where a Medium Break is defined as having a flow rate between 94 kg/s and 320 kg/s. Both high and low pressure injection pumps of the emergency core cooling systems (ECCS) are not available. Based on the accumulators (i.e. passive ECCS) availability and exact location of the break the following cases have been analyzed:

Case 1A: Break is located in the control volume ULEGB1 (see Figure 3.4) and no accumulator is available;

Case 1B: Break is located in the control volume COL1 (see Figure 3.4) and no accumulator is available;

Case 2A: Break is located in the control volume ULEGB1, but all three accumulators are available;

Case 2B: Break is located in the control volume COL1, but all three accumulators are available.

It should be mentioned that availability of the accumulators has strong influence on the accident sequence evolution mainly from the point of view of the duration of the core degradation process and timing of RV lower head failure. This has also considerable influence on the release of the semi and low volatile FP from the degraded core.

Preliminary analyses made with ASTEC code before performing final calculations showed that the results are nearly the same for break location in the control volumes ULEGA1, ULEGAB1 and ULEGB1. But break location in the COL1 volume leads to different gas (steam + H_2) flow paths in the primary loops with the consequence on the FP (SM) transport in the circuit before their leakage through the break outside the circuit.

5 The Analysis of the Results

5.1 Thermal-hydraulic Response of the Reactor Coolant System

The timing of main events as well as the detailed results at predicted time of RV lower head failure is presented for all the cases in the Table 5.1. Note that time of RV lower head vessel failure corresponds to the end of the calculation.
It should be also pointed out that automatic management of DIVA module start was applied in all the cases, which is based on a following double criterion:

- Void fraction in the highest mesh of the CESAR core volume is > 0.99.
- Steam temperature in the highest mesh of the CESAR core volume is > 750 K.

Table 5.1: Timing of main events and selected results at time of RV lower head failure

EVENT	**Case 1A** [s]	**Case 1B** [s]	**Case 2A** [s]	**Case 2B** [s]
Break opening	98.0	98.0	98.0	98.0
Reactor scram (stop of MCP and feedwater flow to SG)	100.0	100.0	100.0	100.0
Start of DIVA	2330.0	2200.0	2325.0	2200.0
Beginning of oxidation	2495.9	2777.0	2476.0	2763.7
Start of SM release	2764.7	2990.8	2764.0	2982.5
Start of FP release	2769.0	2999.6	2772.0	2991.8
Start of accumulators discharge	-	-	3293.5	3471.6
1st total core uncovery	3330.0	3545.0	3300.0	3475.0
1st material slump in lower plenum	3473.9	3663.0	3402.7	3571.0
Melting pool formation	3613.7	3763.0	3745.3	3836.4
Stop of accumulators discharge	-	-	-	15519.7
1st slump of corium with FP	3693.0	3868.0	6036.2	16692.8
1st lateral slump in lower plenum	-	-	6036.2	-
Stop of accumulators discharge	-	-	15149.7	-
Lower head vessel failure	5514.4	5606.7	18753.7	19343.7
Elevation of lower head rupture, [m]	- 2.149	- 2.149	- 2.433	- 2.433
Corium mass in the lower head, [kg]	65310	74070	45597	21939
Corium mass released from the reactor vessel, [kg]	60113	66350	40866	20197
Total mass of H_2 produced, [kg]	133.43	128.15	206.0	226.4
Total aerosols mass produced, [kg]	1476.5	1046.6	1184.0	1627.0
Total aerosols mass leaked from circuit, [kg]	526.62	276.13	487.39	408.9

Case 1A:

Due to leakage of the primary coolant through the break (~243 kg/s of water at the break opening; Figure 5.1), the primary pressure (Figure 5.2) decreases sharply to ~9.5 MPa at t=~250 s, when the

saturation is reached. At this time, the secondary pressure in all three SG increases from ~6.14 MPa to ~8.3 MPa due to the loss of secondary feedwater and the SG water inventory starts to decrease through the opened SG relief valves (Figure 5.3). Later the evolution of the primary pressure is controlled by the secondary pressure (i.e. primary pressure is kept slightly above of the SG relief valves set point ~7.6 MPa). This is due to the fact that the break size is relatively small and primary coolant mass flow rate through the break (Figure 5.1) is insufficient to remove the entire decay heat from the primary circuit. Consequently, a part of the decay heat has to be removed through the opened SG relief valves. This phase lasts till t=~2600 s, when primary pressure starts to decrease below the secondary pressure (Figure 5.2) and the SG secondary water mass stops to decrease following the closing of the SG relief valves. This is a consequence of the decreasing of the core decay heat (Figure 3.2) and on the start of core uncovery (just before start of DIVA module at t=2330 s) with a significant part of the decay heat which heats up the core structures (see rapid increase of fuel temperature in Figure 5.5).

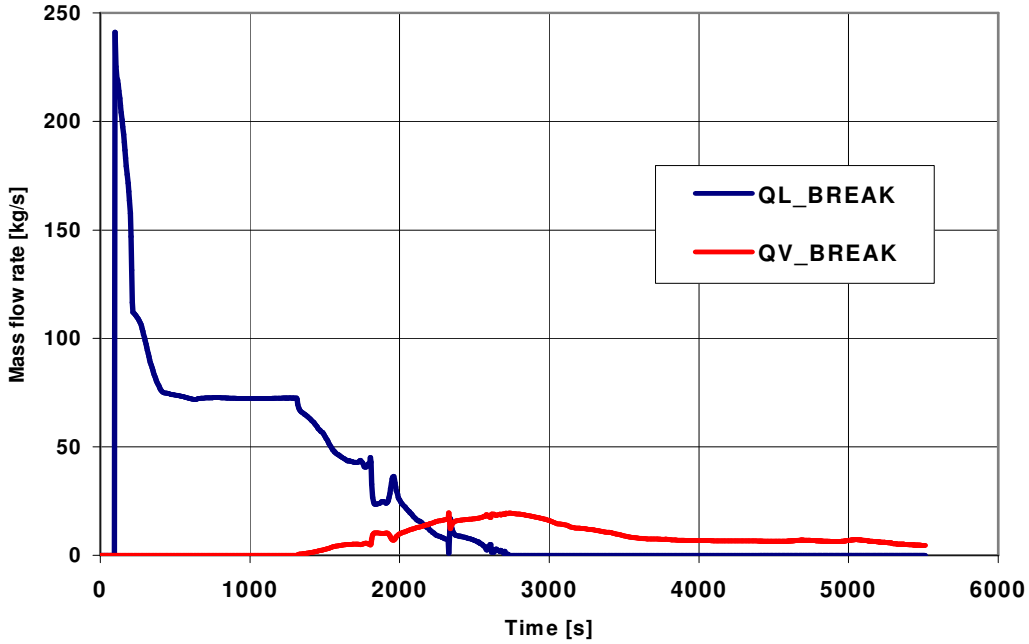

Figure 5.1: Water (QL_) and steam (QV_) mass flow rate through the break (**Case 1A**)

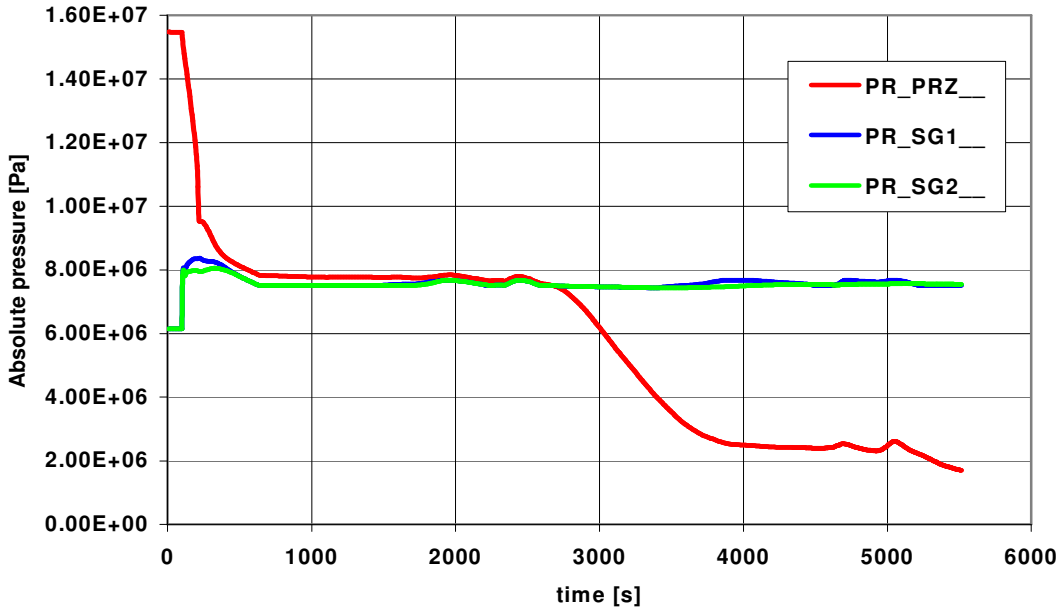

Figure 5.2: Pressure in the primary circuit (PR_PRZ) and in the SG secondary side (**Case 1A**), secondary pressures in SG3 and SG2 are identical

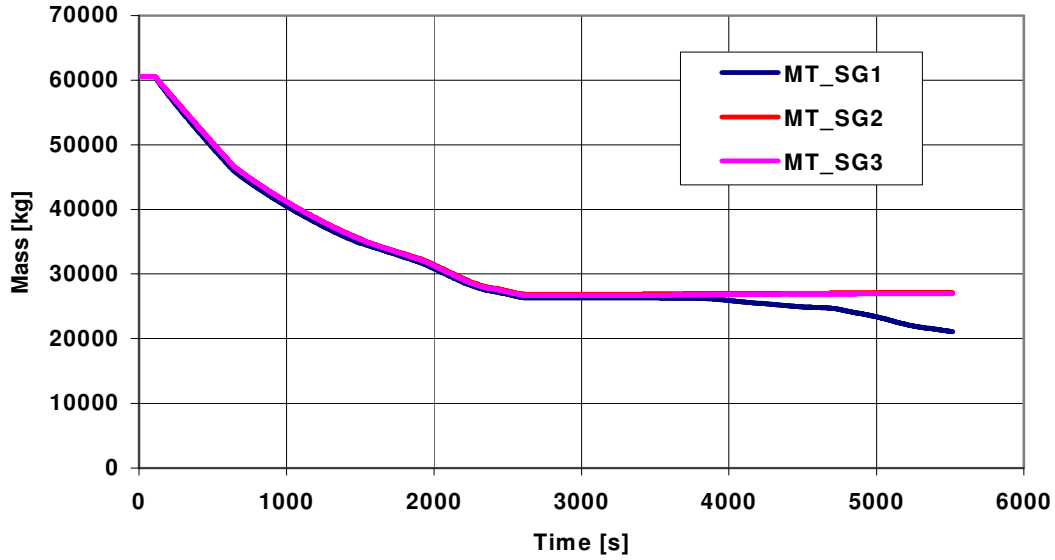

Figure 5.3: Water mass in the SG1, SG2 and SG3 secondary side (**Case 1A**)

After the start of core uncovery (~2300 s), the water level in the core decreases quickly and, as shown in Figure 5.4, the total active core uncovery is reached at t=3330 s. Fuel temperature (Figure 5.5) starts to gradually increase at ~2500 s, i.e. shortly after start of core uncovery, because the heat transfer from fuel rods to steam only is not sufficient to remove the decay heat from the core region. The situation is also similar for control rods and guide tubes, which are heated-up by convective heat transfer from overheated steam and mainly by radiation.

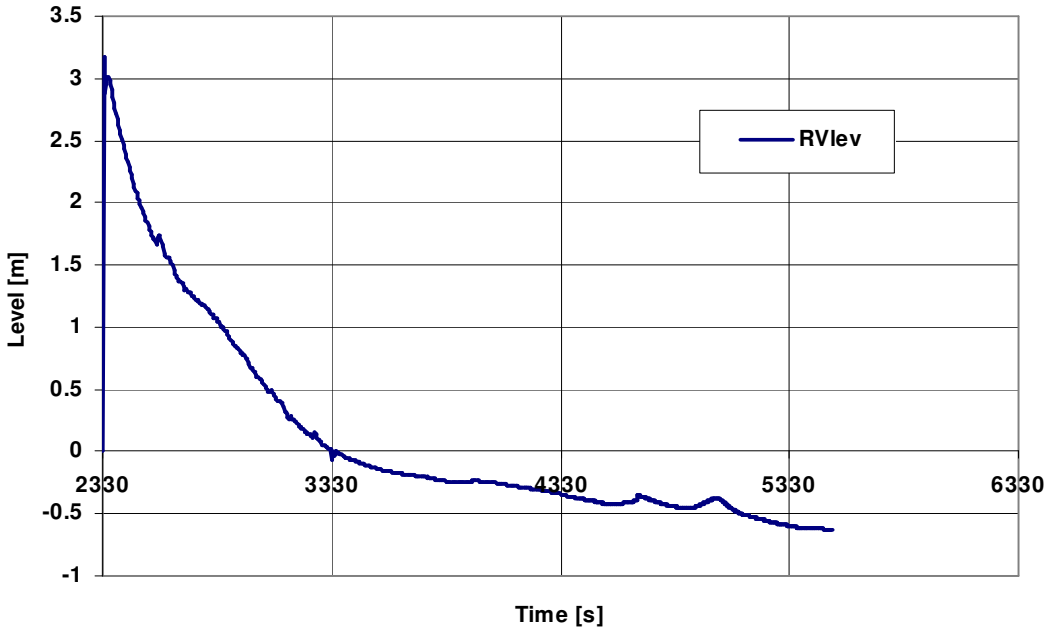

Figure 5.4: Collapsed water level in the active core (DIVA module - **Case 1A**)

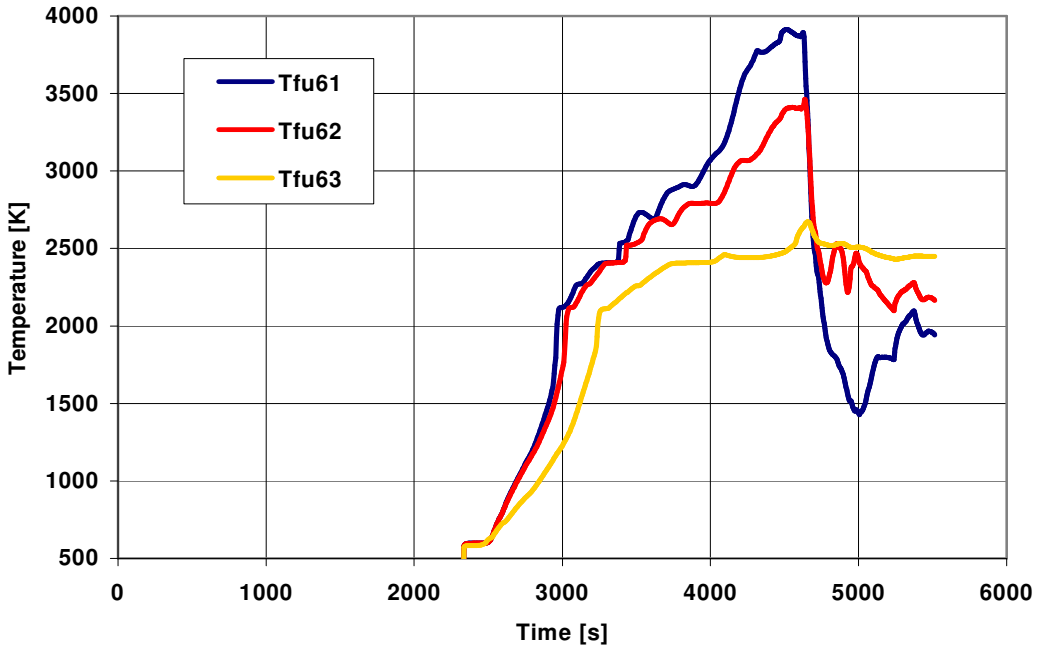

Figure 5.5: Fuel temperature in the 1st (Tfu61), 2nd (Tfu62), 3rd (Tfu63) radial ring (**Case 1A**), 6th axial mesh between the elevations from 1.829m to 2.195m

Increase of fuel rod cladding and guide tube (made also from Zircaloy alloy) temperature above ~1000 K starts the hydrogen production (Figure 5.6) at t=~2700 s. The maximum hydrogen generation rate during the main oxidation period (2800 – 3600 s) reaches the peak values of ~0.8 kg/s, which is lower than steam flow rate through the break (Figure 5.1) during the same time period, which means that steam starvation due to its total consuming in the core by chemical reaction with Zr is not reached.

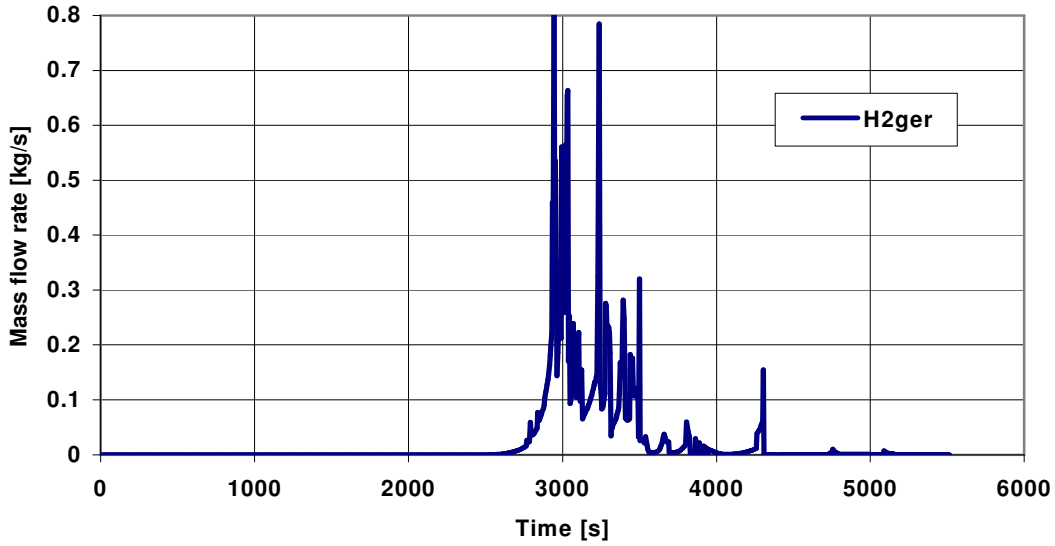

Figure 5.6: Hydrogen generation rate in RV (**Case 1A**)

The first molten material produced in the core region is due to the melting of SIC control rods (temperature reaches 1100 K) at ~2800 s just after start of SM release (see Table 5.1). A complex material mixture U-O-Zr is formed due to UO_2 and ZrO_2 dissolution by molten Zr from the Zircaloy alloy since ~3000 s, when the maximum cladding temperature reaches ~2100 K (see Table 3.1 and Figure 5.5, note that after the start of core heat-up, the fuel and cladding temperatures are nearly identical). Slightly later, at ~3300 s, fuel (U-O-Zr) starts to melt when temperature reaches ~2400 K. Formation of the molten pool is predicted at t=3614 s, i.e. at least in one core mesh all components have a molten fraction greater than 90% and the mesh below is blocked.

The first material slump into RV lower plenum is predicted very soon at t=3474 s, i.e. still before molten pool formation. (see Figure 5.7). This is mainly due to the fact that the core support plate was not included in the model. The first slumped material is only composed of metals (see "Mmeta" on Figure 5.7) mainly coming from molten SIC and molten Zircaloy. The first material containing fuel with FP slumps into RV lower plenum occurs later at t= 3693 s. As shown in Figure 5.7 and 5.8 the masses of oxide molten pool (UO_2, ZrO_2), liquid metals (Zr, Fe) and solid debris in RV lower head gradually increase up to the t= ~4500 s. Then follows a massive slumping mainly of molten fuel into RV lower plenum from the 1st (central) and the 2nd radial core ring, which became nearly empty. This event leads to increased water evaporation from RV lower plenum and the steam produced causes the rapid cooling of the residual fuel (i.e. very small masses) in the 1st and 2nd radial rings as can be seen on Figure 5.5. This is not predicted for fuel in the 3rd ring because part of fuel mass remains in this ring, i.e. not all fuel from this ring is relocated to the RV lower plenum. It should be noted that increased steam mass flow through the break is not observable on Figure 5.1, because this steam is flowing through core (where is overheated) to upper plenum and then mainly to the primary loop containing the break. Here, it condenses in the SG U-tubes and causes a further evaporation of the SG secondary water inventory (see Figure 5.3).

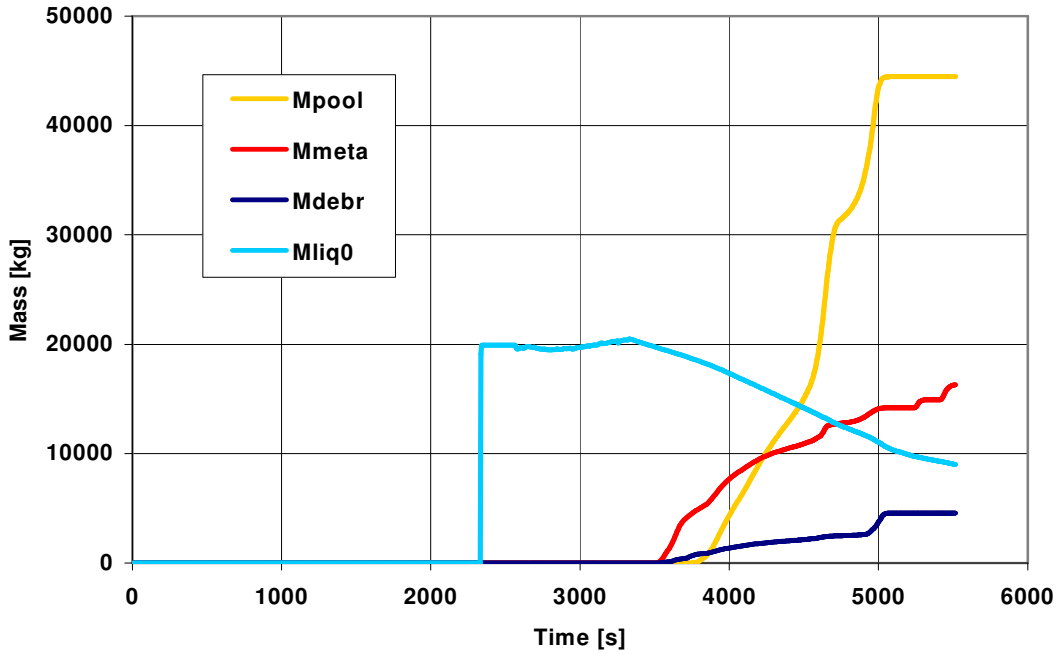

Figure 5.7: Material composition in the RV lower plenum **(Case 1A)**

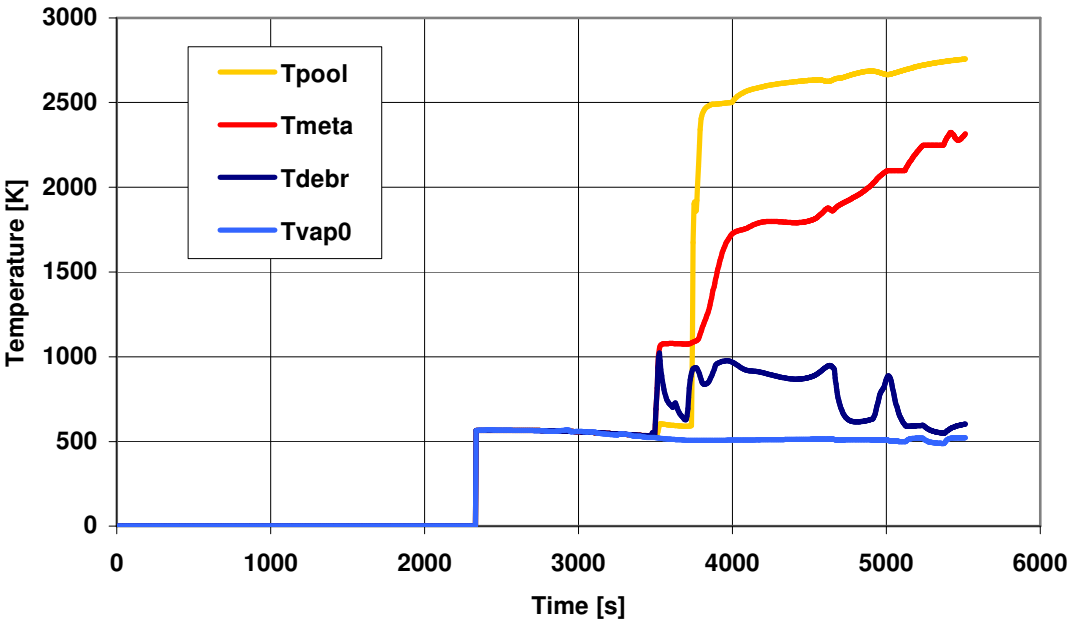

Figure 5.8: Temperature of material components in RV lower plenum (**Case 1A**)

At predicted time of RV lower head plastic rupture (5514.4 s) due to mechanic stress the total mass of materials reached 65.3 tons (see Table 5.1). It is ~70% from total mass of active core materials (~67.9 t of UO_2 + ~24.7 t of SIC and SM = 92.6 t). The remaining mass of water in the RV lower head ("Mliq0" on Figure 5.7) is still ~9 tons.

Case 1B and comparison with Case 1A:

In Case 1B the break location is in the control volume COL1 and not in the control volume ULEGB1 (see Figure 3.4). From the Table 5.1 it appears that this change has small influence on the timing of the

main events. The difference is on the contrary remarkable from the point of view of total mass of aerosols generation and leakage from the circuit. This is mainly a consequence of different carrier gas (steam + hydrogen) flow paths particularly after the start of permanent core uncovery (start of DIVA) as it follows from comparison of the Figure 5.9 with 5.10 and of the Figure 5.11 with 5.12. The main reason is different elevation of ULEGB1 and COL1 volumes, where the break is located (see Table 3.5).

In **Case 1A,** the gas is flowing from UPP_PLEN volume after the start of FP/SM release (~2770 s) mainly to the HOL1 volume (see UP_HOL1 flow rate on Figure 5.9, which continues through SG1 to the break) and partially to DOME volume (negative flow rate DOM_UP). The gas flow through intact loops is negligible. As shown in Figure 5.11 the gas mass flow rate CC_BYP (from COLDCOLL volume to CCBYPASS) corresponds to the gas mass flow rate DOM_UP in Figure 5.9. The difference between gas mass flow rate COL1_CC and CC_BYP flow gives the gas mass flow rate coming from the RV downcomer. After total core uncovery (3330 s) the steam coming from water evaporated from the RV lower plenum is distributed to the downcomer and to the RV cold collector (volume COLDCOLL) and then to the core volume and to the UPP_PLEN volume.

In **Case 1B** (see Figures 5.10 and 5.12), after the start of core uncovery (start of DIVA), strong oscillations of the gas mass flow rates are observed in all primary circuit junctions. These oscillations finish at ~2600 s, i.e. before the start of SM/FP release (~3000 s). Unlike Case 1A, after 3000 s the gas flow rate from UPP_PLEN volume into all hot leg loops (Figure 5.10, flows UP_HOL1, UP_HOL2 and UP_HOL3) is negative or negligible and there is only flow from UPP_PLEN volume to DOME volume (negative flow rate DOM_UP from DOME to UPP_PLEN).

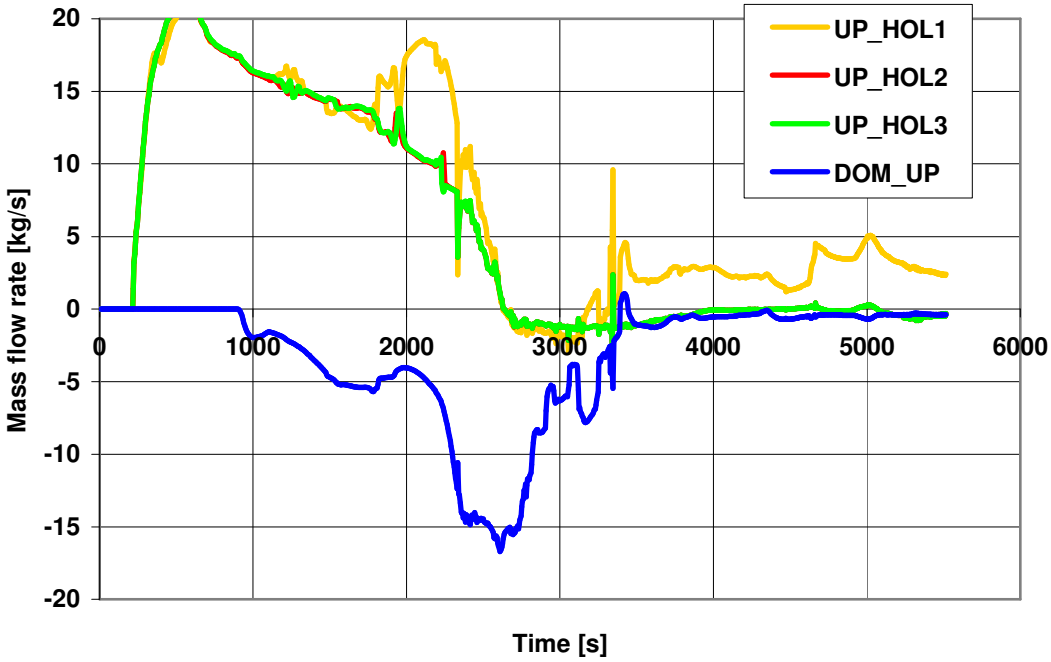

Figure 5.9: Gas mass flow rates in the junctions between UPP_PLEN volume and the adjacent volumes (**Case 1A**)

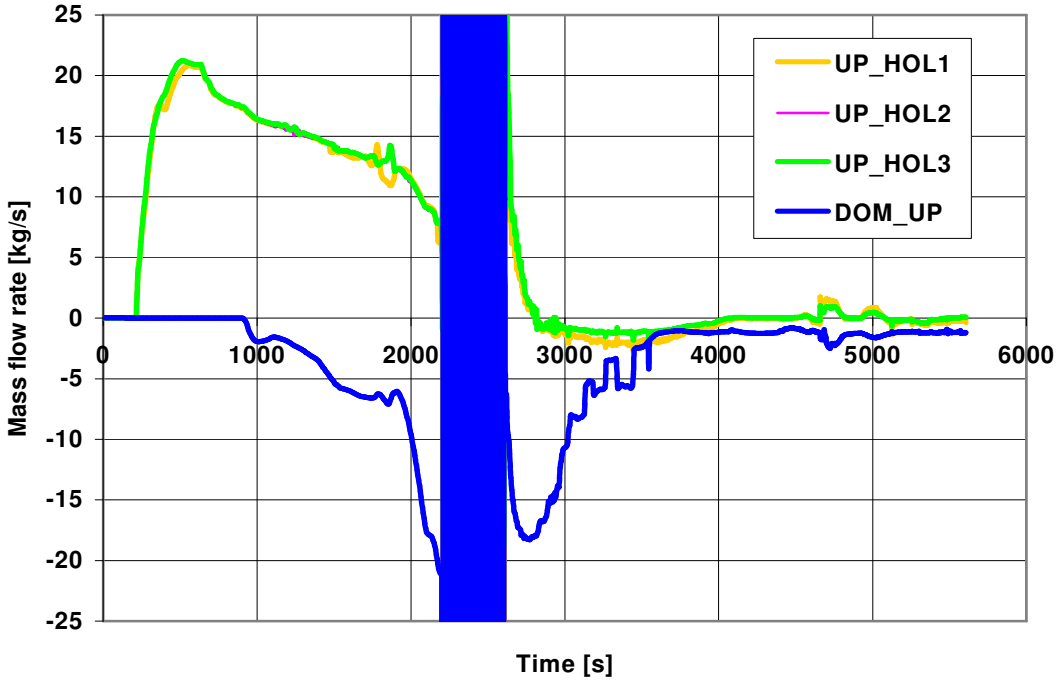

Figure 5.10: Gas mass flow rates in the junctions between UPP_PLEN volume and the adjacent volumes (**Case 1B**)

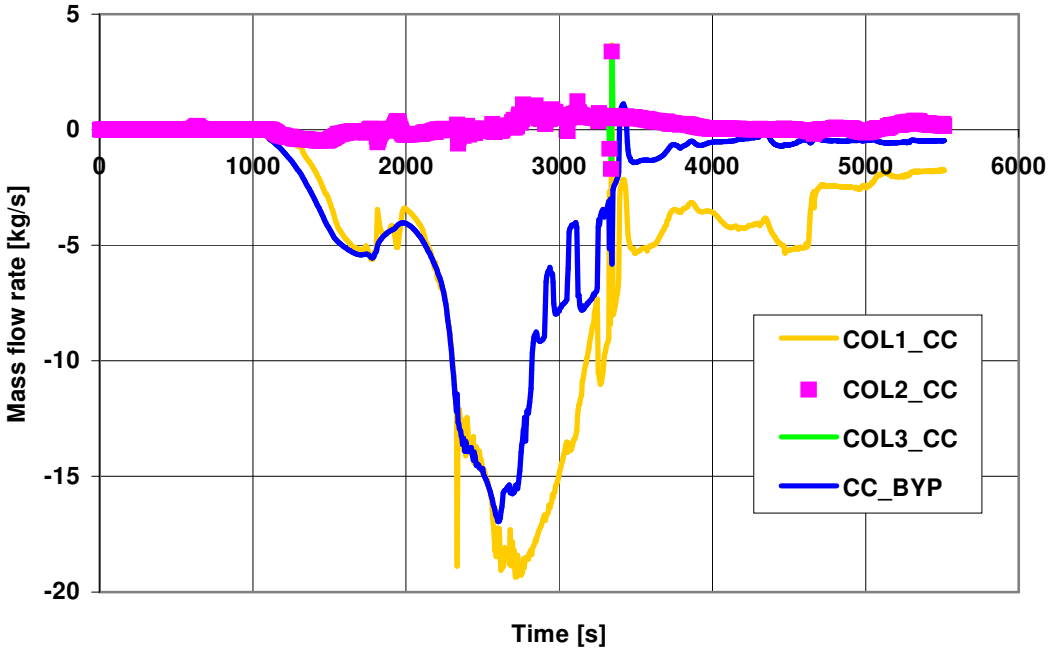

Figure 5.11: Gas mass flow rates in the junctions between COLDCOLL volume and the adjacent volumes (**Case 1A**)

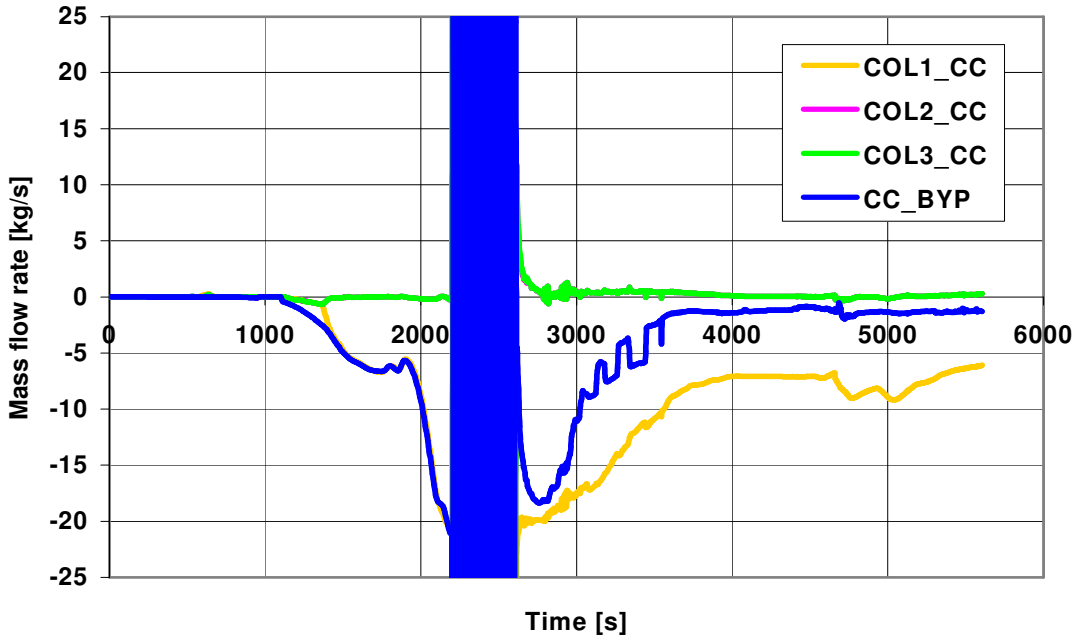

Figure 5.12: Gas mass flow rates in the junctions between COLDCOLL volume and the adjacent volumes (**Case 1B**)

Case 2A and comparison with Case 1A:

Case 2A differs from Case 1A by the fact that all 3 accumulators (ACCU) are available during accident. Therefore, the Case 2A accident evolution is identical to the Case 1A until ACCU discharge occurs at t=3293 s when primary pressure (Figure 5.13) reaches the threshold value of 4.525 MPa.

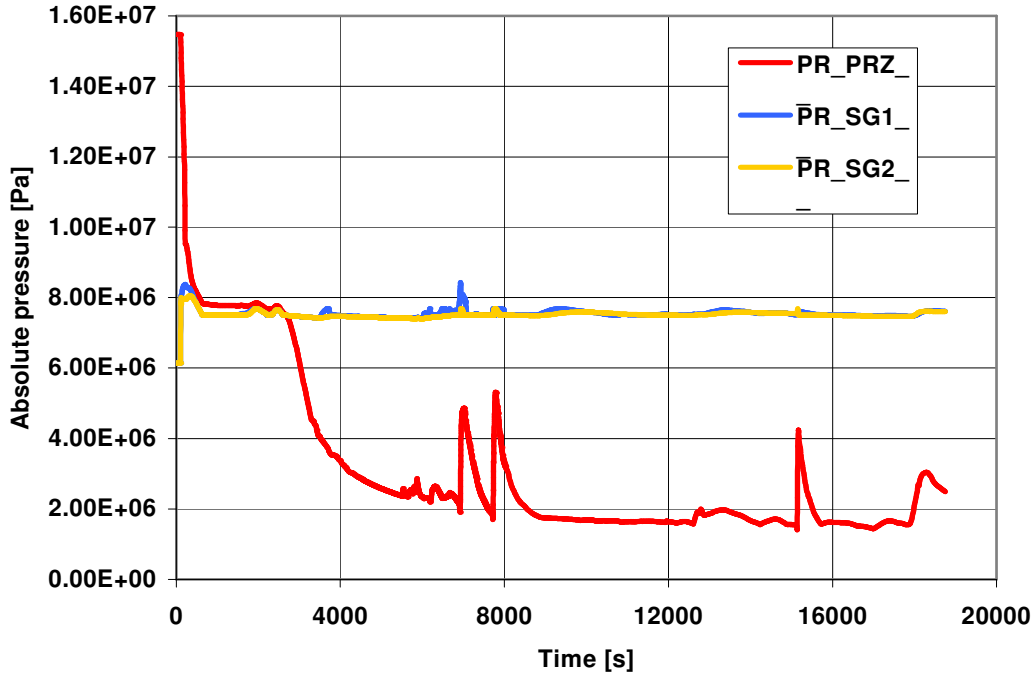

Figure 5.13: Pressure in the primary circuit (PR_PRZ) and in the SG secondary side (**Case 2A**), secondary pressures in SG3 and SG2 are identical

The cumulative water mass released from ACCU1 (note that water mass flow rates from all 3 ACCU are identical) is presented in Figure 5.14. It should be pointed out that the evolution of ACCU depletion and primary pressure are strongly linked: the increase of water level in active core region (Figure 5.15) due to water injection from ACCUs leads to increase of steam generation and consequently of the primary pressure. This in turn leads to the decrease or stop of water flow from ACCUs. Moreover, the primary pressure is influenced also by slumping of the molten materials from the core to RV lower head (see Figure 5.18).

Due to the water discharge of the ACCUs, the lower part of active core is covered by water (Figure 5.15). The water level reaches its maximum value (~2 m) at t=~8000 s. Then the water level in the core decreases gradually and the second total core uncovery is reached at t=~15000 s. Just after this event the last rapid injection from ACCU (~15150 s) occurs. The third last core uncovery occurs ~400 s before RV lower head failure (18754 s).

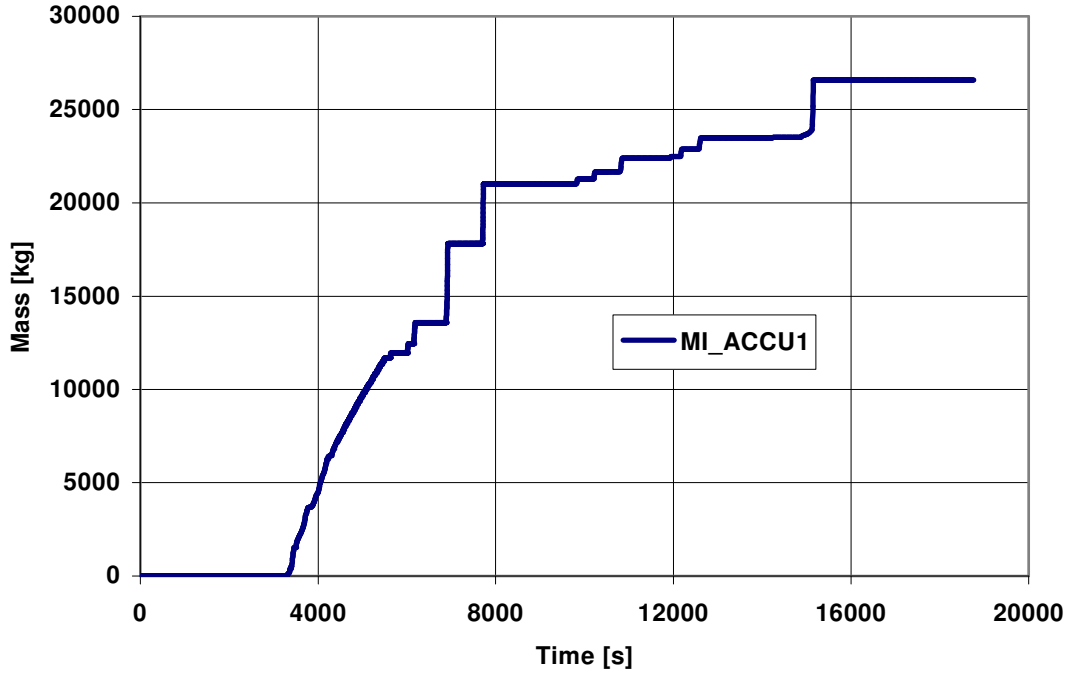

Figure 5.14: Cumulated water mass released from ACCU1 (**Case 2A**)

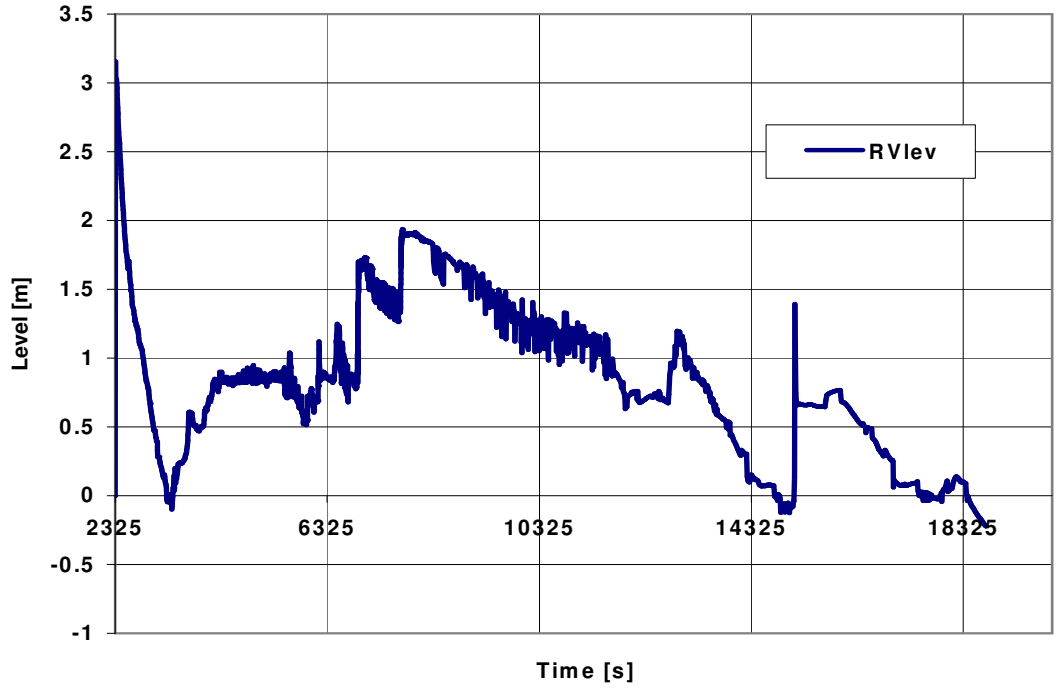

Figure 5.15: Collapsed water level in the active core (DIVA module - **Case 2A**)

The presence of water in the lower part of the core prevents rapid core degradation in the lowest meshes of the fuel and control rods mainly in the 3rd radial ring. On the other hand the steam generated in the lower part of core is not able to cool fully the middle and upper part of core. As shown on Figure 5.16 the temperature increase of the fuel rods with claddings (the situation for control rods and their guide tubes is nearly the same) in the middle part of core during the beginning of heat-up phase (up to ~4000 s) is comparable with Case 1A analysis (Figure 5.5) including the timing of molten pool formation (see Table 5.1). But, with respect to Case 1A, the intensive steam generation in the lower part of active core leads to a significant prolongation of the core degradation process.

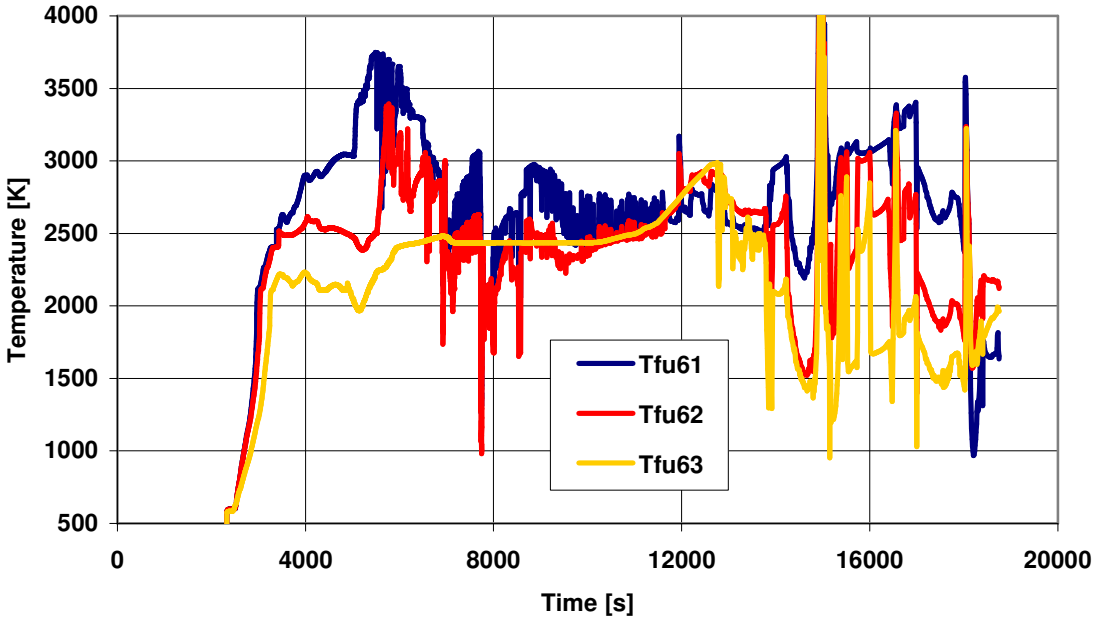

Figure 5.16: Fuel temperature in the 1st (Tfu61), 2nd (Tfu62), 3rd (Tfu63) radial ring (**Case 2A**), 6th axial mesh between the elevations from 1.829m to 2.195m

Also the main oxidation period is longer (2800 s – 5000 s, Figure 5.17) in comparison with Case 1A (2800 s – 3600 s, Figure 5.6). The main reason is the lower rate of material containing non-oxidised Zr relocating into the RV lower plenum (Figure 5.18) in comparison with Case 1A (Figure 5.7). Then the total mass of H_2 produced increases to 206 kg compared to 133.4 kg in Case 1A (Table 5.1).

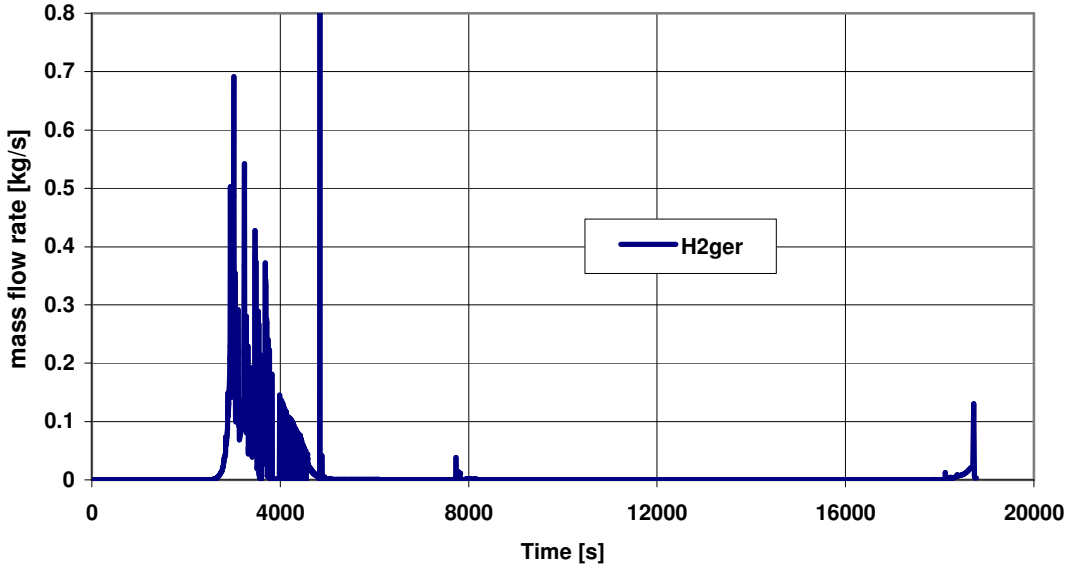

Figure 5.17: Hydrogen generation rate in RV (**Case 2A**)

The comparison of the timing of main events given in the Table 5.1 shows a considerable delay of the timing of the first lateral[1] slump of corium with FP (6036 s) into the RV lower plenum in comparison with Case 1A prediction (3693 s). After this time the masses (see Figures 5.18 and 5.19) of oxide molten pool (UO_2, ZrO_2), liquid metals (Zr, Fe) and solid debris in RV lower plenum start to increase considerably. The total slumped masses are lower in comparison with Case 1A (see Figures 5.7 and 5.8), as a consequence of the generally lower temperatures mainly observed in the lower core regions due to presence and evaporation of the water delivered from ACCUs (Figures 5.14 and 5.15).

At predicted time of RV lower head plastic rupture (18754 s) due to mechanic stress the total mass of materials reached 40.9 tons (see Table 5.1). It is only ~44% (in Case 1A it is ~70%) from total mass of active core materials (~92.6 t). The remaining mass of water in the RV lower plenum ("Mliq0" on Figure 5.18) is still ~14.5 tons.

[1] Lateral slump means that the molten pool reaches a channel limited by a shroud (see component BAFFLE on Figure 3.1) then if the shroud is residual (the face is thus opened) or the molten fraction of the shroud is greater than 90% (no mechanical resistance to the molten pool pressure load), a fraction of the molten pool is added to the corium slumped mass in the RV lower plenum. The fraction is linear from 0 to 1 for components with a molten fraction between 90% and 100% [2].

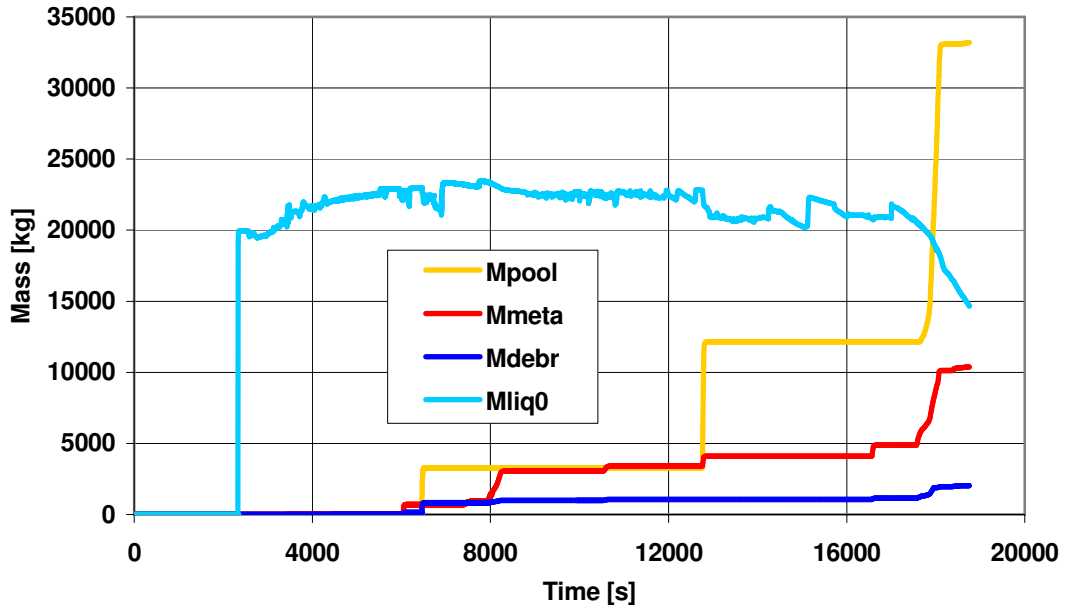

Figure 5.18: Material composition in the RV lower plenum (**Case 2A**)

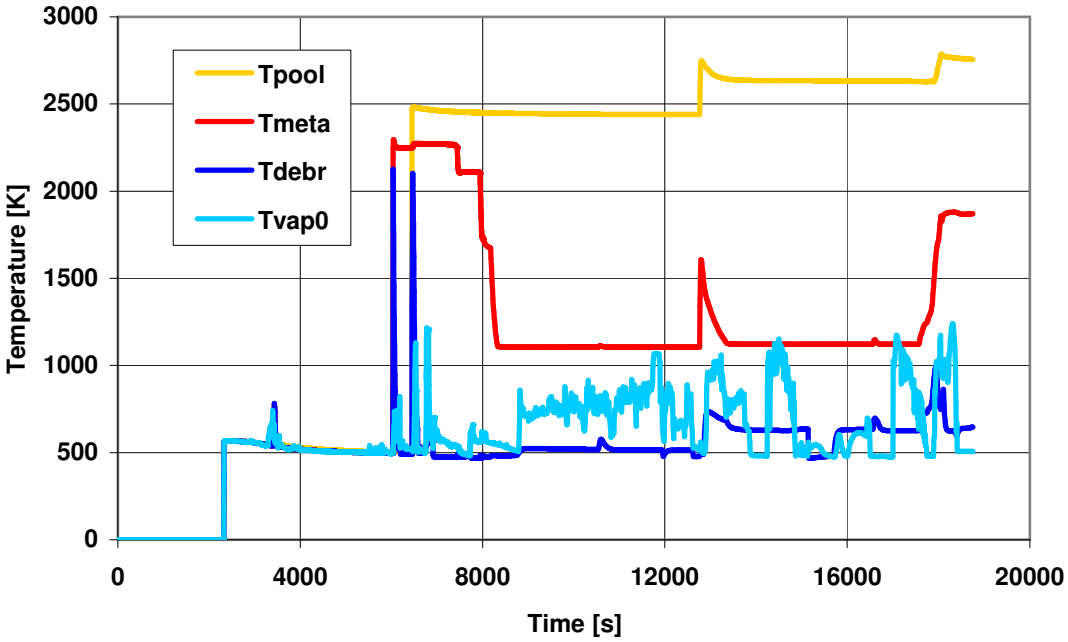

Figure 5.19: Temperature of material components in RV lower plenum (**Case 2A**)

Case 2B and comparison with Case 2A:

Case 2B differs from Case 2A only by definition of the cold leg break location in the control volume COL1 instead of control volume ULEGB1 (see Figure 3.4). From the Table 5.1 it appears that this change has small influence on the timing of the main events up to time of molten pool creation in the core (3836 s). As shown in Figure 5.20, the molten pool remains longer in the active core region and massive relocation (slumping) of the molten materials to RV lower plenum is predicted at t=16693 s, i.e. till after the depletion of ACCU (15520 s). However, the time of RV lower head failure occurs only slightly later than in Case 2A (18754 s) at 19344 s.

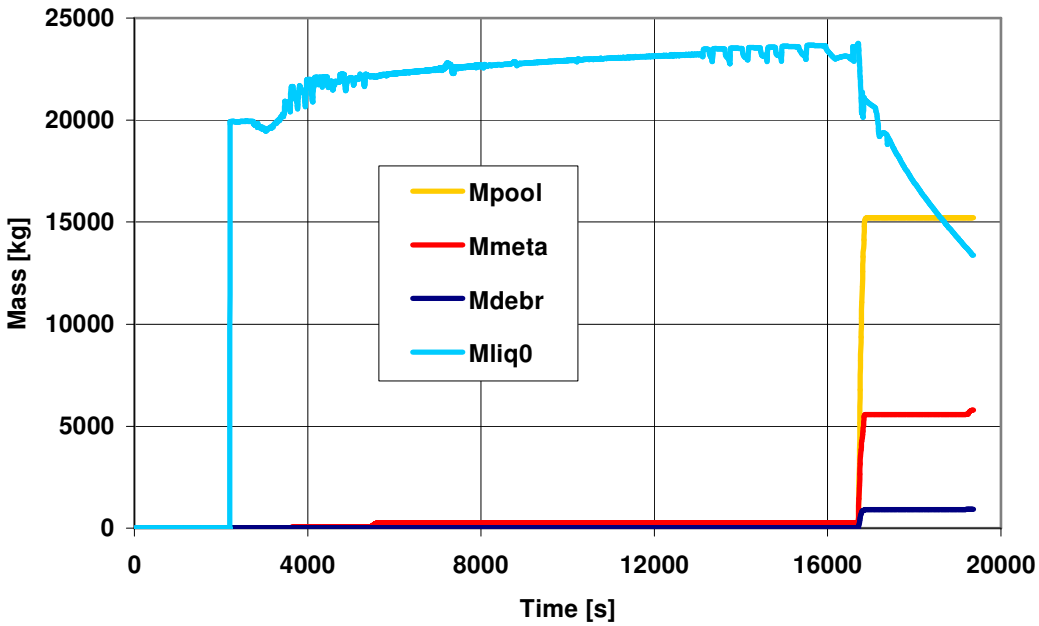

Figure 5.20: Material composition in the RV lower plenum (**Case 2B**)

The fact that the molten pool remains a longer time inside the active core region has two consequences: 1) the total production of hydrogen increases from 206 kg to 226.4 kg, and 2) the total aerosols mass produced increases from 1184 kg to 1627 kg. Moreover, the final mass of materials in the RV lower plenum at time of failure decreases from 45.6 tons (Case 2A) to 21.9 tons (Case 2B), which is only ~22% from total mass of active core materials (~92.6 t).

As it has already been discussed for Case 1A and Case 1B the differences in the Case 2A and Case 2B accident evolutions are also mainly a consequence of the different carrier gas (steam + hydrogen) flow paths particularly after the start of permanent core uncovery (start of DIVA) as it follows from comparison of the Figure 5.21 with 5.22 and of the Figure 5.23 with 5.24. The main reason is again the different location of the break (see Table 3.5).

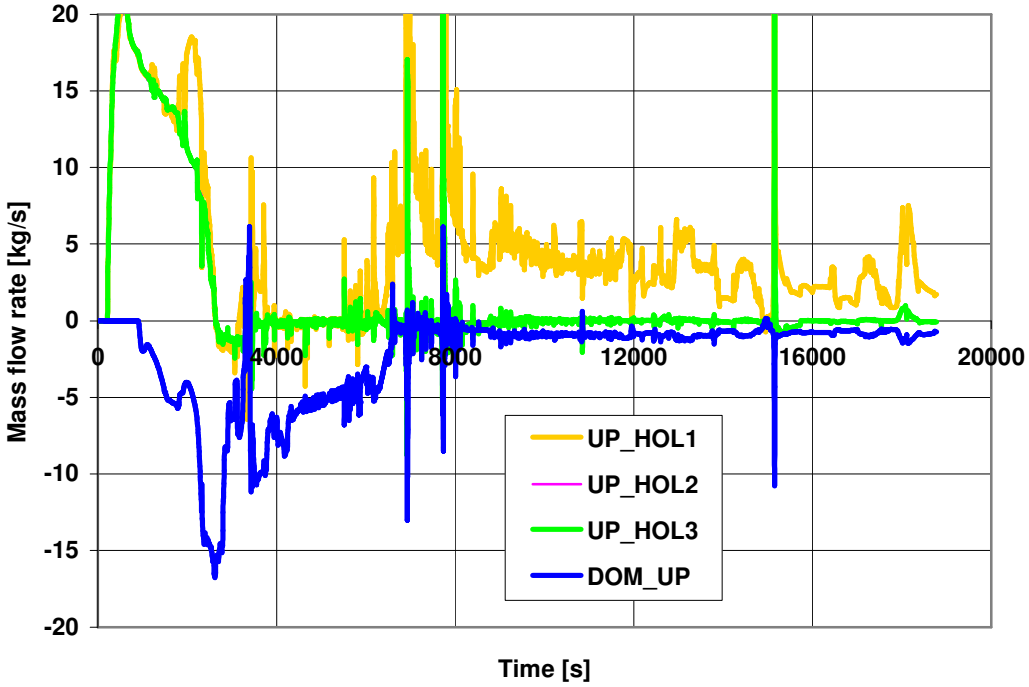

Figure 5.21: Gas mass flow rates in the junctions between UPP_PLEN volume and the adjacent volumes (**Case 2A**)

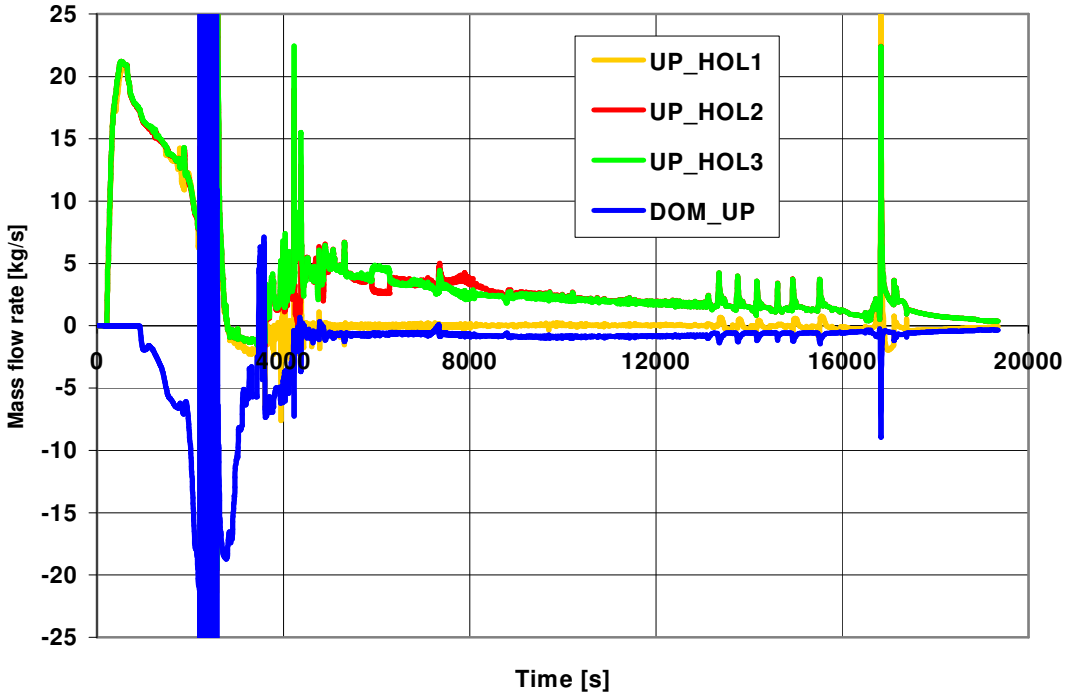

Figure 5.22: Gas mass flow rates in the junctions between UPP_PLEN volume and the adjacent volumes (**Case 2B**)

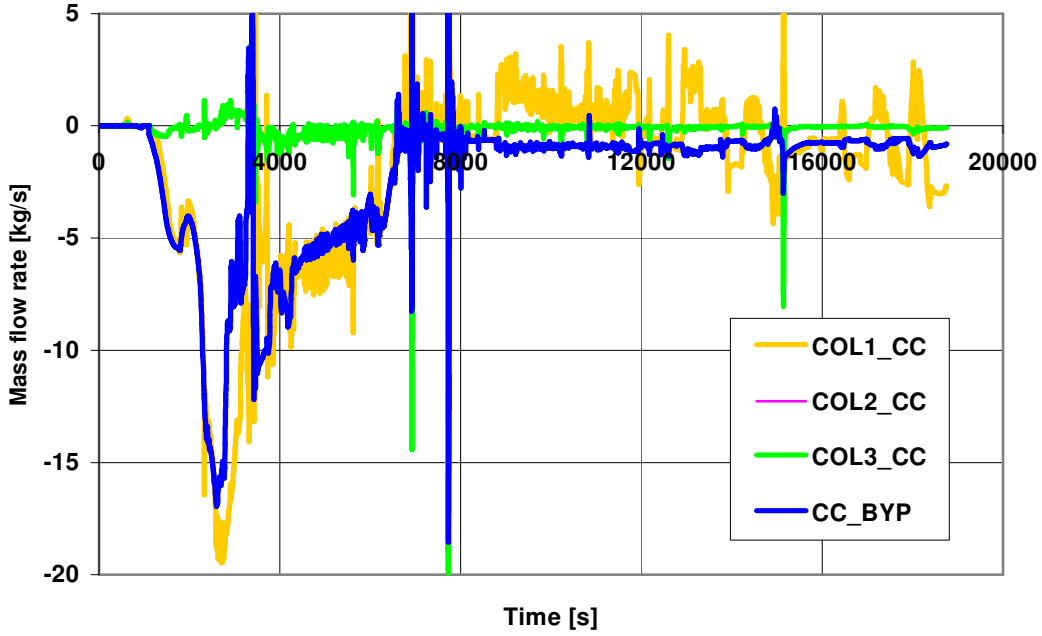

Figure 5.23: Gas mass flow rates in the junctions between COLDCOLL volume and the adjacent volumes (**Case 2A**)

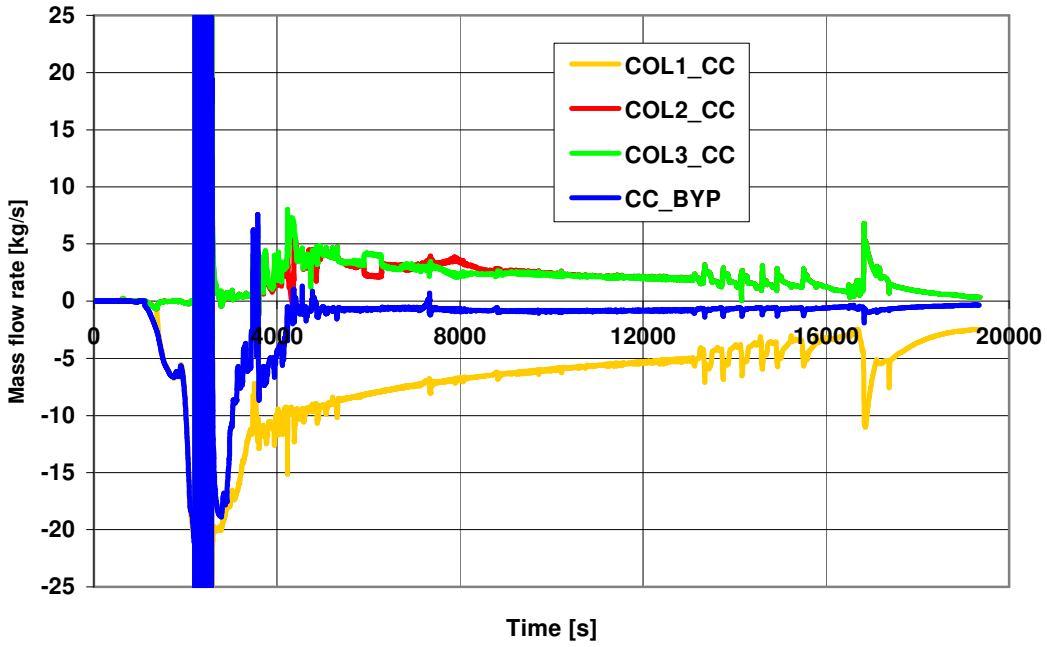

Figure 5.24: Gas mass flow rates in the junctions between COLDCOLL volume and the adjacent volumes (**Case 2B**)

In **Case 2A**, similarly as in Case 1A, the gas from UPP_PLEN volume is flowing after start of FP/SM release (~2770 s) mainly to the HOL1 volume (see UP_HOL1 flow rate in Figure 5.21), and partially to DOME volume (negative flow rate DOM_UP). The gas flow to HOL2 and HOL3, i.e. through intact loops, is negligible. As shown on Figure 5.23 the opposite gas mass flow rate CC_BYP (from COLDCOLL volume to CCBYPASS) corresponds to DOM_UP gas mass flow rate on Figure 5.21. The mass flow rate COL1_CC on Figure 5.23 represents the flow from COL1 volume (break location) to COLDCOLL volume. Between 2770 s – 7000 s and 14000 s – 18754 s the gas is mostly flowing

from COLDCOLL to COL1 volume and through the break, out of the circuit. The situation is inverted between 7000 s – 14000 s when the normal circulation is re-established in the broken loop and part of the gas is discharged through the break.

In **Case 2B** (see Figures 5.22 and 5.24) the accident evolution is identical to Case 1B up to the ACCUs intervention. Unlike Case 2A, after 3000 s, the gas mass flow rate from UPP_PLEN volume is nearly equally distributed between the intact loops (flows UP_HOL2 and UP_HOL3 on Figure 5.22) and flow to broken loop (UP_HOL1) is negligible. Part of the gas (up to ~4000 s) flows from UPP_PLEN volume also to DOME volume (negative flow rate DOM_UP from DOME to UPP_PLEN). As shown on Figure 5.24 the negative flow COL1_CC represents total mass flow rate from COLDCOLL volume to COL1 volume where the break is located. Mass flow COL1_CC comes from COL2 volume (COL2_CC), COL3 volume (COL3_CC) and from the CCBYPASS volume (CC_BYP). Contribution of the gas mass flow rate coming directly from the RV downcomer to COLDCOLL volume is not significant.

5.2 Fission Products and Structural Materials Release from the Core

The calculated fractional release from the core, expressed in the term of "cumulative fraction from initial inventory in %", is compared for all cases in Table 5.2 for FP and in the Table 5.3 for SIC and SM.

In accordance with ELSA module [12] the FP given in the Table 5.2 are split into three categories, based on the volatility of the element. The initial inventory of each element is taken from the Table 3.4.

The initial mass inventory of the control rod (SIC) and of the other structural materials given in the Table 5.3 is calculated automatically by the DIVA module [11] from the data defined for relevant core components (see Table 3.1).

Table 5.2: FP initial inventory and cumulative fractional release from the core

No.	FP / SM [1)]	INVENTORY [kg]	Case 1A [% i.i.]	Case 1B [% i.i.]	Case 2A [% i.i.]	Case 2B [% i.i.]
Highly volatile FP						
1	**Xe**	265.7	94.86	97.45	87.5	82.77
2	**Kr**	20.85	- " –	- " –	- " –	- " –
3	**I**	11.14	94.84	97.44	87.44	82.69
4	**Br**	1.2	- " –	- " –	- " –	- " –
5	**Cs**	139.98	- " –	- " –	- " –	- " –
6	**Rb**	19.71	- " –	- " –	- " –	- " –
7	**Cu**	1.2e-11	94.81	97.42	87.37	82.6
8	**Se**	3.142	91.59	95.36	78.64	75.96
9	**Te**	22.0	91.59	95.36	78.64	75.96
10	**Sb**	0.8284	92.74	96.10	80.59	77.11
11	**Ag**	2.514	94.81	97.42	87.37	82.6
Semi-volatile FP						
12	**Ba**	71.417	0.01058	0.01303	3.457	1.64

13	**Ru**	108.55	1.09e-3	1.71e-3	1.459	0.936
14	**Sr**	54.28	6.66e-5	2.12e-4	0.3132	0.0809
15	**La**	62.85	2.6e-5	9.18e-5	0.0329	0.0258
16	**Eu**	10.47	2.61e-5	1.32e-4	0.0332	0.026
17	**Ce**	151.41	2.6e-5	9.18e-5	0.0329	0.0258
18	**Mo**	162.83	2.021	1.69	9.984	13.07
Low volatile FP						
19	**Cd**	3.246	1.38e-3	0.0252	0.1044	0.0809
20	**Rh**	19.71	1.026e-3	1.092e-3	0.0339	0.0268
21	**Pd**	48.56	2.6e-5	9.183e-5	0.0329	0.0258
22	**Tc**	42.85	- " –	- " –	- " –	- " –
23	**Nb**	2.857	- " –	- " –	- " –	- " –
24	**Zr**	191.4	- " –	- " –	- " –	- " –
25	**Np**	25.14	- " –	- " –	- " –	- " –
26	**Pu**	675.14	- " –	- " –	- " –	- " –
27	**Nd**	185.69	- " –	- " –	- " –	- " –
28	**Pm**	8.284	- " –	- " –	- " –	- " –
29	**Gd**	2.521	- " –	- " –	- " –	- " –
30	**Pr**	57.13	- " –	- " –	- " –	- " –
31	**Am**	3.894	- " –	- " –	- " –	- " –
32	**Cm**	0.992	- " –	- " –	- " –	- " –
33	**Sm**	38.28	- " –	- " –	- " –	- " –
34	**U**	65455.7	- " –	- " –	- " –	- " –
35	**Sn**	2.228	- " –	- " –	- " –	- " –
36	**In**	0.0633	- " –	- " –	- " –	- " –
37	**Y**	27.424	- " –	- " –	- " –	- " –

1) The inventory of the low volatile FP: Zn, As, Ga and Ge is extremely low (< 0.01 kg) and for FP: Tb, Dy, Ho, Er, Tm and Yb is zero.

Table 5.3: Control rod and SM initial inventory and fractional release from the core

No.	**SIC / SM**	**INVENTORY [kg]**	**Case 1A [%]**	**Case 1B [%]**	**Case 2A [%]**	**Case 2B [%]**
1	**Ag**	6434.55	2.077	0.821	1.035	7.276
2	**In**	1285.23	42.55	19.8	27.97	32.39
3	**Cd**	419.1	44.64	23.31	33.12	35.45
4	**Sn**	300.2	48.29	54.93	50.99	50.74
5	**Fe**	20.18	1.6e-16	2.3e-10	5.1e-9	1.5e-8
6	**Ni**	0.0	0.0	0.0	0.0	0.0
7	**Cr**	9.392	3.55e-14	2.25e-8	7.03e-8	1.1e-6
8	**Zr**	16197.7	- **1)**	- **1)**	- **1)**	- **1)**

1) There is no model in the used ASTEC code version for release of the Zr as SM.

ASTEC/ELSA [12] models for FP/SM release

The model of the ELSA module [12] calculates the release of **highly volatile** species from the UO_2 fuel matrix during the heat-up phase at the same rate and reaches the fuel-to-clad gap (i.e. timing of the event "start of FP release" given in the Table 5.1 corresponds to the first clad failure). Some of these

species (Se, Te and Sb) can chemically react with the inner surface of the Zircaloy cladding, depending on the degree of the cladding oxidation. At fuel melting point, 100% of remaining highly volatile species is assumed to be released instantaneously from the fuel liquid fraction. During the accident progression, UO_2 can be dissolved by molten Zr or other material interaction. Here also, 100% of the remaining highly volatile species are released from the dissolved liquid fraction.

Semi-volatile FPs can diffuse to UO_2 grain boundaries at approximately the same rate as the volatile FP but are released from the fuel at lower rates. In the current modelling, the diffusion step has been neglected but with application of the limitation that the instantaneous release of semi-volatile FP cannot exceed the instantaneous release of volatile FP. A rate-limiting process at the grain boundary or outside the grain is therefore supposed to occur. The release into the open porosities of intact fuel and debris bed and then into the bulk atmosphere is assumed to be governed by evaporation and mass transfer processes. It has to be added that no release of semi-volatile FPs is supposed to occur at fuel liquefaction, contrary to volatile FP. Such a release is calculated with the molten pool model activated in the RV lower plenum for reactor applications.

For **low-volatile** FPs, neither diffusion in fuel matrix nor vapour pressure is calculated. Their release from intact fuel as well as debris bed is supposed to be governed by the volatilization of UO_2 and the release is in proportion to the quantity of volatilized fuel.

Release of volatilized **SIC materials** Ag, In and Cd is initiated according to the criteria of cladding status. Three cases are considered: a release through cracks at cladding failure, a release during relocation of molten materials at cladding melting point, and a release from the free surface of the liquid alloy retained within the cladding still in place. Remaining molten SIC in the RV lower head vessel corium pool is released by using the molten pool model.

The model for the release of volatilized SM: **Fe**, **Ni** and **Cr** during candling of steel materials is the same as the one used for the release of SIC materials during candling of control rods. Remaining molten Fe, Ni and Cr in the RV lower head vessel corium pool are released by using the molten pool model.

The simple model of **Sn** release is based on the correlation observed in the Phébus FPT1 test between hydrogen production and tin release. The tin release in each Zircaloy node is taken as being proportional to the rate of formation of ZrO_2. The 60% of the tin contained in the amount of Zr oxide produced is released, and the rest is stored as being unavailable for release.

Case 1A and comparison with Case 1B

As shown in the Table 5.2 according to Case 1A the cumulative release of **highly volatile** FPs is predicted in the range of 91% - 95%. This indicates that more than 90% of fuel reaches melting point. Predicted fractional release is also in agreement with the Phébus FPT1 [23] and FPT2 [24] experiments, where the measured release of the species I, Cs and Te at the bundle outlet was in the range of 70% - 87%. The calculated kinetics of Cs (the same is for I, Rb, Br), Te and Sb release from fuel is shown on Figure 5.25 and correspond to a progression of fuel heat-up and melting (see also Figure 5.5).

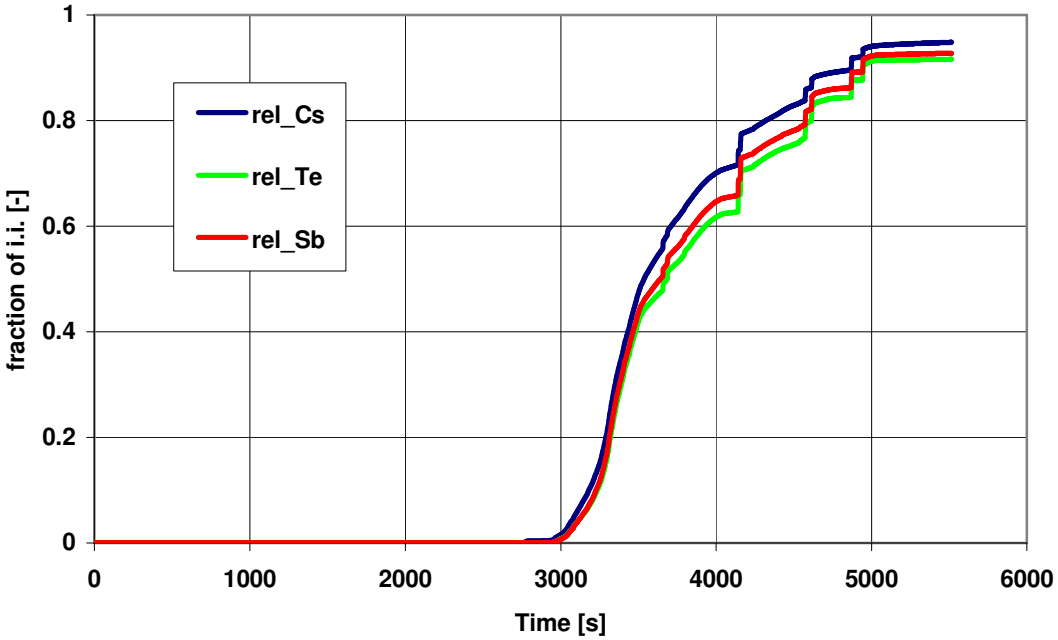

Figure 5.25: Fractional release of the Cs, Te and Sb (**Case 1A**)

The calculated cumulative fractional release of the **semi-volatile** FPs (see Table 5.2) is in the range of ~0.00003% i.i. (La, Eu, Ce) to ~2% i.i. (Mo). As shown on Figure 5.26 the release of Ba and Ru is predicted only during the beginning phase of fuel heat-up and corresponds only to the gap-release (see comment [1)] to Table 3.4), whereas Mo release is governed by its evaporation and mass transfer process. Besides Cd (as FP) and Rh, nearly negligible release of all other **low-volatile** FPs is predicted (see Table 5.2 and release kinetics of U given as representative example also in Figure 5.26).

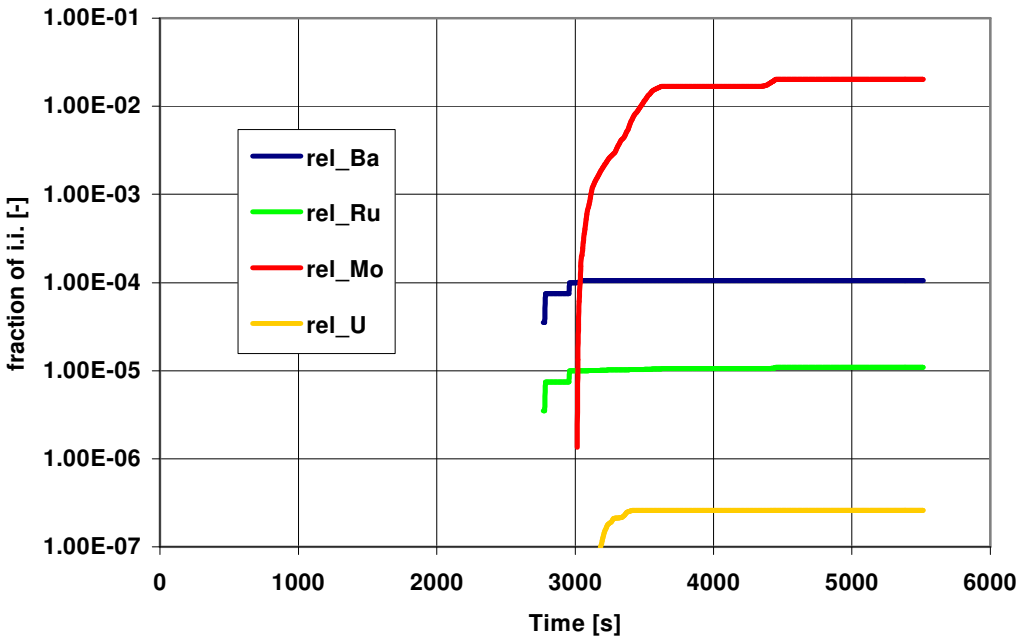

Figure 5.26: Fractional release of the Ba, Ru, Mo and U (**Case 1A**)

The cumulated release of the **SIC materials** (see Table 5.3) is predicted from ~2% i.i. (Ag) to >40% i.i. (In, Cd). From the other SM only the predicted release of Sn is significant (~50% i.i.), whereas release of Fe and Cr is negligible. As shown on Figure 5.27 the release kinetics of Sn corresponds to the kinetics of Zr oxidation (see Figure 5.6), whereas Cd, In and mainly Ag are significantly released also during late degradation phase after ~4500 s, when the massive slumping of corium (molten pool) to RV lower head is predicted (see also Figure 5.7).

As it follows from the Table 5.2, in **Case 1B** the cumulative release of the high-volatile and most of the semi-volatile FPs is similar to what predicted for Case 1A. The released fractions of the SIC materials Ag, In and Cd (see Table 5.3) are lowered by a factor ~2, because only small release is predicted after ~4500 s.

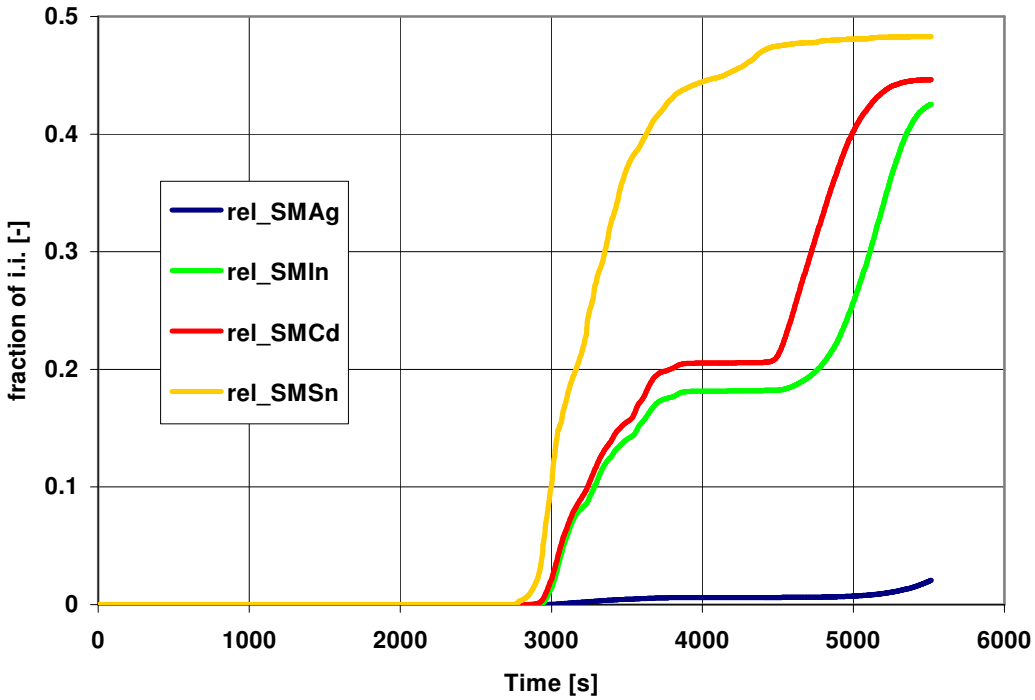

Figure 5.27: Fractional release of the SIC materials and Sn (**Case 1A**)

Case 2A and comparison with Case 1A

As it has been already observed the process of core degradation and molten material relocation into the RV lower plenum is significantly slower in Case 2A compared to Case 1A. As shown in the Table 5.2, besides highly-volatile FPs, the consequence on FP/SM release is significant.

According to Case 2A the cumulative release of **highly volatile** FPs is predicted in the range of 79% - 88%, i.e. as expected slightly lower compared to Case 1A, because also the extent of fuel melting was slightly lower (compare the masses of corium in RV lower plenum at time of failure in Table 5.1). The calculated kinetics of Cs, Te and Sb release from fuel is shown on Figure 5.28 and corresponds to a progression of fuel heat-up and melting (see also Figure 5.16).

On the contrary to the Case 1A, the cumulative fractional release of the **semi-volatile** FPs is significantly increased by 2 (Ba) to 4 (Sr) orders of magnitude and 5 times for Mo. The situation is similar for **low-volatile** FPs where the increase is of 3 orders of magnitude (Cd and Rh up to 2 orders). The release kinetics are shown on Figure 5.29.

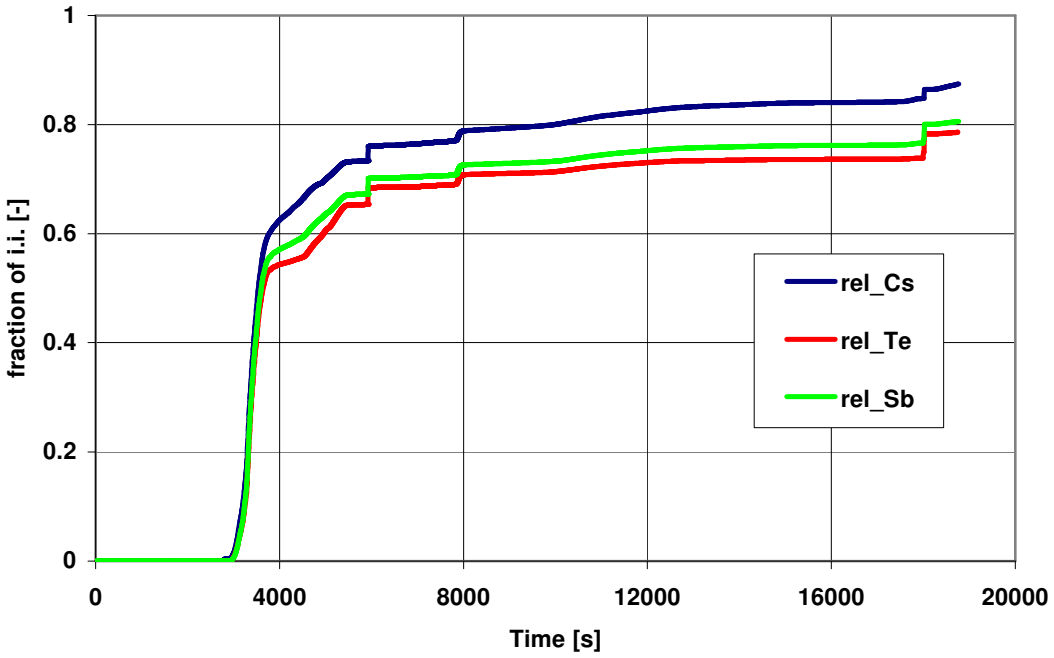

Figure 5.28: Fractional release of the Cs, Te and Sb (**Case 2A**)

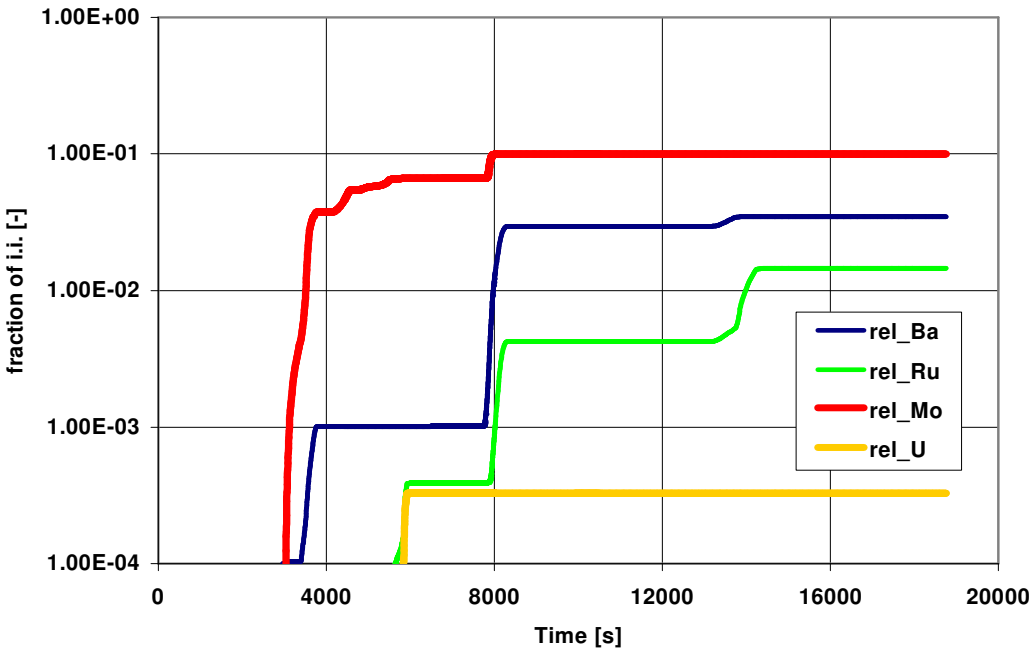

Figure 5.29: Fractional release of the Ba, Ru, Mo and U (**Case 2A**)

The cumulated release of the **SIC materials** and Sn (see Table 5.3) is predicted for Case 2A approximately similar to Case 1A. As shown on Figure 5.30 the release kinetics of Sn corresponds to the kinetics of Zr oxidation (see Figure 5.17), whereas Cd, In and Ag are considerably released also during late degradation phase.

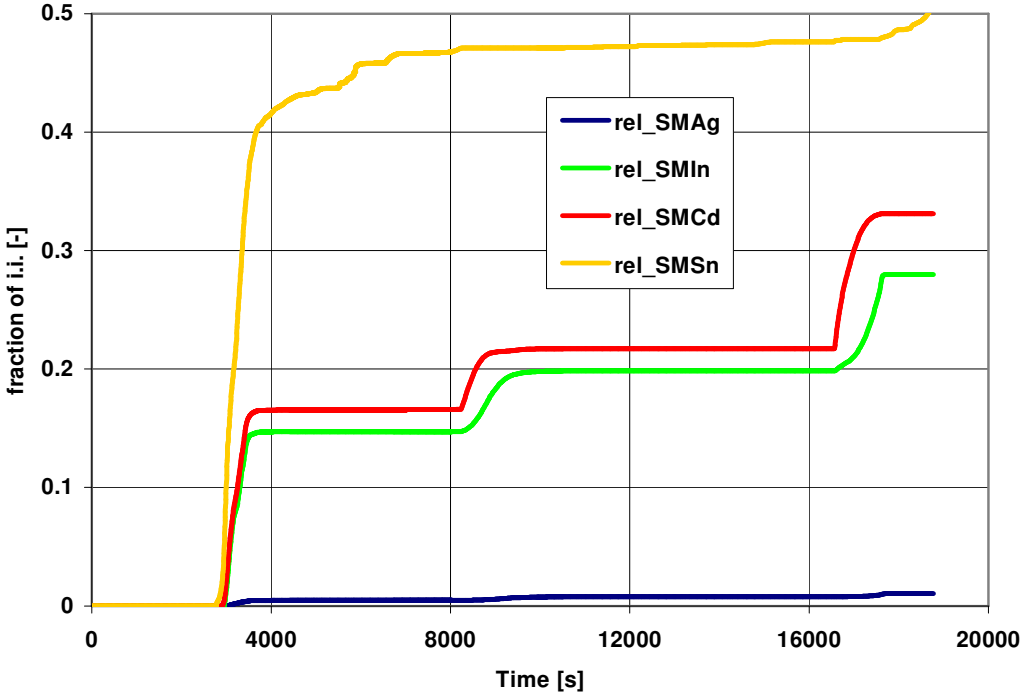

Figure 5.30: Fractional release of the SIC materials and Sn (**Case 2A**)

As it follows from the Table 5.2, in **Case 2B** the cumulative release of the high-volatile, semi and low volatile FP is similar to what predicted for Case 2A. This is the same for most of SIC materials and Sn (Table 5.3). Evidently higher cumulated release is predicted only for SIC material Ag (factor of ~7). This increased release of Ag is predicted during massive material slumping after 16000 s (see Figure 5.20).

5.3 Fission Products and Structural Materials Transport in the Circuit

The transport and deposition of the FP/SM (either as aerosols or as direct vapour condensation on the walls) depend mainly on the leakage pathways through primary circuit, release kinetics from the core and on their chemical speciation.

As discussed earlier (§5.1), the main leakage pathways for FP/SM transport from the core to the break are not identical for all cases and as will be shown later this has considerable influence on the total retention in the circuit.

Case 1A

In accordance with predicted gas mass flow rates in the circuit after start of FP/SM release from the core (t=~2770 s) (Figures 5.9 and 5.11), the considered main FP/SM leakage pathways for SOPHAEROS module are (see also Figure 3.4): **1)** from RV upper plenum through broken loop to the break, and **2)** from RV upper plenum through RV dome and cold collector to the break. Numbering of the control volumes is given in the Table 5.4.

Table 5.4: Numbering of the volumes on FP/SM leakage pathways (**Case 1A**)

1 - UPP_PLEN	**4** - TUBES1	**7** - ULEGAB1	**10** - COLDCOLL
2 - HOL1	**5** - COLDBOX1	**8** - ULEGB1	**11** - CCBYPASS
3 - HOTBOX1	**6** - ULEGA1	**9** - COL1	**12** - DOME

The main data characterizing FP/SM cumulated deposition in all considered volumes of the primary circuit (total retention factor defined as the ratio of deposited mass to inlet mass) and leaked mass through the break are presented for all elements in Table 5.5. Besides noble gases (Xe, Kr) the calculated RF is in the range of **~0.2** (Ba, Ru, Sb) to **~0.66** (SM Ag). Predicted RF for elements Y and SMCr are still higher but source masses of these elements are negligible.

The calculated deposition profiles along the considered circuit volumes (see Table 5.4) are presented for iodine, Mo and Rb in Figure 5.31 and for Cs, Ag and Cd in Figure 5.32. As it can be seen from these figures the deposition dominates in the SG tubes volume (No.4) and in RV cold collector (No.10). In SG tubes (No.4) it is mainly due to thermo-phoresis and partly due to bend impaction, but for iodine (Cs_2I_2, CsI) and mainly for Cd (nearly all Cd exists only in elementary form – see §5.4) it is also due to direct vapour condensation on the walls. In the RV cold collector (No.10) eddy and turbulent impaction dominate. The deposition is predicted to be significant also in the horizontal volumes No.2, 7 and 9, where the prevailing effect has gravitational settling.

In spite of very large surface area defined for 1 – UPP_PLEN volume (600 m^2, see Table 3.8) there is no or negligible retention of the I, Cd, Rb and Mo species due to their high volatility, i.e. exist in vapour form at sufficiently high gas and wall temperatures in this volume. On the other hand, predicted

deposition in this volume of the Cs is due to sorption of CsOH and in case of Ag it is due to aerosols thermo-phoresis.

Table 5.5: FP/SM deposition in the circuit and leak from the circuit (**Case 1A**)

No.	FP	Released (inlet) mass, [kg]	Deposited mass, [kg]	Circuit RF [-]	Leaked mass from circuit, [kg]
1	**Xe**	252.03	1.41 [2)]	0.006	250.62
2	**Kr**	19.78	0.11 [2)]	0.006	19.67
3	**I**	10.57	4.939	0.467	5.631
4	**Br**	1.138	0.544	0.478	0.594
5	**Cs**	132.8	67.49	0.508	65.31
6	**Rb**	18.69	8.552	0.457	10.14
7	**Se**	2.878	1.291	0.449	1.587
8	**Te**	20.15	9.762	0.484	10.39
9	**Sb**	0.7683	0.1573	0.205	0.611
10	**Ba**	7.56e-3	1.45e-3	0.192	6.11e-3
11	**Ru**	1.18e-3	2.34e-4	0.198	9.45e-4
12	**Sr**	3.61e-5	2.24e-5	0.619	1.38e-5
13	**La**	1.63e-5	8.91e-6	0.546	7.40e-6
14	**Eu**	2.74e-6	1.44e-6	0.527	1.29e-6
15	**Ce**	3.93e-5	2.155e-5	0.548	1.775e-5
16	**Mo**	3.291	1.459	0.443	1.832
17	**Rh**	2.02e-4	3.63e-5	0.18	1.66e-4
18	**Pd**	1.26e-5	6.78e-6	0.538	5.82e-6
19	**Tc**	1.11e-5	6.04e-6	0.543	5.08e-6
20	**Nb**	7.41e-7	4.08e-7	0.55	3.34e-7
21	**Zr**	4.97e-5	2.73e-5	0.55	2.34e-5
22	**Np**	6.52e-6	3.58e-6	0.55	2.94e-6
23	**Pu**	1.75e-4	9.38e-5	0.536	8.12e-5
24	**Nd**	4.82e-5	2.59e-5	0.537	2.23e-5
25	**Pm**	2.15e-6	1.17e-6	0.545	9.79e-7
26	**Gd**	6.54e-7	3.58e-3	0.548	2.96e-7
27	**Pr**	1.48e-5	8.06e-6	0.544	6.77e-6
28	**Am**	1.01e-6	5.27e-7	0.522	4.83e-7
29	**Cm**	2.57e-7	1.39e-7	0.538	1.19e-7
30	**Sm**	9.94e-6	5.35e-6	0.539	4.59e-6
31	**U**	0.017	0.00922	0.542	0.00778
32	**Y**	7.12e-6	4.90E-6	0.688	2.22e-6
33	**SM Ag** [1)]	136.02	89.68	0.659	46.34
34	**SM Cd** [1)]	187.1	114.3	0.611	72.78
35	**SM In** [1)]	546.4	310.36	0.568	236.04
36	**SM Sn** [1)]	145.0	69.66	0.48	75.34
37	**SM Fe**	3.29e-17	0.0	0.0	3.29e-17
38	**SM Cr**	3.3e-15	2.4e-15	0.724	9.1e-16

[1)] Masses of Ag, Cd, In and Sn as FP (substantially lower than SM) are included.
[2)] Mass suspended inside the circuit volumes.

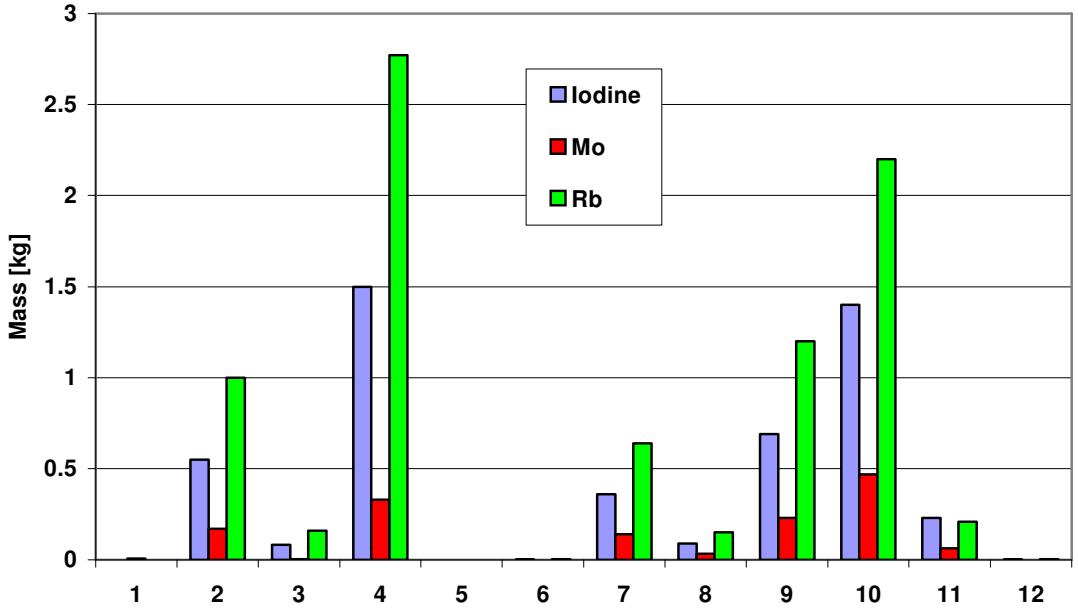

Figure 5.31: Deposited masses of the I, Mo and Rb in the circuit volumes (**Case 1A**)

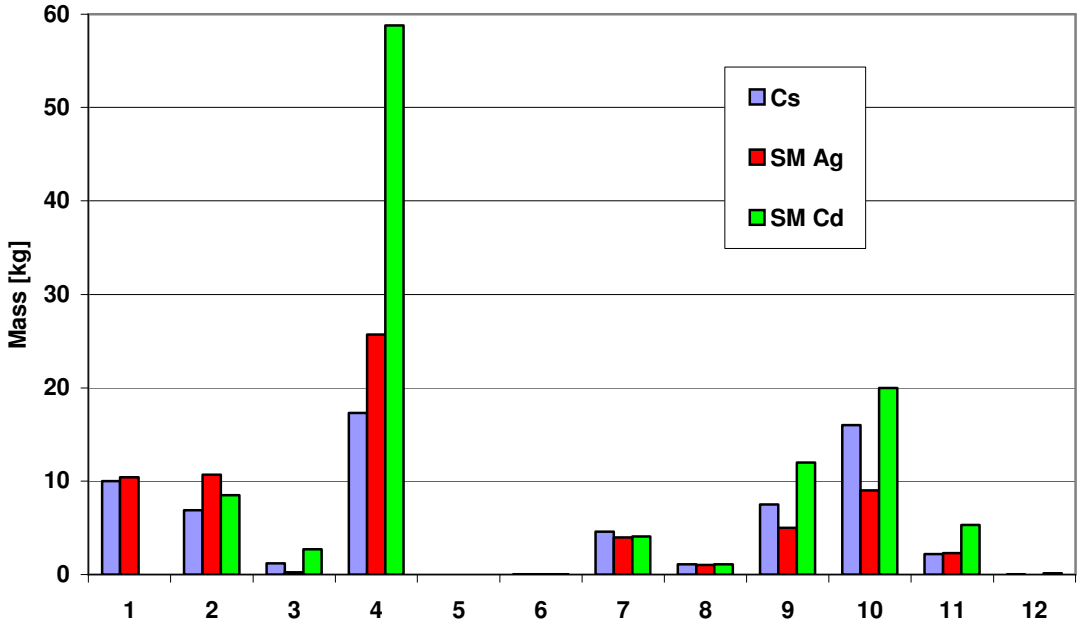

Figure 5.32: Deposited masses of the Cs, Ag and Cd in the circuit volumes (**Case 1A**)

As the inlet masses of Te, In and Sn are also significant (see Table 5.5), the deposition profile for Te is similar to Cs and deposition profile of In and Sn is similar to Ag.

Case 1B

In accordance with predicted gas mass flow rates in the circuit after start of FP/SM release from the core (~3000 s) (Figures 5.10 and 5.12) the considered FP/SM leakage pathway for SOPHAEROS module is from RV upper plenum through RV dome and cold collector to the break in the COL1 volume (see also Figure 3.4). Numbering of the control volumes is given in the Table 5.6.

Table 5.6: Numbering of the volumes on FP/SM leakage pathway (**Case 1B**)

1 - UPP_PLEN	**3** - CCBYPASS	**5** – COL1
2 - DOME	**4** - COLDCOLL	

The main data characterizing FP/SM cumulated deposition in all considered volumes of the primary circuit and leaked mass through the break are presented for all elements in Table 5.7. Besides noble gases (Xe, Kr) and Ba (Ru, Rh) the calculated RF is in the range of **~0.6** (Cs, Rb) to **~0.73** (low volatiles), i.e. generally still higher than in Case 1A.

The calculated deposition profiles along the considered circuit volumes (see Table 5.6) are presented for Iodine, Mo and Rb in Figure 5.33 and for Cs, Ag and Cd in Figure 5.34. As it can be seen from these figures the deposition dominates in the last two volumes: RV cold collector (No.4) and in COL1 volume. As in Case 1A, the dominant deposition process in RV cold collector is turbulent-eddy impaction and deposition in the horizontal COL1 volume is caused mainly by gravitational settling.

The deposition is small or negligible in the first three volumes and is mainly due to thermo-phoresis. Small deposition of I and Cs in the first volume (RV upper plenum) is caused mainly by condensation of the CsI vapour and by thermo-phoretic deposition of the Cs_2Te aerosols.

As the inlet masses of Te, In and Sn are also significant (see Table 5.7) as in Case 1A, the deposition profile for Te is similar to Cs and deposition profile of In and Sn is similar to Ag.

Table 5.7: FP/SM deposition in the circuit and leak from the circuit (**Case 1B**)

No.	FP	Released (inlet) mass, [kg]	Deposited mass, [kg]	Circuit RF [-]	Leaked mass from circuit, [kg]
1	**Xe**	258.9	2.0 [2)]	0.008	256.9
2	**Kr**	20.32	0.16 [2)]	0.008	20.16
3	**I**	10.86	7.476	0.688	3.384
4	**Br**	1.169	0.8081	0.691	0.3609
5	**Cs**	136.4	84.2	0.617	52.2
6	**Rb**	19.21	10.62	0.553	8.591
7	**Se**	2.997	2.087	0.696	0.9096
8	**Te**	20.98	13.8	0.658	7.174
9	**Sb**	0.7961	0.5418	0.681	0.2543
10	**Ba**	9.31e-3	2.7e-3	0.29	6.61e-3
11	**Ru**	1.86E-3	7.10E-4	0.382	1.15e-3
12	**Sr**	1.15e-4	6.38e-5	0.555	5.12e-5
13	**La**	5.77e-5	4.22e-5	0.731	1.55e-5
14	**Eu**	1.38e-5	6.78e-6	0.491	7.02e-6
15	**Ce**	1.39e-4	1.02e-4	0.734	3.73e-5
16	**Mo**	2.752	1.954	0.71	0.7975
17	**Rh**	2.15e-4	5.00e-5	0.233	1.65e-4
18	**Pd**	4.46e-5	3.26e-5	0.731	1.20e-5
19	**Tc**	3.94e-5	2.88e-5	0.731	1.06e-5
20	**Nb**	2.62e-6	1.92e-6	0.731	7.04e-7

21	**Zr**	1.76e-4	1.29e-4	0.733	4.71e-5
22	**Np**	2.31e-5	1.69e-5	0.732	6.19e-6
23	**Pu**	6.20e-4	4.54e-4	0.732	1.66e-4
24	**Nd**	1.71e-4	1.25e-4	0.731	4.57e-5
25	**Pm**	7.61e-6	5.49e-6	0.721	2.12e-6
26	**Gd**	2.32e-6	1.70e-6	0.733	6.21e-7
27	**Pr**	5.25e-5	3.84e-5	0.732	1.41e-5
28	**Am**	3.58e-6	2.58e-6	0.721	9.96e-7
29	**Cm**	9.11e-7	6.67e-7	0.732	2.44e-7
30	**Sm**	3.52e-5	2.51e-5	0.713	1.01e-5
31	**U**	0.06011	0.044	0.732	0.01612
32	**Y**	2.52e-5	1.84e-5	0.73	6.75e-6
33	**SMAg** [1)]	55.3	38.51	0.696	16.79
34	**SMCd** [1)]	97.7	63.61	0.651	34.09
35	**SMIn** [1)]	254.3	172.6	0.679	81.7
36	**SMSn** [1)]	164.9	104.0	0.631	60.9
37	**SMFe**	4.62e-11	3.21e-11	0.695	1.41e-11
38	**SMCr**	2.11e-9	1.39e-9	0.659	7.16e-10

[1)] Masses of Ag, Cd, In and Sn as FP (substantially lower than SM) are included.
[2)] Mass suspended inside the circuit volumes.

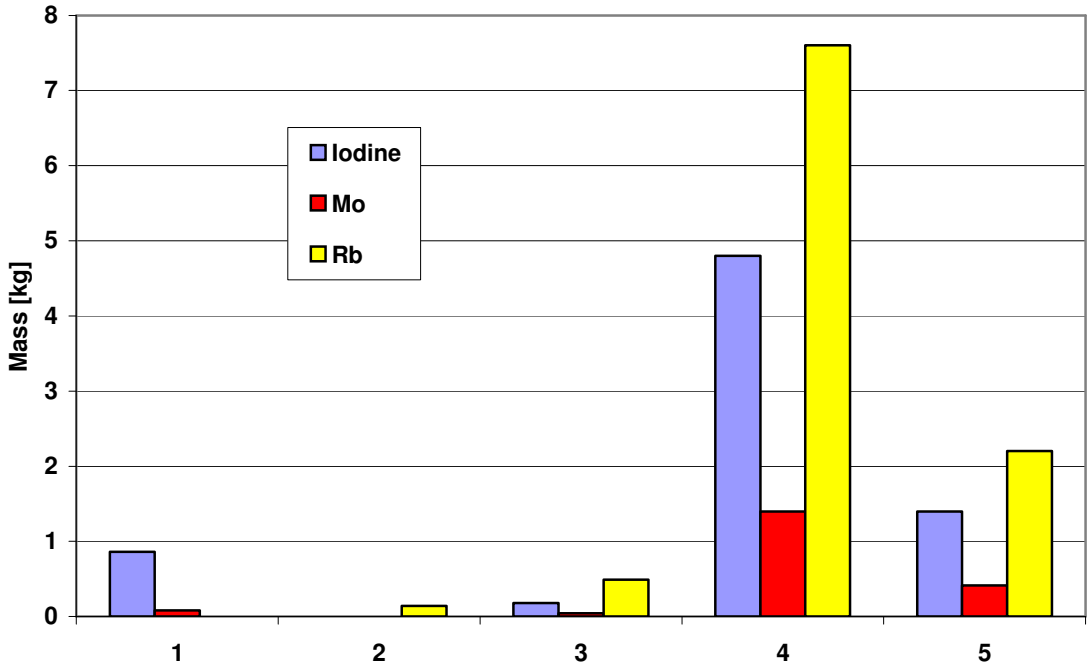

Figure 5.33: Deposited masses of the I, Mo and Rb in the circuit volumes (**Case 1B**)

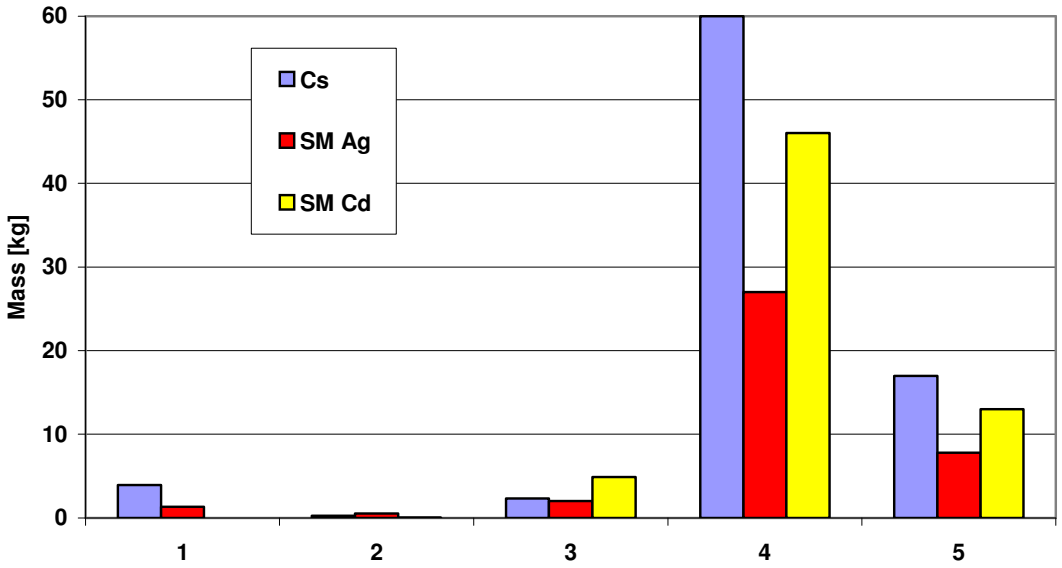

Figure 5.34: Deposited masses of the Cs, Ag and Cd in the circuit volumes (**Case 1B**)

Case 2A

In accordance with predicted gas mass flow rates in the circuit after start of FP/SM release from the core (~2770 s) (Figures 5.21 and 5.23) the considered main FP/SM leakage pathways for SOPHAEROS module are the same as for Case 1A (see also Figure 3.4), i.e.: **1)** from RV upper plenum through broken loop to the break, and **2)** from RV upper plenum through RV dome and cold collector to the break on broken loop (ULEGB1 volume). Numbering of the control volumes is given in the Table 5.4 and remains unchanged in comparison with Case 1A.

The main data characterizing FP/SM cumulated deposition in all considered volumes of primary circuit and leaked mass through the break are for all elements summarized in the Table 5.8. Besides noble gases (Xe, Kr) and low-volatile FP the calculated RF is in the range of **~0.15** (Ba, Ru) to **~0.53** (Cs, SM Ag, SM In). In comparison with Case 1A the calculated RF is comparable for highly-volatile FP and for SM (besides Cd, Fe and Cr, but source masses of the last two are negligible), whereas is evidently lower for semi-volatile FP and mainly for low-volatile FP. The explanation is given in the next paragraphs.

As shown on Figures 5.35 and 5.36 for highly-volatile FP (I, Rb, Cs), semi-volatile Mo and SIC materials (Ag, Cd) the deposition dominates only in the volumes No.9 to 11 (i.e., in COL1 – gravitational settling and in COLDCOLL and CCBYPASS – thermo-phoresis), whereas negligible deposition is predicted in the hot leg part of the broken loop No.1 (including SG tubes) or is very small in the cold leg part (No. 5 to 8). As has been already analyzed in the chapter 5.1 the duration of the

degradation period in Case 2A is substantially longer compared to Case 1A. Therefore, as shown on Figure 5.37, hot gas coming to broken loop No.1 causes overheating of the broken loop walls including SG No.1 pipes walls (note that SG pipes are completely uncovered at time ~8000 s due to evaporation of the secondary water). The temperatures of all cells of SG No.1 tubes are very similar (i.e. TW_CEL6 is representative). This leads to re-evaporation already deposited volatile species and these can reach the break and leak out of the circuit. On the other hand this negligible deposition in the SG tubes is partly compensated by higher deposition in the COL1 and COLDCOLL volumes.

The lower retention factor predicted in Case 2A compared to Case 1A for semi and low-volatile FP can be explained through their mostly not continuous release kinetics from the core (see Figures 5.26 and 5.29), i.e. in Case 2A lower fraction of these FP released from the core during relative short time periods is realized via broken loop No.1 (i.e. through SG No.1 tubes), while higher fraction is flowing via RV dome to cold collector. This is prove e.g. by the fact that in Case 1A ~11% of all deposited U mass is in SG pipes, whereas it is only ~5% in Case 2A

Finally, it should be noted that considerable deposition of Cs in the RV upper plenum and in SG No.1 tubes (volumes No.1 and No.4 on Figure 5.36) is caused by sorption of CsOH vapours, i.e. such deposit can't be re-evaporated. Also considerable deposition of the Ag in SG tubes (volume No.4 on Figure 5.36) is due to elementary Ag vapour condensation. Since elementary Ag is highly non-volatile the re-evaporation is not predicted.

Table 5.8: FP/SM deposition in the circuit and leak from the circuit (**Case 2A**)

No.	FP	Released (inlet) mass, [kg]	Deposited mass, [kg]	Circuit RF [-]	Leaked mass from circuit, [kg]
1	**Xe**	232.5	1.0 [2)]	0.004	231.5
2	**Kr**	18.25	0.08 [2)]	0.004	18.17
3	**I**	9.742	4.644	0.477	5.098
4	**Br**	1.049	0.4956	0.472	0.5534
5	**Cs**	122.4	64.8	0.529	57.6
6	**Rb**	17.24	7.265	0.442	9.615
7	**Se**	2.471	1.117	0.452	1.354
8	**Te**	17.3	8.315	0.481	8.985
9	**Sb**	0.6676	0.1806	0.271	0.487
10	**Ba**	2.469	0.3	0.122	2.169
11	**Ru**	1.584	0.272	0.172	1.312
12	**Sr**	0.17	0.0524	0.308	0.1176
13	**La**	0.0207	0.0022	0.106	0.0185
14	**Eu**	3.48e-3	4.50e-4	0.129	3.03e-3
15	**Ce**	0.04977	0.00588	0.118	0.04389
16	**Mo**	16.26	4.29	0.264	11.97
17	**Rh**	6.68e-3	3.00e-5	0.005	6.65e-3
18	**Pd**	0.016	0.0016	0.100	0.0144
19	**Tc**	0.01409	0.00157	0.111	0.01252
20	**Nb**	9.39e-4	1.09e-4	0.116	8.30e-4
21	**Zr**	0.0629	0.0075	0.119	0.0554
22	**Np**	0.00826	0.00111	0.134	0.00715
23	**Pu**	0.2219	0.0257	0.116	0.1962
24	**Nd**	0.061	0.006	0.098	0.055
25	**Pm**	0.00272	0.00027	0.100	0.00245
26	**Gd**	8.29e-4	9.20e-5	0.111	7.37e-4

27	**Pr**	0.0188	0.002	0.106	0.0168
28	**Am**	1.28e-3	3.48e-4	0.272	9.32e-4
29	**Cm**	3.26e-4	3.30e-5	0.101	2.93e-4
30	**Sm**	0.01258	0.00158	0.126	0.011
31	**U**	21.52	2.41	0.112	19.11
32	**Y**	9.02e-3	1.23e-3	0.136	7.79e-3
33	**SMAg** [1)]	68.78	36.33	0.528	32.45
34	**SMCd** [1)]	138.8	49.84	0.359	88.96
35	**SMIn** [1)]	359.3	191.9	0.534	167.4
36	**SMSn** [1)]	153.1	75.39	0.492	77.71
37	**SMFe**	1.03e-9	2.90e-10	0.282	7.40e-10
38	**SMCr**	6.60e-9	1.27e-9	0.192	5.33e-9

[1)] Masses of Ag, Cd, In and Sn as FP (substantially lower than SM) are included.
[2)] Mass suspended inside the circuit volumes.

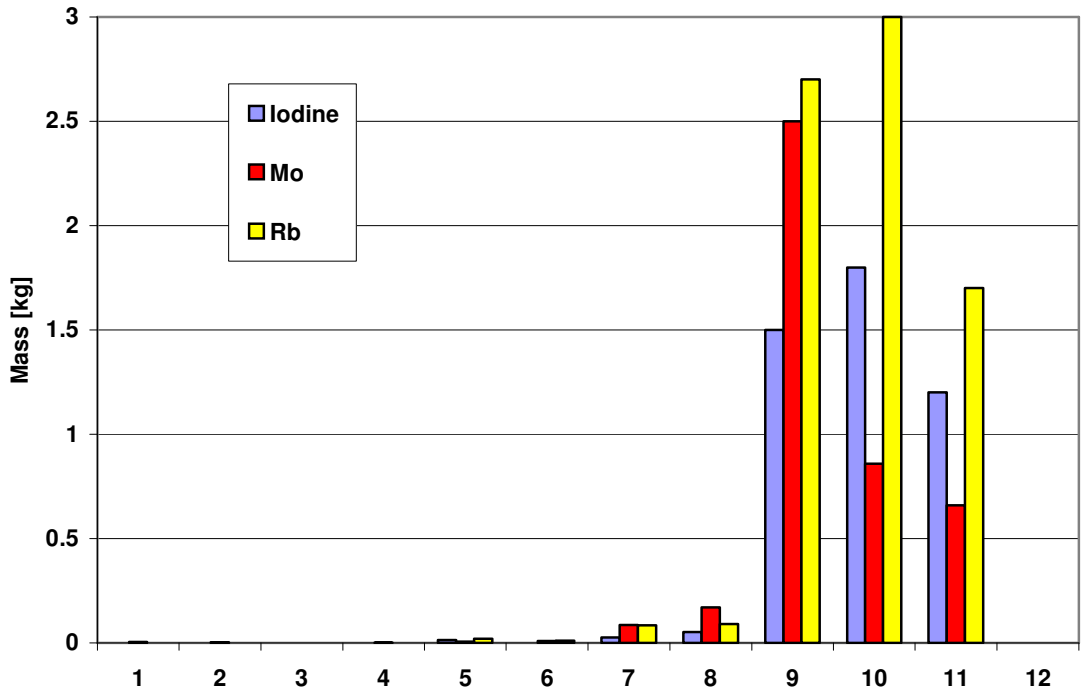

Figure 5.35: Deposited masses of the I, Mo and Rb in the circuit volumes (**Case 2A**)

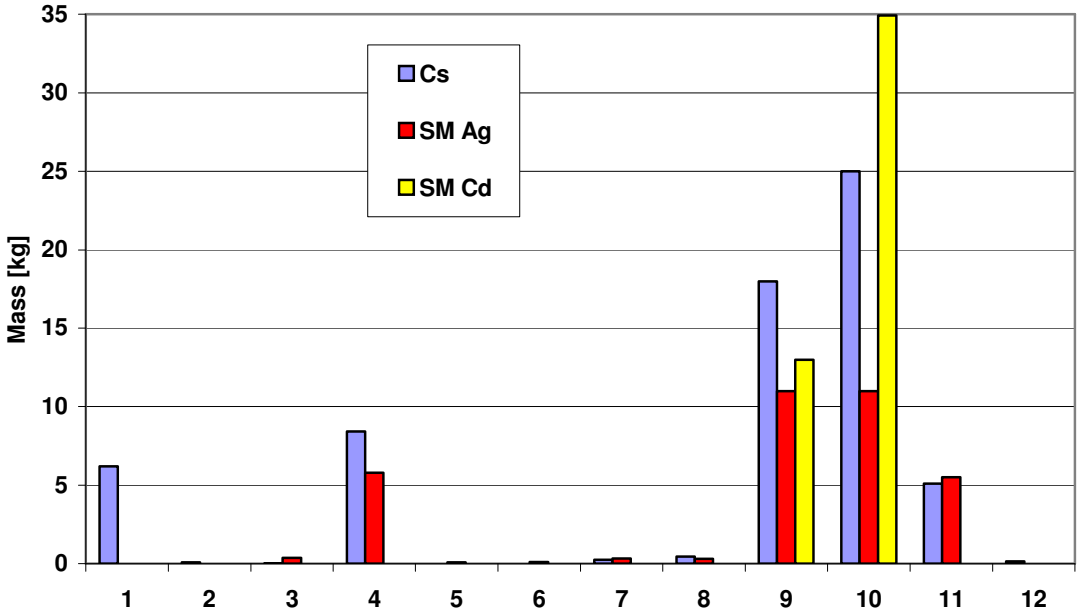

Figure 5.36: Deposited masses of the Cs, Ag and Cd in the circuit volumes (**Case 2A**)

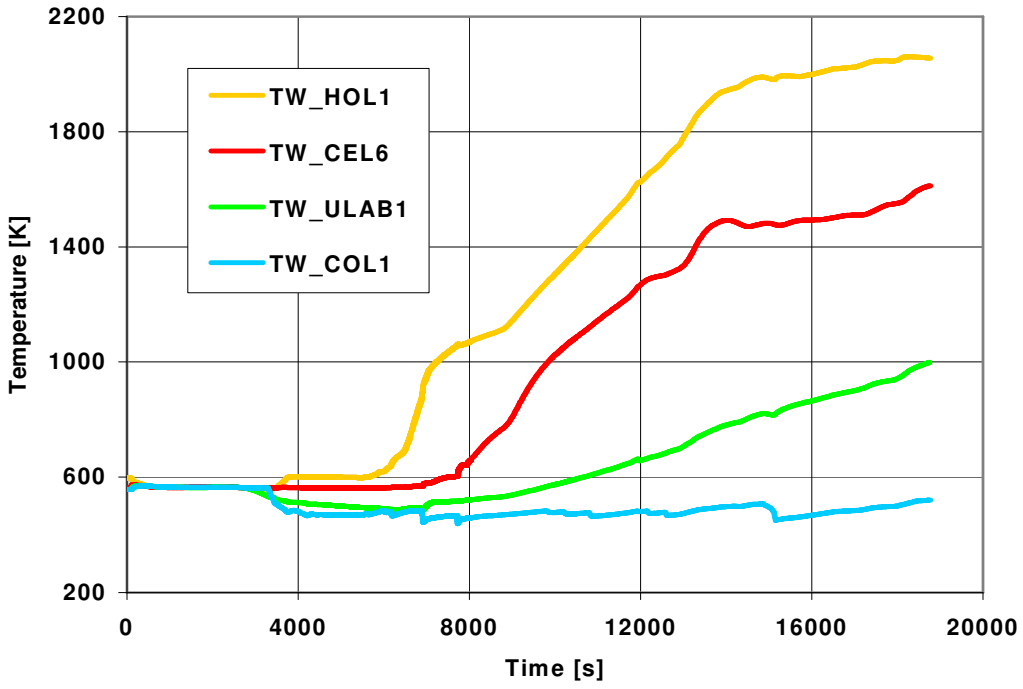

Figure 5.37: Wall temperatures in the volumes HOL1, CELL6, ULEGAB1 and COL1 (**Case 2A**)

Case 2B

As observed earlier (§5.1) for Case 2B, after start of FP/SM release from the core (~3000 s) the gas mass flow rate from UPP_PLEN volume is nearly equally distributed into intact loops (see Figures

5.22 and 5.24) and flow to broken loop is negligible. The FP/SM leakage pathways through RV dome to cold collector remains as in the Case 2A. Therefore, numbering of the control volumes of three FP/SM leakage pathways is that as given in the Table 5.9 for Case 2B.

Table 5.9: Numbering of the volumes on FP/SM leakage pathways (**Case 2B**)

1 - UPP_PLEN	**7** – ULEGAB2	**13** – COLDBOX3	**19** – COLDCOLL
2 – HOL2	**8** – ULEGB2	**14** – ULEGA3	**20** – CCBYPASS
3 – HOTBOX2	**9** – COL2	**15** – ULEGAB3	**21** - DOME
4 - TUBES2	**10** – HOL3	**16** – ULEGB3	**-**
5 – COLDBOX2	**11** – HOTBOX3	**17** – COL3	**-**
6 - ULEGA2	**12** – TUBES3	**18** – COL1	**-**

The main data characterizing FP/SM cumulated deposition in all considered volumes of the primary circuit and leaked mass through the break are summarized for all elements in the Table 5.10. In comparison with Case 2A the calculated RF is slightly increased for highly-volatile FPs (up to factor ~1.3 for Te) and also for SIC and Sn materials (up to factor ~1.8 for In and Cd). The increased deposition is more evident for semi-volatile FPs (up to factor ~4 for Ba) and for low-volatile (up to factor ~8 for Tc, but mostly is about 3 to 4 times higher).

As shown on Figures 5.38 and 5.39, in Case 2B compared to Case 2A, the deposition of some high volatile (e.g. Rb), semi-volatile (Mo) species and of SIC (Ag, not highly volatile Cd) and Sn materials is significant also in the tubes of the intact loop SGs (volume No.4 and No.12). It should be noted that also in Case 2B the hot gases coming to intact loops cause evaporation of the secondary water from these SGs (since 8000 – 8500s the tubes are uncovered) but the following overheating mainly of the SG tubes walls is not so strong as in Case 2A (see Figure 5.40). Therefore, re-evaporation of some already deposited Rb and Mo species (e.g. Rb_2MoO_4) is not so extensive as it was in the previous Case 2A.

Besides SG tubes the deposition is significant mainly in the "cold" volumes COL2 (No.9) and COL3 (No.17) due to gravitational settling, in COLDCOLL (No.19) due to eddy impaction and also in the CCBYPASS (No.20) due to thermo-phoresis.

Table 5.10: FP/SM deposition in the circuit and leak from the circuit (**Case 2B**)

No.	**FP**	**Released (inlet) mass, [kg]**	**Deposited mass, [kg]**	**Circuit RF [-]**	**Leaked mass from circuit, [kg]**
1	**Xe**	219.9	1.8 [2)]	0.08	218.1
2	**Kr**	17.26	0.14 [2)]	0.08	17.12
3	**I**	9.212	4.722	0.513	4.49
4	**Br**	0.9921	0.4987	0.503	0.4934
5	**Cs**	115.7	72.03	0.623	43.67
6	**Rb**	16.3	8.59	0.527	7.709
7	**Se**	2.387	1.118	0.468	1.269
8	**Te**	16.71	10.25	0.613	6.456
9	**Sb**	0.6388	0.1786	0.28	0.4602
10	**Ba**	1.171	0.6413	0.548	0.5297
11	**Ru**	1.016	0.292	0.287	0.724
12	**Sr**	0.0439	0.029	0.661	0.0149
13	**La**	0.0162	0.00626	0.386	0.00994
14	**Eu**	2.72e-3	1.06e-3	0.39	1.66e-3
15	**Ce**	0.0391	0.0152	0.389	0.0239

16	**Mo**	21.28	9.7	0.456	11.58
17	**Rh**	5.28e-3	4.0e-5	0.008	5.24e-3
18	**Pd**	0.0125	4.97e-3	0.398	7.53e-3
19	**Tc**	0.0111	9.77e-3	0.88	1.33e-3
20	**Nb**	7.37e-4	2.87e-4	0.389	4.50e-4
21	**Zr**	0.494	0.0185	0.375	0.0309
22	**Np**	6.48e-3	2.51e-3	0.387	3.97e-3
23	**Pu**	0.1742	0.068	0.39	0.1061
24	**Nd**	0.0479	0.0183	0.382	0.0296
25	**Pm**	2.14e-3	8.20e-4	0.383	1.32e-3
26	**Gd**	6.50e-4	2.52e-4	0.388	3.98e-4
27	**Pr**	0.0147	5.67e-3	0.386	9.03e-3
28	**Am**	1.0e-3	2.07e-4	0.207	7.93e-4
29	**Cm**	2.56e-4	1.44e-4	0.563	1.12e-4
30	**Sm**	9.87e-3	3.84e-3	0.389	6.03e-3
31	**U**	16.86	6.3	0.374	10.56
32	**Y**	7.07e-3	2.75e-3	0.389	4.32e-3
33	**SMAg** [1)]	470.3	371.5	0.79	98.83
34	**SMCd** [1)]	148.6	98.13	0.66	50.47
35	**SMIn** [1)]	415.9	308.9	0.743	107.0
36	**SMSn** [1)]	152.3	88.2	0.579	64.1
37	**SMFe**	3.02e-9	1.09e-9	0.361	1.93e-9
38	**SMCr**	1.03e-7	7.22e-8	0.701	3.08e-8

[1)] Masses of Ag, Cd, In and Sn as FP (substantially lower than SM) are included.
[2)] Mass suspended inside the circuit volumes.

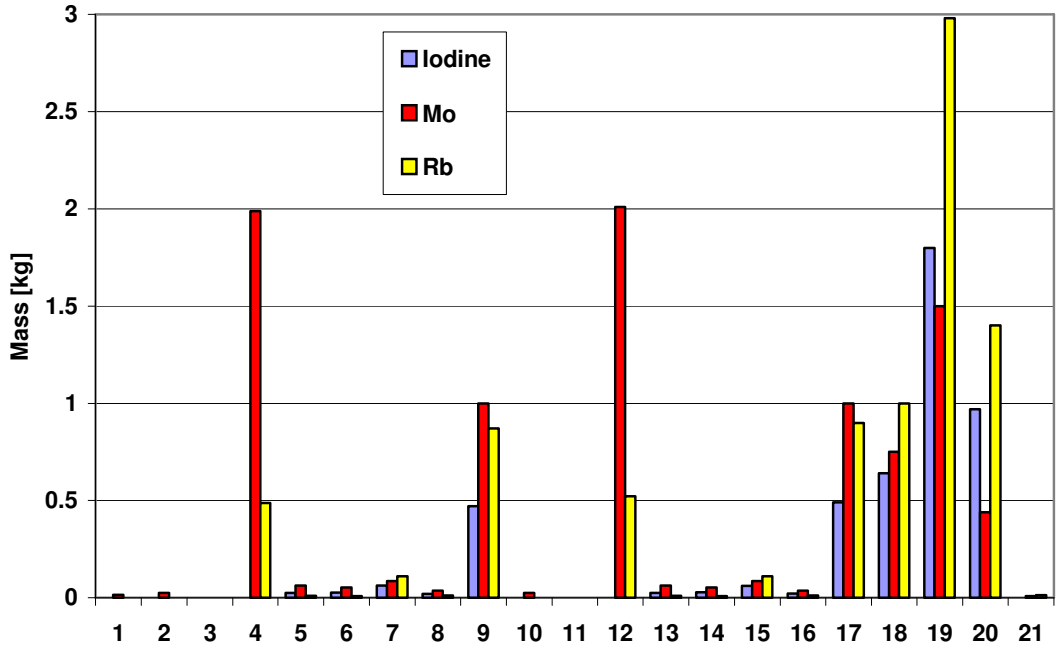

Figure 5.38: Deposited masses of the I, Mo and Rb in the circuit volumes (**Case 2B**)

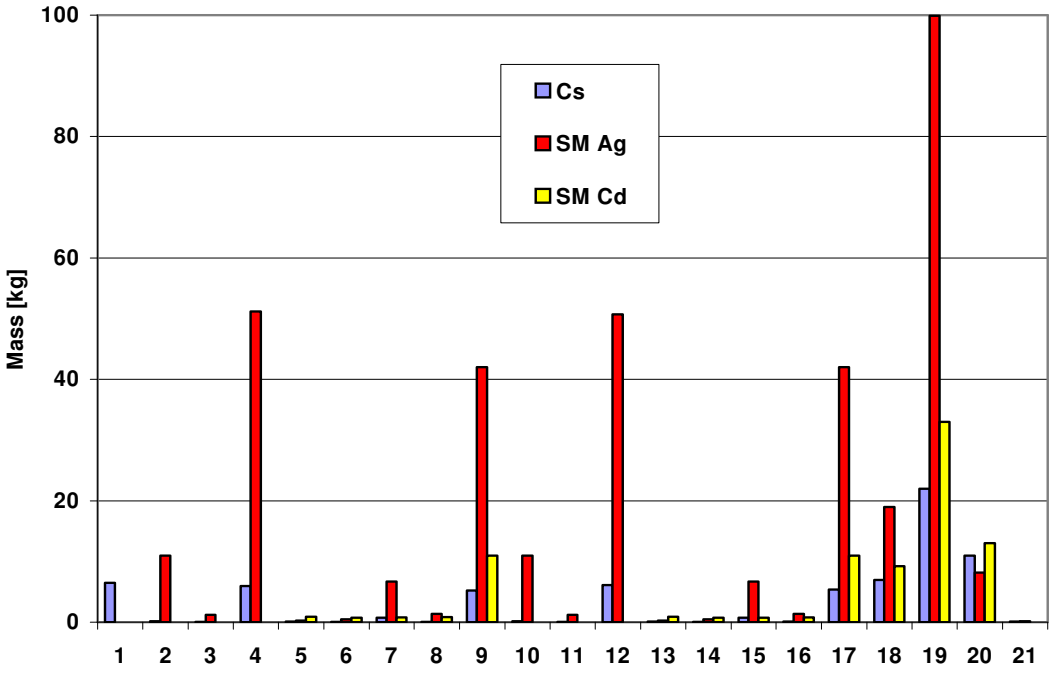

Figure 5.39: Deposited masses of the Cs, Ag and Cd in the circuit volumes (**Case 2B**)

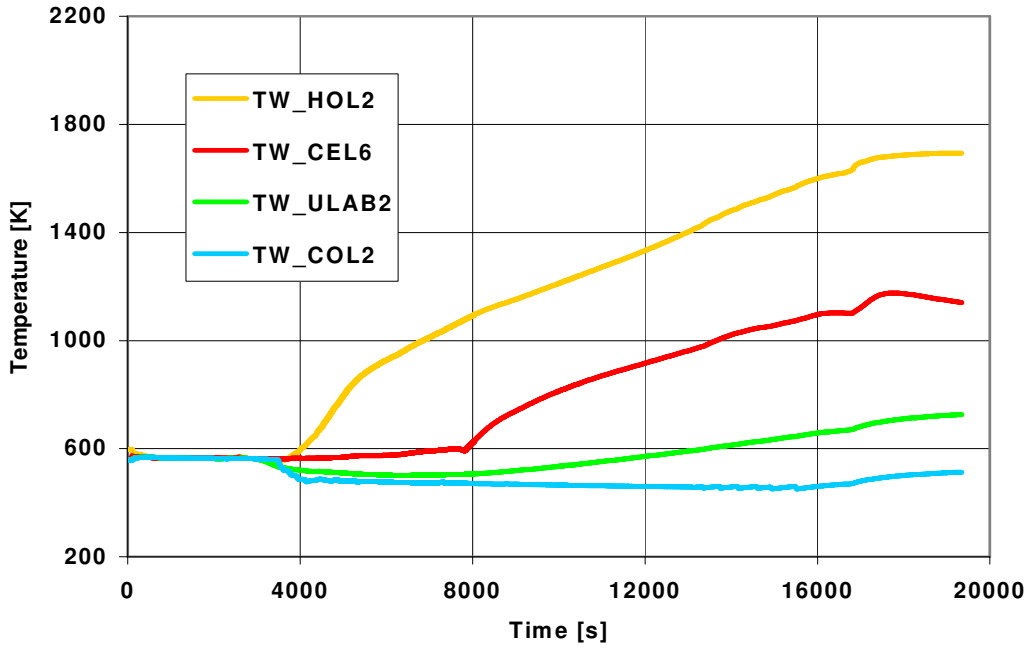

Figure 5.40: Wall temperatures in the volumes HOL2, CELL6, ULEGAB2 and COL2 (**Case 2B**)

5.4 Detailed Analysis of the Source Term

The ASTEC (module SOPHAEROS [13]) chemistry model calculates the gaseous-species masses in thermodynamic chemical equilibrium in each control volume from the masses of the elements, the temperature and the volume. The model is based on the following main hypotheses:

- chemical equilibrium is assumed to be reached instantaneously within the gaseous phase;
- chemical reactions are neglected in condensed phases, i.e. aerosols or deposits;
- mass exchanges between different phases are not in equilibrium but kinetics-controlled, i.e. a species condensed on an aerosol is not in equilibrium with its gaseous phase but its condensation rate is proportional to the deviation from the equilibrium (difference between its partial pressure and its saturation pressure).

Besides noble gases and Cs (partially also Rb, Te, Ba, Ru, Mo) the iodine is one of the most important nuclide from the point of view of source term and radiological consequences. Calculations performed with SOPHAEROS/ASTEC module for integral Phébus FP experiments [25], clearly indicated that the key species responsible for the iodine chemical speciation in the primary circuit are mainly Cs (Rb), Mo and Cd; partially iodine can react also with Ag, Ba, Sr, In and Sn. The strong influence of both their release kinetics and related species thermodynamic properties on the iodine speciation in different environment (reducing/oxidizing) were discussed, too. It has been shown [25], that the key species responsible for the volatile iodine persistence in the RCS of Phébus FP tests is molybdic acid (H_2MoO_4) because a non-negligible part of it remains as vapour in the upper plenum above fuel bundle. Then, this H_2MoO_4 consumes a significant part of Cs from CsOH or from molecular Cs_2 to form Cs_2MoO_4 and almost does not allow formation of CsI and RbI (note that behaviour of Rb is similar to Cs) if the Mo/Cs(Rb) bundle release molar ratio is sufficiently high. In such a case the ASTEC V1.3 chemistry model predicts significant reaction of iodine with Cd by formation of cadmium iodides, mostly CdI_2 (i.e., if SIC control rod is present – this is a case of FPT1 [23] and FPT2 [24] tests). When SIC is not present (FPT3 test [26]) the significant part of iodine remains in gaseous form of HI and also creation of highly volatile species I_2MoO_2, SnI_4, SnI_2 is predicted. On the other hand when the Mo/Cs(Rb) molar ratio is low (i.e. there is a surplus of Cs and Rb) the predicted dominant iodine species are CsI (RbI) and their dimmers. In this case Cd has negligible influence on iodine chemistry.

Case 1A

The calculation (Figure 5.41) predicts a significant surplus of Cs (Rb) released mass from the core compared to released mass of Mo (Cs: ~133 kg, Mo: ~3.3 kg) and the release kinetics of the Iodine in term of fractional release from the core is the same as for Cs and Rb (see also cumulative fractional release of I, Cs and Rb from the core given in Table 5.2).

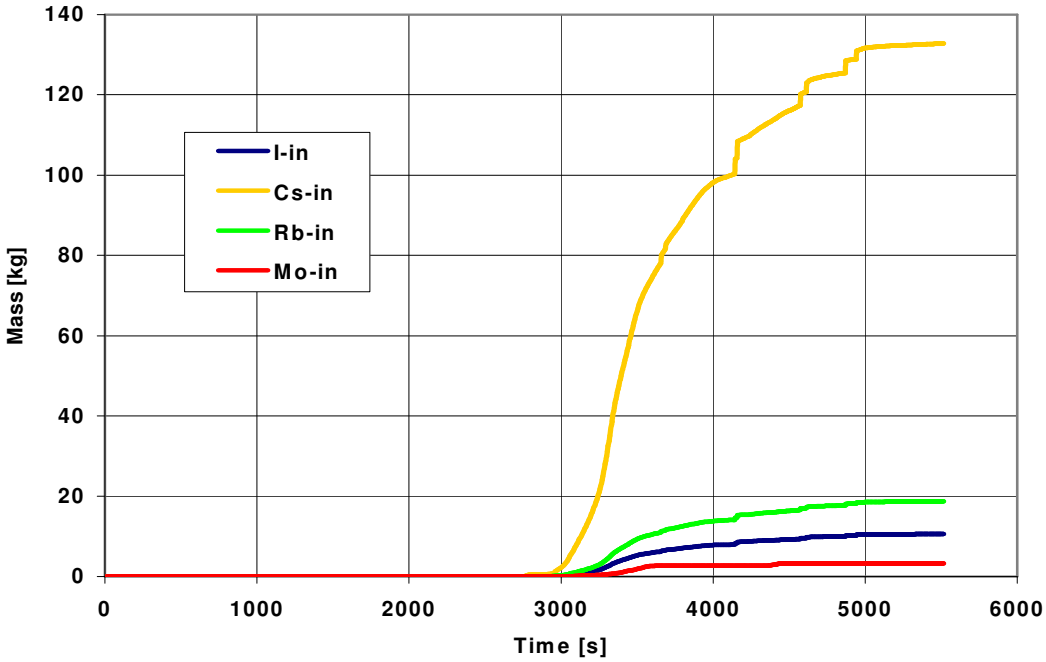

Figure 5.41: Inlet masses of I, Cs, Rb and Mo from core to the circuit (**Case 1A**)

Due to this fact, only a very small portion of Cs (Rb) is captured by Mo (by the reaction of H_2MoO_4 with CsOH and Cs_2, as already mentioned above). Therefore, as shown in Table 5.11 (masses concern net mass of I in a given compound), nearly all iodine (**~98%**) exists and will reach the containment in the form of caesium iodide and its dimmer and the remaining mass of iodine is bonded in rubidium iodide and its dimmer. The formation of another iodine species (e.g. AgI, CdI, InI, SnI_2, I_2MoO_2, BaI_2, SrI_2) is predicted to be negligible. Note that the inlet sources to circuit of the SIC (Ag, Cd, In) and of the Sn materials are significant (see Table 5.5), but the affinity of the Iodine to react with available Cs and Rb is substantially higher. On the other hand the inlet sources to circuit, Mo, Ba and Sr, are small or negligible (see Table 5.5).

Table 5.11: Final **iodine** integrated chemical speciation, time 5514 s (**Case 1A**)

Com-pound	**Suspended mass, [kg]**	**Deposited mass, [kg]**			**Leak from RCS, [kg]**	**The sum [kg]**
		CoW [1)]	**DAe** [1)]	**The sum**		
Cs_2I_2	0.0182	0.0673	2.494	2.561	3.412 **60.6%**	5.991 **56.7%**
CsI	0.0384	0.388	1.775	2.163	2.151 **38.2%**	4.352 **41.2%**
RbI	0.0003	0.118	0.018	0.136	0.0417 **0.74%**	0.178 **1.68%**
I_2Rb_2	0.0003	0.006	0.0116	0.0176	0.0264 **0.47%**	0.0443 **0.42%**

AgI	1.12E-4	1.18E-4	~0	1.18E-4	2.3E-19 **4.0E-18%**	2.3E-4 **2.2E-3%**
HI (gas)	4.2E-5	-	-	-	- **-**	4.2E-5 **4.0E-4%**
InI	2.4E-5	~0	~0	~0	~0 **~0 %**	2.4E-5 **2.3E-4%**
Elem. **I**	1.6E-5	~0	~0	~0	~0 **~0 %**	1.6E-5 **1.5E-4%**
CdI	~0	4.35E-6	~0	4.35E-6	~0 **~0 %**	4.35E-6 **4.2E-5%**
The sum	0.0574	0.579	4.3	4.88	5.631 **100%**	10.568 **100%**

1) **C**o**W** – Condensed on the Walls, **DA**e – Deposited Aerosols

Integrated chemical speciation of the Cs in the circuit at the end of calculation (5514 s) is presented in Table 5.12 (masses concern net mass of Cs in a given compound). The main predicted Cs compound is caesium hydroxide and its dimmer (**~59%** of the Cs mass) and ~24% of Cs exists in the form of caesium tellurides. The percentage of Caesium in CsI and its dimmer (~8%) is limited by the total Iodine source. Only ~4% of Cs source mass to circuit is chemically bonded with Mo (as di-caesium molybdate) and the reason is the very limited Mo source compared to Cs source (see Table 5.5).

Table 5.12: Final **Cs** integrated chemical speciation, time 5514 s (**Case 1A**)

Com-pound	**Suspended mass, [kg]**	**Deposited mass, [kg]**			**Leak from RCS, [kg]**	**The sum [kg]**
		CoW **1)**	**DA**e **1)**	**The sum**		
CsOH	0.08	6.532	9.445	26.3 **2)**	15.19 **23.82 %**	41.57 **31.3%**
$Cs_2H_2O_2$	0.272	0.734	15.7	16.3	20.21 **31.67%**	36.9 **27.8%**
Cs_2Te	0.092	0.0061	12.54	12.55	15.49 **24.29%**	28.13 **21.2%**
Cs_2I_2	0.019	0.0704	2.612	2.682	3.573 **5.6%**	6.274 **4.73%**
CsI	0.038	0.406	1.86	2.265	2.253 **3.53%**	4.557 **3.43%**
Cs_2MoO_4	0.011	0.0027	2.22	2.223	2.754 **4.31%**	4.988 **3.76%**
Cs_2	~0	~0	1.744	1.745	1.142 **1.79 %**	2.887 **2.18%**
Cs_2Te_2	0.029	0.179	1.052	1.231	2.184 **3.24 %**	3.444 **2.6%**
BrCs	0.012	0.0353	0.841	0.876	0.984 **1.54 %**	1.872 **1.41%**
The sum	0.553	7.966	48.01	66.3 **2)**	63.78	130.62 **3)**

					100%	**98.4%**

[1] **CoW** – Condensed on the Walls, **DAe** – Deposited Aerosols.
[2] The net mass of Cs 10.33 kg deposited due to CsOH sorption is included.
[3] The total source of Cs is 132.8 kg (see Table 5.5), i.e. Cs net mass from other compounds as Cs_2Te_3, $CsTe_2$ e.t.c. is not included.

It should be also pointed out that in the current analysis the presence of Boron in the primary coolant has been neglected. Due to this fact the role of Boron on Caesium and, as a consequence, on Iodine chemistry, as suggested in [27] was not taken into account. Note that Boron can also considerably consume Cs (Rb) by creation of the Caesium (Rubidium) metaborates ($BCsO_2$, $BRbO_2$).

The existing connection between iodine, Cs (Rb) and Mo chemistry is also shown in Figures 5.42 and 5.43, in which the evolution of the I and Cs integrated speciation at the end of three time instances (computational times) is presented:

- 3760 s: end of oxidation run away period (see also Figure 5.6),
- 4761 s: after this time the hydrogen production is negligible,
- 5514 s: final calculation time.

As shown in Figure 5.42 the change in predicted integrated Iodine chemical speciation during the analyzed transient phase is negligible and the main reason is a strong surplus of the Cs (Rb) inlet mass source to the circuit compared to Mo source (Figure 5.41) during the analyzed phase. It is only remarkable that during the main hydrogen generation period ~99.5 % of iodine is chemically bonded with Cs and ~0.5 % with Rb, whereas later ~98 % of iodine is bonded with Cs and ~2 % with Rb, which is mainly due to lower fraction of Rb, which remains in elementary form at higher temperatures after ~4500 s (see also Figure 5.44). Note that the fraction of Rb, which remains in elementary form decreases from ~8% at 3760 s to ~4% after ~4500 s.

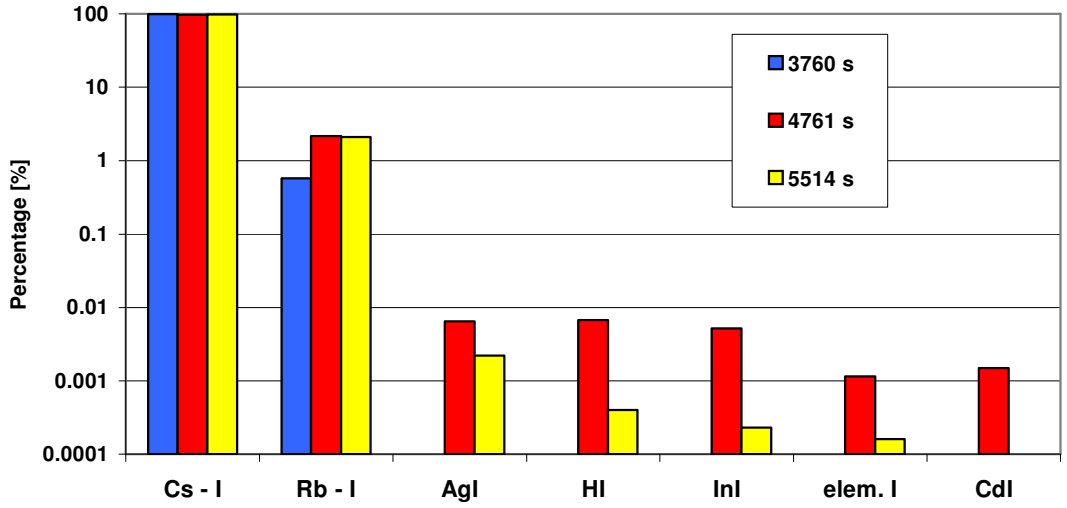

Figure 5.42: **Iodine** integrated speciation at a given time instances (**Case 1A**)

As shown in Figure 5.43 also the change in the predicted Cs chemical speciation during the analyzed transient phase is also not significant. The fraction of Cs in caesium molybdate decreases after ~3800 s

due to lower source of Mo (see Figure 5.26) and on the other hand the fraction of Cs in caesium hydroxide increases.

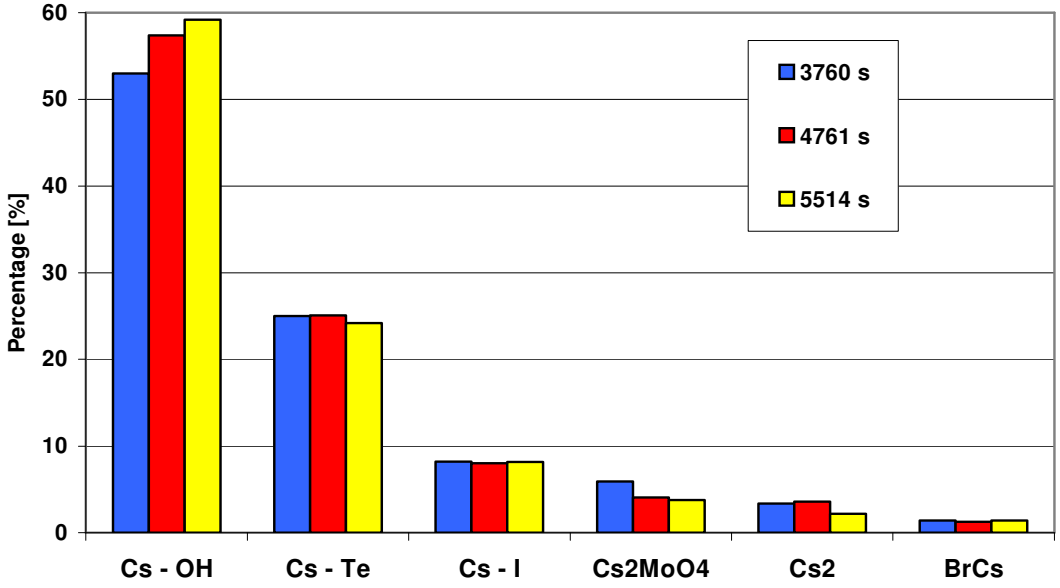

Figure 5.43: **Caesium** integrated speciation at a given time instances (**Case 1A**)

The predicted integrated (up to final time of analysis) chemical speciation of the other important FPs and SMs (see also Table 5.5) is the following:

Rubidium: The essential amount of Rb (~83%) released from the core (18.69 kg) forms rubidium hydroxide and its dimmer and ~12% of Rb exists as rubidium molybdate. The rest of Rb remains in elementary form (~3.7%) or forms RbI (~0.7%).

Molybdenum: Most of the Mo mass released from the core (3.29 kg) is chemically bonded in molybdates: Cs_2MoO_4 (~55%) and Rb_2MoO_4 (~36%). The rest of Mo remains in elementary form (~8.7%) and the negligible fraction exists as molybdic acid - H_2MoO_4 (<0.001 %) due to its consumption in reaction with CsOH and RbOH to create the corresponding molybdates.

Tellurium: The Te released mass from the core (20.15 kg) is chemically bonded mainly in the caesium tellurides - Cs_2Te and Cs_2Te_2 (~87%), the rest creates AgTe (~11%) and SnTe (~1%).

Cadmium: Nearly all mass of Cd (>99.9%) released mainly from the control rods (187.1 kg) does not react and remains in the elementary form.

Silver: More than 98% of the Ag released mass mainly from the control rods (136 kg) exists in elementary or molecular form. The rest is chemically bonded in AgTe and AgSe.

Indium: ~81% of the In mass released from the control rods (546.4 kg) creates di-Indium tri-oxide (In_2O_3) and ~18.5% of In remains in elementary form. The rest exists as In_2Se, In_2O and In_2Te.

Tin: The Sn mass released from the core (145 kg) is chemically bonded mainly in the tin hydroxide $Sn(OH)_2$ (~45%) or remains in the molecular form of Sn_2 (~44%). The rest exits as H_2SnO_3 (~7.3%), SeSn (~2.6%), elementary Sn and SnTe.

Case 1B

As it has already been shown in §5.1 and §5.3, from the point of view of chemical speciation, the main difference of the Case 1B in comparison with Case 1A is the fact that after start of FP/SM release from the core (~3000 s) and mainly after total core uncovery (~3500 s), the larger part of the gas (i.e. steam, because hydrogen generated in the core region is flowing mainly to RV upper plenum) mass flow rate flows through the downcomer to RV cold collector (see negligible mass flow from RV upper plenum to all 3 hot legs on Figure 5.10), whereas in the Case 1A there is always significant flow of overheated gas in the core to RV upper plenum and then continuing mainly to the hot leg of broken loop (see Figure 5.9). As shown in Figure 5.44, this is the main reason why the gas temperature in the RV upper plenum is in Case 1B significantly lower compared to Case 1A. As a consequence some differences in chemical speciation are predicted, since chemical reactions depend mainly on temperature of the carrier gas in the RV upper plenum.

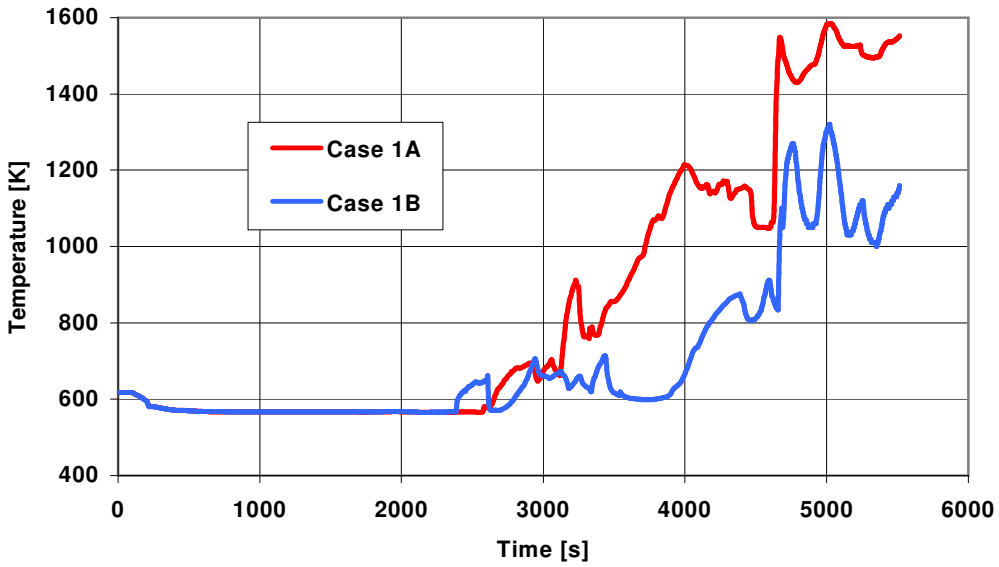

Figure 5.44: Temperature of the gas in the RV upper plenum (volume UPP_PLEN)

As shown in Figure 5.45 for the iodine integrated chemical speciation at the end of three time instances:

- 3990 s: end of oxidation run away period,
- 4990 s: after this time the hydrogen production is negligible,
- 5606 s: final calculation time,

the change in predicted speciation during the analyzed transient phase is negligible (i.e. all iodine reacts with Cs and only partly with Rb) and, as in Case 1A, the main reason is a strong surplus of the Cs (Rb) inlet masses to RCS compared to Iodine and Mo sources (see also Table 5.7) during the analyzed phase. Moreover, the relatively low carrier gas temperature in the RV upper plenum (Figure 5.44) prevents the creation of any Mo species, i.e. all Mo remains in the elementary form. Creation of the other iodine species as InI, AgI, CdI is predicted to be negligible.

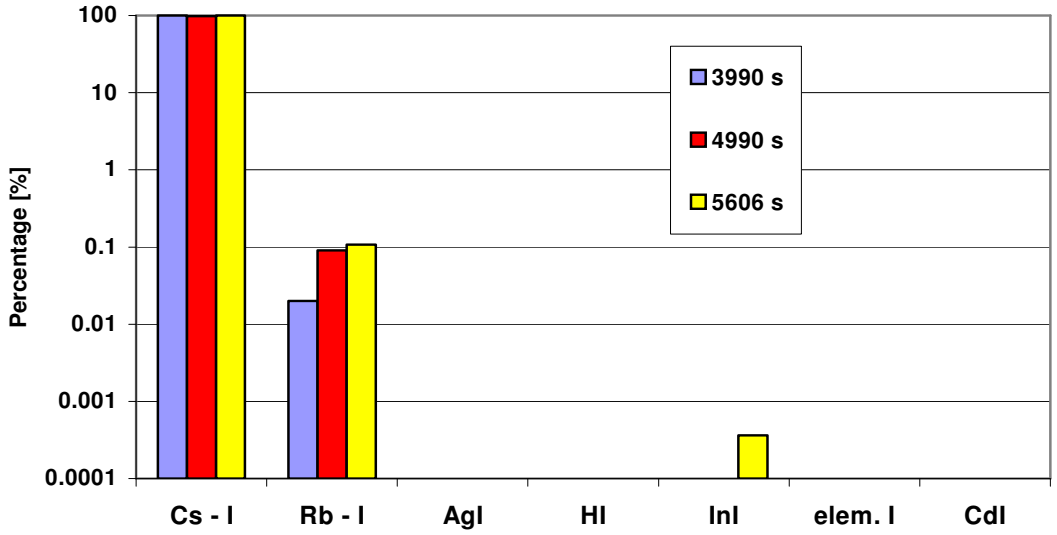

Figure 5.45: **Iodine** integrated speciation at given time instances (**Case 1B**)

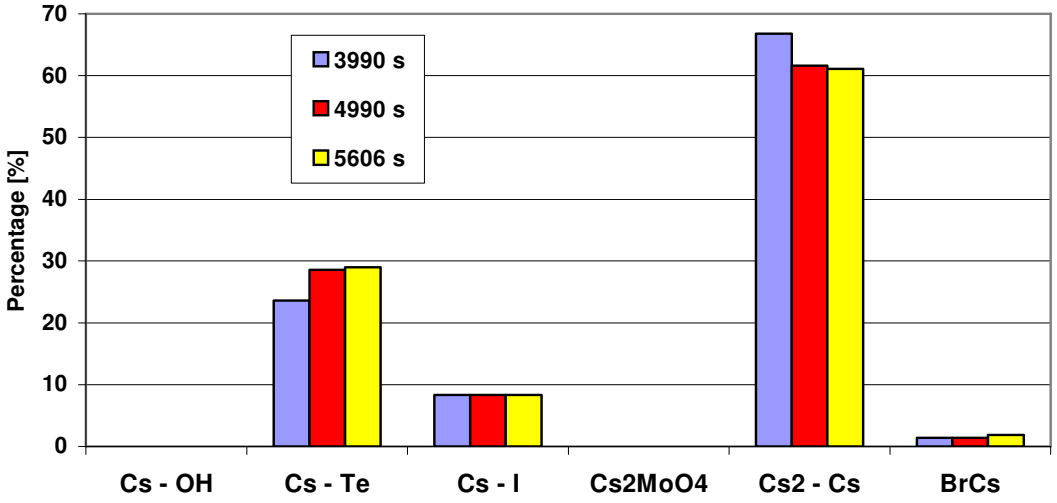

Figure 5.46: **Caesium** integrated speciation at given time instances (**Case 1B**)

As shown in Figure 5.46 also the change in predicted integrated Cs chemical speciation during the transient phase is not significant. On the contrary with Case 1A, the relatively low carrier gas temperature in the RV upper plenum (Figure 5.44) prevents creation of any CsOH and Cs_2MoO_4 (also Mo does not create molybdic acid) and most of Cs remains in the molecular (Cs_2) or elementary forms (their decreased fraction in later phases from time of 4990 s are due to increased gas temperature – see Figure 5.44).

The predicted integrated chemical speciation of the other important FP and SM (see also Table 5.7) is the following:

Rubidium: Due to relatively low temperature in the RV upper plenum nearly all Rb remains in the elementary form (~99.9%) and only ~0.1% of Rb exists as RbI (see Figure 5.45).

Molybdenum: As is already mentioned above, 100% of Mo remains in the elementary form.

Tellurium: Similarly as in the Case 1A most of the Te released from the core (20.98 kg) is chemically bonded mainly in the Cs_2Te (~90%), the rest creates In_2Te (~9.8%) and SnTe (~0.1%).

Cadmium: As in the Case 1A, all mass of Cd (~100%) remains in the elementary form.

Silver: Similarly to Case 1A, more than 99% of the Ag exists in elementary or molecular form. The rest is chemically bonded in Ag_2Se and AgSe.

Indium: ~96.5% of the In mass remains in elementary form. The rest exists as In_2Se and In_2Te.

Tin: As for Ag, ~99% of the Sn mass exists in molecular or elementary form. The rest creates SeSn (~1%) and SnTe (<0.01%).

Case 2A

In spite of the fact that the cumulated released mass of Mo (~16.3 kg, see Table 5.8) is several times larger compared to Case 1A (~3.3 kg) and Case 1B (~2.8 kg) and that the cumulated released mass of Cs (Rb) is slightly decreased (by ~10%, see Table 5.2), the surplus of the Cs (Rb) released mass compared to Mo released mass remains still significant, as it is shown in Figure 5.47. Therefore, as expected, the dominant iodine compound remains CsI and its dimmer (see Table 5.13).

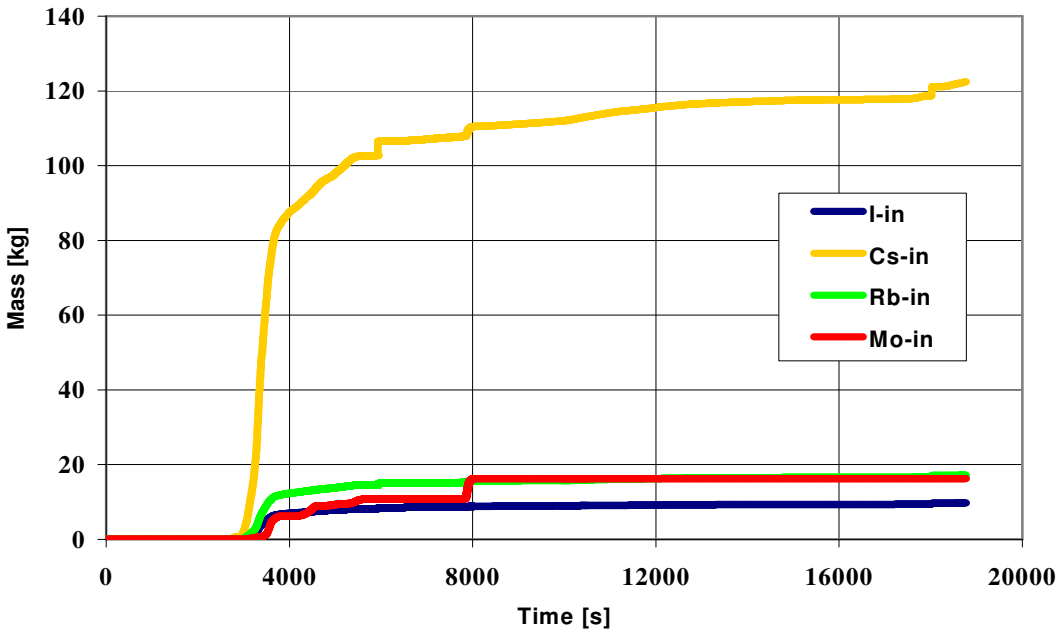

Figure 5.47: Inlet masses of I, Cs, Rb and Mo from core to the circuit (**Case 2A**)

Integrated chemical speciation of the iodine in the circuit at the end of calculation (18753 s) is presented in Table 5.13 (masses concern net mass of iodine in a given compound). In comparison with

the Case 1A (see Table 5.11) it is evident, that the fraction of iodine chemically bonded in CsI and its dimmer decreases from ~98% (Case 1A) to **~91**% and, that this fraction is increased for all other iodine compounds (e.g. RbI, AgI, CdI_2, BaHIO, BaI_2). Moreover, iodine is predicted to be present on not negligible level also in the form of hydrogen iodide (HI gas) and as highly volatile compounds: molybdenum iodide oxide (I_2MoO_2) and tin iodides (SnI_2, SnI_4), which exist in vapour form at temperatures greater than 150 ºC (i.e. no deposition in the circuit – see Table 5.13). This is mainly a consequence of the increased Mo source, which through molybdic acid (H_2MoO_4) consumes more Cs to create caesium molybdate (Cs_2MoO_4, see also Table 5.14 given later). In case of iodine compounds with Ba (BaHIO and BaI_2) it is also consequence of substantially increased Ba source in Case 2A compared to Case 1A and Case 1B (see Table 5.2).

Table 5.13: Final **iodine** integrated chemical speciation, time 18753 s (**Case 2A**)

Com-pound	**Suspended mass, [kg]**	**Deposited mass, [kg]**			**Leak from RCS, [kg]**	**The sum [kg]**
		CoW [1)]	**DAe** [1)]	**The sum**		
CsI	0.0147	0.393	2.073	2.466	2.044 **40.1%**	4.525 **46.4%**
Cs_2I_2	0.0075	0.034	2.004	2.04	2.325 **45.6%**	4.373 **44.9%**
RbI	0.0077	0.0659	0.00108	0.067	0.254 **4.98%**	0.329 **3.38%**
I_2Rb_2	7.2E-5	9.58E-4	4.48E-3	5.44E-3	0.0266 **0.52%**	0.032 **0.33%**
AgI	4.2E-4	1.63E-3	7.57E-3	9.2E-3	0.0684 **1.34%**	0.078 **0.8%**
CdI_2	~0	0.012	5.7E-3	0.0177	0.1 **1.96%**	0.118 **1.21%**
BaHIO	4.2E-6	1.47E-3	2.06E-3	3.53E-3	0.05 **0.98 %**	0.0535 **0.55%**
BaI_2	~0	1.34E-6	3.02E-4	3.03E-4	5.63E-3 **0.11 %**	5.93E-3 **0.06%**
Elem. **I**	1.76E-3	~0	~0	~0	~0 **~0 %**	1.76E-3 **0.02%**
HI (gas)	0.004	-	-	-	0.0664 **1.3%**	0.0704 **0.72%**
I_2MoO_2	-	-	-	-	0.103 **2.02%**	0.103 **1.06%**
$SnI_{2(4)}$	-	-	-	-	0.053 **1.0%**	0.053 **0.54%**
The sum	0.036	0.51	4.1	4.61	5.096 **99.91%**	9.742 **100%**

[1)] **C**o**W** – Condensed on the Walls, **DA**e – Deposited Aerosols

Integrated chemical speciation of the Cs in the circuit at the end of calculation (18753 s) is presented in Table 5.14 (masses concern net mass of Cs in a given compound). As in Case 1A the main predicted Cs compound is caesium hydroxide and its dimmer (**~56%** of the Cs mass, Case 1A: 59%). In comparison with Case 1A the fraction of Cs mass chemically bonded in caesium tellurides decreases from ~24% to ~17% and, as already mentioned, increases for caesium molybdate from ~4% to ~14%.

The fraction of Cs mass bonded in CsI (Cs_2I_2) decreases not significantly, from 8.2% (Case 1A) to 7.6%. Since the cumulated released mass of iodine is more than 10 times lower compared to Cs (Table 5.8), then this decrease is from the point of view of iodine bonded in CsI more evident (i.e. as already mentioned from 98% to 91%).

Table 5.14: Final **Cs** integrated chemical speciation, time 18753 s (**Case 2A**)

Com-pound	**Suspended mass, [kg]**	**Deposited mass, [kg]**			**Leak from RCS, [kg]**	**The sum [kg]**
		CoW [1]	**DAe** [1]	**The sum**		
CsOH	~0	7.17	7.6	29.77 [2]	14.81 **25.8%**	44.58 **36.4%**
$Cs_2H_2O_2$	0.0202	0.366	11.84	12.23	12.47 **21.75%**	24.7 **19.9%**
Cs_2Te	0.0027	1.96E-3	9.74	9.74	9.09 **15.9%**	18.83 **15.4%**
Cs_2I_2	0.0078	0.0357	2.1	2.135	2.436 **4.25%**	4.579 **3.74%**
CsI	0.0064	0.412	2.17	2.582	2.14 **3.73%**	4.728 **3.86%**
Cs_2MoO_4	1.4E-4	0.0494	5.257	5.306	12.2 **21.3%**	17.51 **14.3%**
Cs_2	~0	0.001	0.932	0.933	1.283 **2.24%**	2.216 **1.81%**
Cs_2Te_2	0.049	0.0274	0.735	0.762	1.113 **1.94%**	1.924 **1.57%**
BrCs	0.0023	0.0353	0.0546	0.719	0.694 **1.21%**	1.415 **1.16%**
Br_2Cs_2	5.4E-5	7.8E-5	0.0291	0.0292	0.79 **1.38%**	0.819 **0.67%**
Cs_2Te_3	~0	0.196	0.0883	0.284	0.288 **0.5%**	0.572 **0.47%**
The sum	0.553	7.966	48.01	66.3 [2]	57.31 **100%**	121.9 [3] **99.3%**

[1] **CoW** – Condensed on the Walls, **DAe** – Deposited Aerosols.
[2] The net mass of Cs ~15 kg deposited due to CsOH sorption is included.
[3] The total source of Cs is 122.4 kg (see Table 5.8).

As shown on Figure 5.48 for the iodine integrated chemical speciation at the end of three time instances:

- 4360 s: end of main oxidation run away period,
- 9360 s: after this time the hydrogen production is very low,
- 18753 s: final calculation time,

nearly all (>99%) iodine exists as CsI and its dimmer up to end of main oxidation run away period because of a strong surplus of Cs source against Mo source. The creation of another iodine compounds

on a remarkable (but not significant) level is predicted till after this period when the mass (also molar) ratio Cs/Mo is mainly decreased during relatively short time period before 8000 s (see Figures 5.29 and 5.47). Besides the mentioned event, increased creation of the other iodine compounds than CsI and its dimmer is also caused by increased gas temperature in the RV upper plenum after ~9000 s (see Figure 5.50 given later). This concern mainly Rb, when the fraction of elementary Rb decreases from ~5% at 4360 s to a negligible level at the end (see also discussion for Rb in Case 1B). The increased reaction of iodine with Ba, Cd and Ag it is also due to their increased release kinetics from the core (see Figures 5.29 and 5.30).

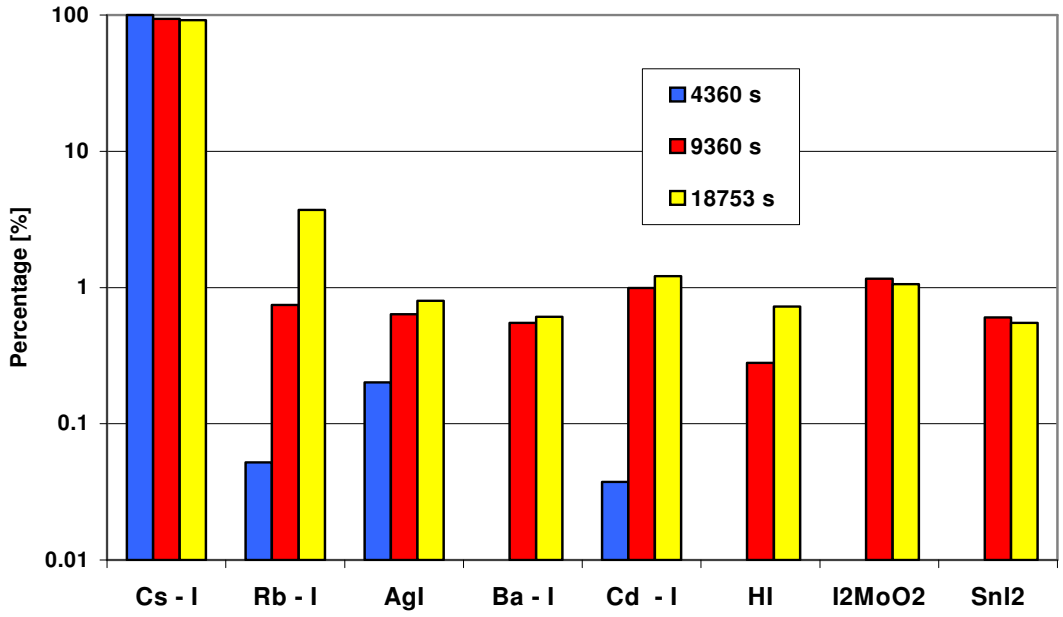

Figure 5.48: **Iodine** integrated speciation at a given time instances (**Case 2A**)

As shown in Figure 5.49 the change in predicted integrated Cs chemical speciation during the analyzed transient phase is not significant. The fraction of Cs chemically bonded in caesium hydroxide and its dimmer and in caesium tellurides is mainly influenced by the evolution of the gas temperature in the RV upper plenum (see Figure 5.50), i.e. the affinity of Cs to create hydroxides increases with gas temperature (see also the results given above for Case 1B, i.e. at relatively low temperature there is no creation of CsOH, but reaction of Cs with Te to create Cs_2Te is predicted).

As has been already explained, the increased fraction of caesium molybdate (Cs_2MoO_4) in the later time periods (Figure 5.49) is a consequence of the increased Mo source just before 8000 s (Figure 5.29).

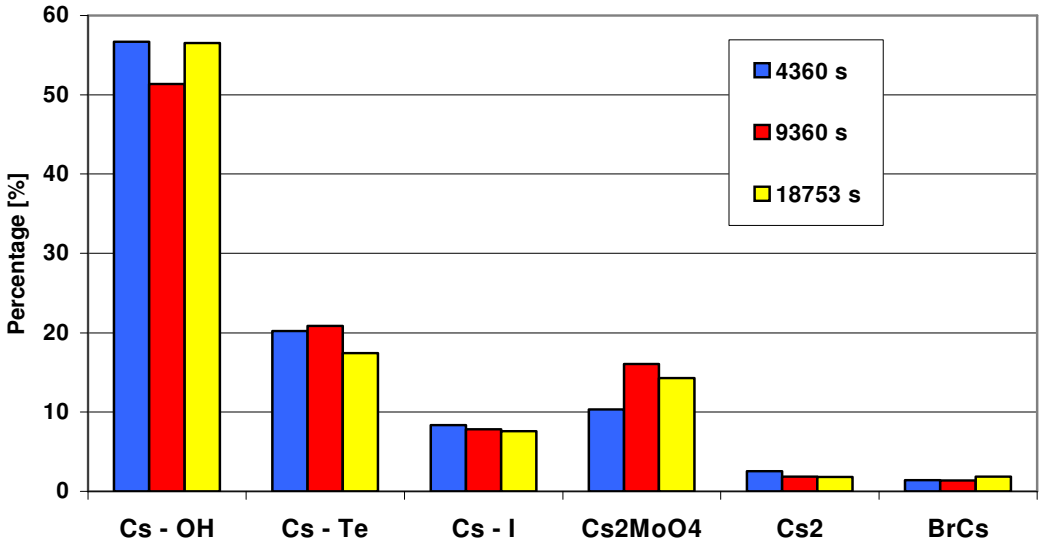

Figure 5.49: **Caesium** integrated speciation at a given time instances (**Case 2A**)

The predicted integrated chemical speciation of the other important FPs and SMs (see also Table 5.8) is the following:

Rubidium: In comparison with Case 1A, mainly due to larger released mass of the Mo in Case 2A, the fraction of released Rb mass (17.2 kg) bonded in RbOH and $Rb_2(OH)_2$ is decreased from ~83% to ~47% and, the fraction bonded in rubidium molybdate is increased from ~12% to 48%. The rest of Rb reacts with iodine and Br and negligible fraction of Rb mass (<0.1%) remains in elementary form.

Molybdenum: Similarly to Case 1A, most of the Mo mass released from the core (16.3 kg, note that it is only ~3.3 kg in Case 1A) is chemically bonded in molybdates: Cs_2MoO_4 (~39%) and Rb_2MoO_4 (~29%). In contrary with Case 1A, a considerable fraction of Mo remains in the form of molybdic acid: H_2MoO_4 (~22%) and creates molybdenum oxides: Mo_3O_9 and Mo_2O_6 (~8%). Only small fraction (~1.5%) remains in elementary form.

Tellurium: Te released from the core (17.3 kg) is chemically bonded mainly in the caesium tellurides - Cs_2Te, Cs_2Te_2 and Cs_2Te_3 (~68%), the rest creates AgTe (~18%), SnTe (~5%) and Te_2 (~7%).

Cadmium: Essential fraction of Cd mass (~97.6%) released mainly from the control rods (138.8 kg) remains in the elementary form. The rest exists as $Cd(OH)_2$ (~2.3%), CdI_2 and CdTe.

Silver: Similarly to Case 1A more than 95% of the Ag released mass mainly from the control rods (68.8 kg) exists in elementary or molecular forms. The rest is chemically bonded in AgTe, Ag_2Te and Ag_2Se and AgI.

Indium: ~74.5% of the In mass released from the control rods (359.3 kg) creates di-Indium tri-oxide (In_2O_3) and ~25% of In remains in elementary form. The rest exists as In_2Se, $HInO_2$ and In_2Te.

Tin: The Sn mass released from the core (153 kg) is chemically bonded mainly in the tin hydroxide $Sn(OH)_2$ (~39%) or remains in the molecular form of Sn_2 (~38%). The rest exits as H_2SnO_3 (~10%), HO_2Sn (~9%), SeSn (~1.8%), elementary Sn and SnTe.

As predicted released masses of Ba, Ru and uranium are also considerable – see Table 5.8 (note that in the Case 1A and Case 1B their release is negligible), then their predicted chemical speciation is as follows:

Barium: More than 95% of Ba released mass (~2.5 kg) is chemically bonded in barium hydroxide $Ba(OH)_2$. The rest exists as BaHIO, barium molybdate ($BaMoO_4$) and barium oxide (BaO).

Ruthenium: Essential fraction (~67%) of Ru released mass (1.58 kg) remains in the elementary form. The main Ru compounds are ruthenium oxides - RuO_2 and RuO (~25% of Ru mass) and ruthenium hydroxide – RuOH (~4.8% of Ru mass). It should be noted that not negligible fraction of Ru mass (~1.5%) creates highly volatile ruthenium tri-oxide (RuO_3). Formation of highly volatile ruthenium tetra-oxide RuO_4 is predicted to be negligible.

Uranium: 85.4% of released U mass (21.5 kg) exists as uranium di-oxide (UO_2) and 14.4% is chemically bonded in hydrated uranium oxides (HO_2U, HO_3U). Formation of highly volatile uranium tri-oxide (UO_3) is predicted on very low level (~0.2% of released U mass).

Case 2B

As shown in Figure 5.50 the carrier gas temperature in the RV upper plenum is generally lower in Case 2B compared to Case 2A, which is a consequence of the different mass flow rates in the junctions between RV and primary loops (see §5.1). This can have some influence on the chemical speciation, but the gas temperature in RV upper plenum is sufficiently high in Case 2B not to block chemical reaction of Rb and mainly of Mo, as it is predicted for Case 1B. Therefore, the main difference between the Cases 2A and 2B from the point of view of chemical speciation is the difference in Mo release kinetics from the fuel (see Figure 5.51), which is mainly due to different evolution of core degradation and fuel relocation to RV lower plenum, as it was already analyzed in §5.1.

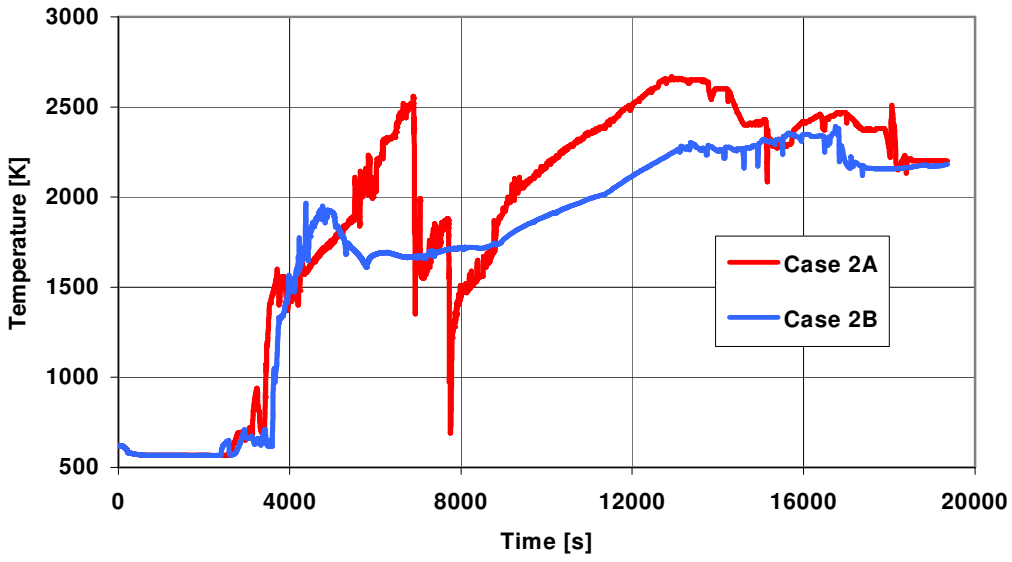

Figure 5.50: Temperature of the gas in the RV upper plenum (volume UPP_PLEN)

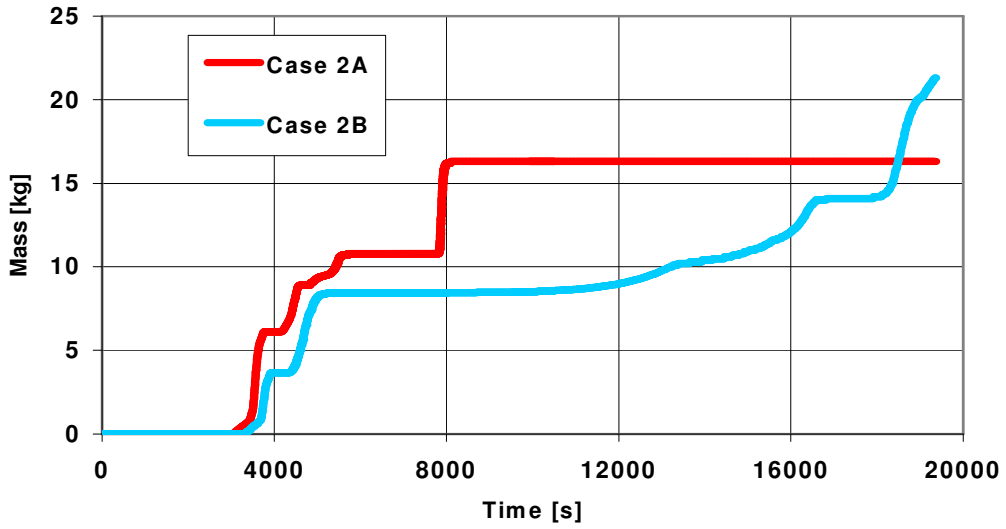

Figure 5.51: Inlet masses of **Mo** from the core to the circuit for Cases 2A and 2B

The iodine integrated chemical speciation at the end of three time instances:

- 3980 s: end of main oxidation run away period,
- 9980 s: after this time the hydrogen production is very low,
- 19343 s: final calculation time,

is presented in Figure 5.52. As in the previous Case 2A the dominant iodine compounds remains CsI and its dimmer. From the comparison of the Figures 5.52 and 5.48 it follows that also the formation of another iodine species is very similar. The main difference is the fact that highly volatile iodine species (HI, I_2MoO_2, SnI_2) are created on remarkable level in Case 2B till after ~10000 s, whereas their creation is predicted sooner in the Case 2A. This is strongly connected with differences in predicted Mo release kinetics from the core, as mentioned above (see Figure 5.51). In Case 2B a more or less continuous Mo release is predicted till after ~9000 s and after Cs source becomes less significant (see Figure 5.47 – note that Cs release kinetics is nearly the same for Cases 2A and 2B). Due to this fact more of Cs is consumed by Mo to create Cs_2MoO_4 (see also Figure 5.53) and consequently iodine can react with other elements.

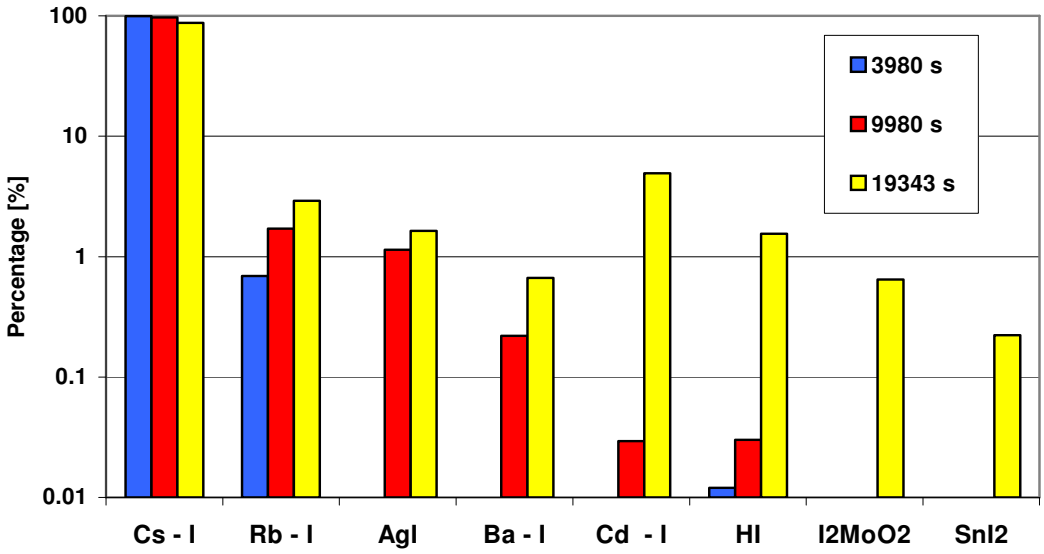

Figure 5.52: **Iodine** integrated speciation at a given time instances (**Case 2B**)

As shown in Figure 5.53 the change in predicted integrated Cs chemical speciation during the analyzed transient phase is not significant and is very similar to previous Case 2A (see also Figure 5.49). As already explained, the increased fraction of caesium molybdate (Cs_2MoO_4) and decreased fraction of the molecular non-reacted Cs_2 later in time is mainly a consequence of the increased Mo source after ~9000 s in combination with a gradual increase of carrier gas temperature (Figure 5.50). Here, it should be noted that the fraction of the Mo mass which remains in non-reacted elementary form decreases from ~16% (3980 s) to ~7% (9980 s) and decreases to ~2% at the end.

The predicted integrated (up to final time of analysis) chemical speciation of the other important FP and SM (see also Table 5.10) is the following:

Rubidium: The speciation is very similar to Case 2A, i.e. the fraction of released Rb mass (16.3 kg) bonded in RbOH and $Rb_2(OH)_2$ is ~45% and the fraction bonded in rubidium molybdate is ~49%. The rest of Rb reacts with iodine and Br. The fraction of Rb mass remaining in elementary form is ~5%, while this fraction is negligible in Case 2A, probably due to higher predicted gas temperature in RV upper plenum (Figure 5.50).

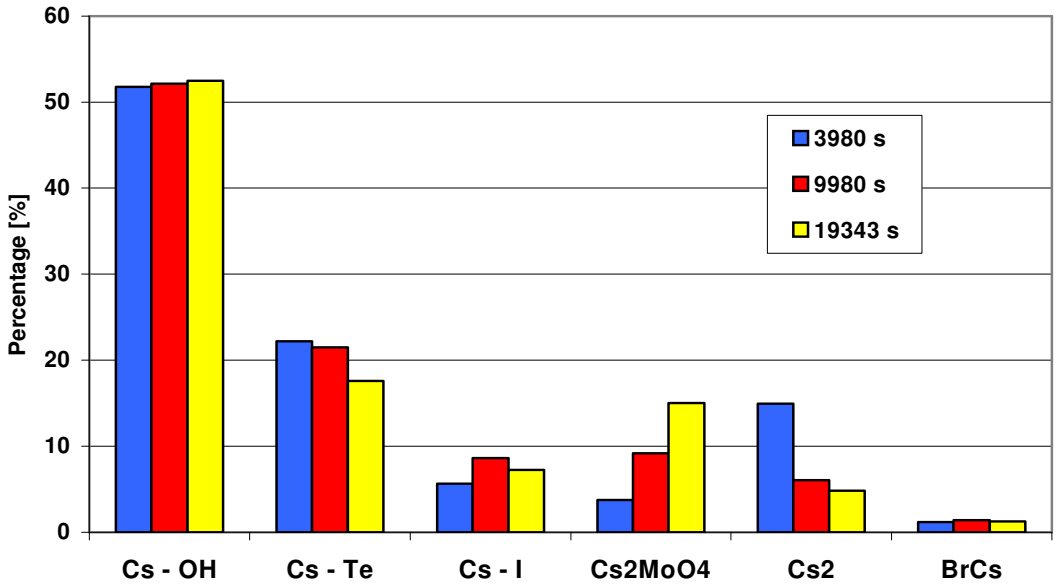

Figure 5.53: **Caesium** integrated speciation at a given time instances (**Case 2B**)

Molybdenum: Similarly to Case 2A, most of the Mo mass released from the core (21.3 kg) is chemically bonded in molybdates: Cs_2MoO_4 (~30%) and Rb_2MoO_4 (~21%). The relatively large fraction of Mo remains in the form of molybdic acid: H_2MoO_4 (~38%) mainly due to increased source of Mo after the time of ~12000s (Figure 5.51) and limited source of Cs (Figure 5.47) after this time. The rest of Mo mass exists as hydrated molybdenum oxide: $HMoO_2$ (~5%), barium molybdate: $BaMoO_4$ (~2%) and elementary Mo (~2%). Molybdenum oxides (Mo_3O_9 and Mo_2O_6) are created on negligible level (<0.5%).

Tellurium: Te released from the core (17.2 kg) is chemically bonded mainly in the caesium tellurides - Cs_2Te, Cs_2Te_2 and Cs_2Te_3 (~69%), as in the Case 2A. The rest creates AgTe (~7%), SnTe (~9%), Te_2 (~10%) and In_2Te (~2%).

Cadmium: As in Case 2A, an essential fraction (~98%) of released Cd mass (74.3 kg) remains in the elementary form. The rest exists as $Cd(OH)_2$ (~2%), CdI_2 and CdTe.

Silver: Nearly all (>99%) of Ag released mass (470.3 kg) exists in elementary or molecular forms, i.e. still larger fraction than in Case 2A.

Indium: In comparison with Case 2A, on one hand the fraction of In released mass (415.9 kg) bonded in In_2O_3 decreases from ~74.5% to ~56% and, on the second hand more In mass (~42%) remains in elementary from. The rest exists as In_2O, In_2Se, $HInO_2$, and In_2Te.

Tin: The main difference in comparison with Case 2A is the fact, that larger fraction (~62%) of the Sn released mass (152.3 kg) remains in molecular form and lower fraction (~20%) creates $Sn(OH)_2$.

The predicted released masses of Ba, Ru and uranium are slightly lower compared to Case 2A, but are also on considerable level – see Table 5.10. Their final chemical speciation is as follows:

Barium: With respect to Case 2A, the main Ba (total source is 1.17 kg) compound is barium molybdate $BaMoO_4$ (~52% of released Ba mass) instead of barium hydroxide $Ba(OH)_2$ (~22% of

released Ba mass). The main reason is increased Mo source in later phases of the transient phase (see Figure 5.51). The rest of Ba mass exists as BaHIO, BaO and BaBrOH.

Ruthenium: As in Case 2A, an essential fraction (~66%) of Ru released mass (1.02 kg) remains in the elementary form. The main Ru compounds are ruthenium oxides - RuO_2 and RuO (~25% of Ru mass) and ruthenium hydroxide – RuOH (~9% of Ru mass). In contrary with Case 2A, the formation of highly volatile ruthenium tri-oxide (RuO_3) is negligible, what is mainly a consequence of generally lower gas temperature in the RV upper plenum (see Figure 5.50).

Uranium: In comparison with Case 2A, the fraction of released U mass (16.9 kg) chemically bonded in hydrated uranium oxides (HO_3U, HO_2U) increases from 14.4% (Case 2A) to ~72% and, the fraction bonded in the uranium di-oxide (UO_2) decreases from ~85% (Case 2A) to ~20%. The rest of U mass (~8%) forms highly volatile uranium tri-oxide (UO_3).

6 Summary of the Results

The main results from the performed analyses can be summarized as follows:

1) As expected, the timing of main events up to predicted time of RV lower head failure is very similar for Case 1A and Case 1B. However, it was found that the difference in break location has considerable influence on the different gas (steam + H_2) flow paths in the primary loops with consequences on the FPs (SMs) transport in the circuit to the break.

2) The availability of the accumulators, as passive emergency core cooling system, has strong influence on the accident sequence evolution mainly from the point of view of the duration of the core degradation process and timing of RV lower head failure, which is postponed from 5514 s to 18753 s for Case 2A and from 5606 s to 19343 s for Case 2B. This has considerable influence on the total generated mass of hydrogen, which is increased from 133 kg to 206 kg for Case 2B and from 128 kg to 226 kg for Case 2A. Also, the cumulated released mass of the semi and low volatile FPs from the degraded core is increased significantly (see point 3).

3) FP/SM release from the core:

• Due to a very rapid core heating and degradation process in the Case 1A and Case 1B the cumulated released fractions of the **highly volatile** FPs (I, Cs, Te …) is predicted in the range of 92 – 97% i.i., whereas this fraction is in the range 76 – 88% i.i. in the Case 2A and Case 2B, i.e. slightly decreased due to slightly lower degree of core melting up to predicted time of RV lower head failure (cooling effect from evaporation of the water delivered by accumulators). These results are in agreement with the fractional release of I, Cs and Te measured in the FPT1 [23] and FPT2 [24] tests (70 – 87%i.i.).

• The situation is opposite for **semi** and **low-volatile** FPs. Their predicted cumulated release fractions in the Case 1A and Case 1B are negligible (<0.01%i.i., mostly <0.0001%i.i.) or on very low level (Mo: 1.7 – 2 %i.i., Ba: 0.01 %i.i.). Due to the fact that in the Cases 2A and 2B heated and molten fuel remains substantially for longer time in the core region (i.e. not quickly slumped to the water in RV lower plenum) the cumulative fractional release of the **semi-volatile** FPs is increased by 2 (Ba) to 4 (Sr) orders of magnitude and ~5 times for Mo. The situation is similar for **low-volatile** FPs where the increasing is by a factor of ~3 orders of magnitude. Despite of this increasing, the predicted released fractions seem to be underestimated compared to available measured fractions in the FPT1 and FPT2 tests (Mo: ~50%i.i., Ba: 1 – 6%i.i., Ru: 1 – 10%i.i., U: ~0.14%i.i.).

• The calculated cumulative release fractions of the control rod materials (Ag, In, Cd) and of the tin from Zircaloy alloy (fuel rod claddings, guide tubes) are predicted on the similar level in all cases, i.e. Ag: 1 – 2%i.i. (only in Case 2B it is ~7%), In: 20 - 40%i.i., Cd: 25 – 45%i.i. and for Sn: ~50%. These results are basically in agreement with available measured fractions in the FPT1 and FPT2 tests (Ag: ~15%i.i., In: >9%i.i., Cd: 25 – 65%i.i., Sn: >38%i.i.). Only the predicted Ag release seems to be underestimated.

4) The performed analyses shown that the main leakage pathways for FP/SM transport from the core to the break are not always identical and this fact can have considerable influence on their total retention in the circuit.

• In Case 1A, the FPs/SMs are transported from RV upper plenum to the break by two pathways. One pathway is from the core to the broken loop and through the SG U-tubes to the break in the cold leg. The retention dominates in the SG pipes mainly due to thermo-phoresis. The other one is from the core to the RV dome and through the RV cold collector to the break in the cold leg. Significant deposition is predicted in RV cold collector mainly due to turbulent-eddy impaction and in the horizontal part of the cold leg due to gravitational settling. The total calculated retention factor is **~65**%.

• In Case 1B nearly all FP/SM are transported from RV upper plenum to the RV dome and through RV cold collector to the break in cold leg. Main deposition is predicted in RV cold collector mainly due to turbulent-eddy impaction and in the horizontal part of the cold leg due to gravitational settling. The total calculated retention factor is **~74%**. This is a higher in comparison with previous case: higher aerosols concentration leads to an enhanced agglomeration process by creating larger particles and to increased turbulent-eddy impaction and gravitational settling.

• In Case 2A the FP/SM leakage pathways are the same as for Case 1A. Main deposition is predicted in RV cold collector mainly due to thermo-phoresis and in the horizontal part of the cold leg due to gravitational settling. The total calculated retention factor is **~59%**. This is lower in comparison with Case 1A mainly due to lower retention of the low volatile FPs. They are released during a very short time interval in both cases, but in Case 1A the flow to the break comes from the upper plenum of the RV and not via the broken loop SG.

• In Case 2B there are three FPs/SMs leakage pathways from RV upper plenum to the break. One pathway is through the RV dome to RV cold collector and then to the break. The other two pathways are to the hot legs of the intact primary loops and then through the SG U-tubes to the RV cold collector and finally to the break in the broken loop. The total calculated retention factor is therefore the highest one ~7**5**%.

5) From the point of view of predicted iodine chemistry in the circuit the results of performed calculations are consistent with the conclusion of the SOPHAEROS/ASTEC analyses of the Phébus tests given in [25]. Mainly it means that according to current ASTEC V1.3 rev.2 chemistry model, the key species responsible for the volatile iodine persistence in the circuit is molybdic acid (H_2MoO_4) because a non-negligible part of it remains as vapour in the upper plenum above the core. Then, this H_2MoO_4 consumes a significant part of Cs from CsOH or from molecular Cs_2 to form Cs_2MoO_4 and almost does not allow formation of CsI and RbI (note that behaviour of Rb is similar to Cs) if the Mo/Cs(Rb) bundle release molar ratio is sufficiently high. In such a case the ASTEC V1.3 chemistry model predicts significant reaction of iodine with Cd by formation of cadmium iodides, mostly CdI_2 (i.e., if SIC control rod is present – as it was the case of FPT1 [23] and FPT2 [24] tests). When SIC is not present (FPT3 test [26]) the significant part of iodine remains in gaseous form of HI and also creation of highly volatile species I_2MoO_2, SnI_4, SnI_2 is predicted. On the other hand when the Mo/Cs(Rb) molar ratio is low (i.e. there is a surplus of Cs and Rb) the predicted dominant iodine species are CsI (RbI) and their dimmers. In this case Cd has small or negligible influence on iodine chemistry.

In all 4 performed calculations of the MBLOCA a significant surplus of the Cs (Rb) source is calculated compared to Mo source during the entire transient period. Therefore, as shown on Figure 6.1 for the source term to containment, the predicted dominant iodine species are CsI and its dimmer. As in the Cases 2A and 2B this surplus is partly reduced due to increased Mo source, some fraction of iodine is allowed to react also with other FP/SM.

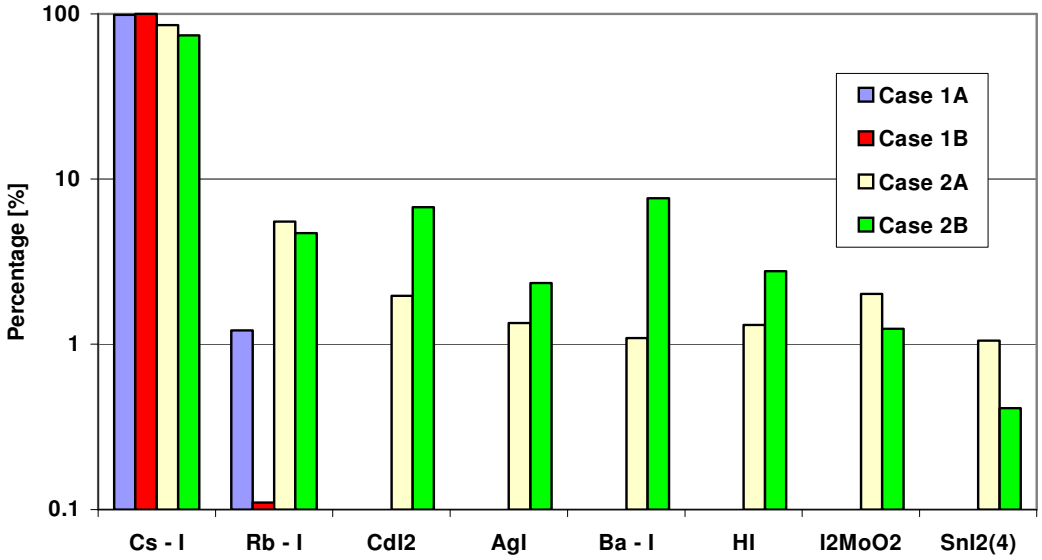

Figure 6.1: Integrated iodine chemical speciation in the leak from the circuit

7 Conclusions

This report has presented the analysis of the severe accident initiated by a Medium Break on the cold leg (d_e = 51.6 mm), combined with the total loss of electric power supply (Black-Out) using the last version of the integral code ASTEC V1.3 rev2. As reference reactor a 3-loop PWR type with a nominal thermal power of ~3000 MWt at the end of equilibrium fuel cycle has been used.

Besides the detailed analysis of the primary and secondary circuits thermal-hydraulic response and core degradation processes (timing of main events), the analyses have been concentrated on FP/SM release form fuel and SIC control rods, their transport and chemical speciation inside the primary circuit and at the break (source term to containment).

A sensitivity analysis has been performed in terms of break position and accumulator availability.

The different location of the break in the cold leg can have an impact on the carrier gas flow paths in the primary circuit affecting the temperature in the RV Upper Plenum where the main chemical reactions occur. This in turn has an effect on the chemical speciation of the FPs.

In particular, the affinity of Mo to react with Cs is strongly dependant on the carrier gas temperature. At temperatures below ~1200K the reaction of Mo with Cs is suppressed and the dominant Iodine species are CsI and its dimmer. Under the same temperature conditions the Rb remains in elementary form and the reaction with Iodine becomes negligible.

Different pathways have clearly a considerable influence on the total retention of FPs/SMs in the circuit. Indeed the highest retention factor (~75%) is predicted when several pathways go through the intact loops resulting in a high deposition in the SGs U-tubes due to thermo-phoresis, in the horizontal part of the cold leg due to gravitational settling and at cold leg collector due to turbulent-eddy impaction.

The accumulator availability extends the duration of the core degradation process before RV failure occurs. This increases significantly the total production of hydrogen and the cumulated released mass of semi (Ba, Mo, Ru) and low volatile (U, Pu) FPs since the heated and molten fuel remains longer in the core region. On the contrary the cumulated released mass of highly volatile FPs (I, Cs, Te) is slightly decreased due to the lower amount of core melt because of the cooling effect from evaporation of the water discharged from the accumulators.

The SIC release occurs mainly during relocation of molten guide tubes materials and depends on the amount of molten pool and on the slumping. When accumulators are not available a larger molten pool is present with a rapid slumping process. The availability of accumulators produces a smaller molten pool with slower slumping but occurring in several steps. The compensating effect results in calculated cumulative release fractions of the control rod materials which are predicted on a similar level for all cases.

According to the ASTEC V1.3 rev2 equilibrium chemistry model, the Mo/Cs(Rb) molar ratio has the most influence on the fraction of Iodine which can reach the containment in the gaseous or highly volatile form. In all the analyses performed, a significant surplus of Cs (Rb) source is calculated over the Mo source. Therefore the predicted dominant Iodine species to the containment are CsI and its dimmer. When this surplus is partly reduced to an increase in the Mo source, some fraction of Iodine is allowed to react also with other FPs/SMs (Ba, Ag, Cd). A 3-4% of Iodine which reaches the break exists in gaseous (HI) and highly volatile metal-iodides (I2MoO2, SnI2, SnI4) species.

REFERENCES

[1] Fauske & Associated Incorporated, 1994. MAAP4-Modular Accident Analysis Program for LWR Power Plants.

[2] Gauntt, R.O. et al., 2000, MELCOR Computer Code Manuals: Version 1.8.5, NUREG/CR-6119.

[3] Allelein H.-J. et al. Final report of the project FI4S-CT98-0054, "VASA – Validation Strategies for Severe Accident Codes"

[4] Allelein H.-J. et al. Final report of the project FIKS-CT-199-00010, "EVITA – European Validation of the Integral code ASTEC"

[5] Micaelli J.C. Project EC-SARNET/FI60-CT-2004-509065, "SARNET – Network of Excellence for Sustainable Integration of European Research on Severe Accident Phenomenology"

[6] US Nuclear Regulatory Commission (USNRC), 1990. Severe Accident Risks: An Assessment for Five U.S. Nuclear Power Plants, NUREG-1150.

[7] Poloski J.P. et al., 1999 Rates of initiating events at U.S. nuclear power plants: 1987–1995, NUREG/CR-5750

[8] Van Dorsselaere, J.P. et al.: User's Guidelines for the integral code ASTEC v1.3 rev0, Project reference ASTEC-V1/DOC/06-34, December 2006

[9] Van Dorsselaere, J.P. et al.: Evolution of the integral code ASTEC v1.3rev2 with respect to the v1.3rev0 version, Project reference ASTEC-V1/DOC/07-23, November 2007

[10] Trégourès, N., Moal, A.: CESAR physical and numerical modeling, ASTEC V1 code, ASTEC-V1/DOC/07-18, October 2007

[11] Guillard, G., Jacq, F., Pignet, S., Majumdar, P., Siméone, A: DIVA physical modeling, ASTEC V1 code, ASTEC-V1/DOC/07-19, October 2007

[12] Plumecocq, W., Guillard, G.: ELSA module: fission product and structural element release from intact and degraded cores, Project reference ASTEC-V1/DOC/06-08, April 2006

[13] Cousin, F.: ASTEC V1.3 SOPHAEROS module: Theoretical manual rev.1, Project reference ASTEC-V1/DOC/06-15, December 2006

[14] Cranga, M., Giordano, P., Passalacqua R., Caroli, C., Walle, L.: ASTEC V1.3 RUPUICUV module: Ex-vessel corium discharge and corium entrainment to containment, Rev.1, Project reference ASTEC-V1/DOC/03-19, December 2003

[15] Seropian, C., Jacq, F., Walle, L.: Description of the CORIUM module of the ASTEC code, Rev.0, ASTEC-V1/DOC/04-11, December 2004

[16] Langhans, J., Spengler, C., Druwe, H.: ASTEC V1 Description of WEX 3.1 (improved version of WECHSL 3.5), Rev.0, ASTEC-V1/DOC/01-33, November 2002

[17] Duval, F., Cranga, M., Commandé, A.: ASTEC V1.3 MEDICIS MCCI module, Theoretical manual rev.1, ASTEC-V1/DOC/06-26, December 2006

[18] Klein-Hessling, W., Schwinges, B.: ASTEC V0 CPA module, Program Reference Manual, Rev.0, ASTEC-V0/DOC/01-34, November 1998

[19] Arndt, S., Weber, G.: ASTEC V0 FIPHOST - A module to calculate the Fission Product Transport in a Containment, Rev.0, ASTEC-V0/DOC/99-21, April 1998

[20] Bosland, L., Cantrel, L.: ASTEC V1.3 code, IODE module: Iodine and ruthenium behaviour in the containment, Rev.1, ASTEC-V1/DOC/06-20, September 2007

[21] Jacq, F.: ASTEC V0, ISODOP code for isotope treatment, Theoretical manual, Rev.0, ASTEC-V0/DOC/00-10, September 2001

[22] Guillard, G., Jacq, F., Seropian, C., Plumecocq, W.: ASTEC V1 code, SYSINT module – Management of events and safety systems interactions, Rev.1, ASTEC-V1/DOC/07-21, October 2007

[23] Jacquemain D., Bourdon S., de Bremaecker A., Barrachin M.: FPT1 Final Report: Volume 1 - 4, December 2000

[24] DATA BOOK FPT2, Phébus PF IP 2004-0555 and CPEX NT 2004-0084, IRSN/JRC, CD-ROM, March 2004

[25] Girault N., Fiche C., Bujan A., Dienstbier J.: Towards a better understanding of iodine chemistry in RCS of nuclear reactors, The 2nd European Review Meeting on Severe accident Research (ERMSAR-2007), Forschungszentrum Karlsruhe GmBH, Germany, 12-14 June 2007

[26] FPT3 PRELIMINARY REPORT – March 2007, CDROM

[27] OECD/NEA: Level 2 PSA Methodology and Severe Accident Management.
OECD/GD/198, (1997)

European Commission

EUR 23797 EN – Joint Research Centre – Institute for Energy
Title: ASTEC V1.3rev2 Code Application on Medium Cold Leg Break Accident for a reference PWR 1000 Reactor
Author(s): A. Bujan, L. Ammirabile, J. Slaby, A. Bieliauskas
Luxembourg: Office for Official Publications of the European Communities
2008 – 86 pp. – 210 x 297 cm
EUR – Scientific and Technical Research series – ISSN 1018-5593

Abstract
During a hypothetical severe accident in a nuclear reactor most of the radioactivity would be released from the damaged core and the broken primary circuit in form of aerosols and chemical vapours and gases. However the radio-toxicity of released materials depends both on the released mass and on the chemical form as well. The fission products release and transport in the circuit has been analysed for a Medium Break cold leg Loss Of Coolant Accident (MBLOCA) for a reference PWR 1000 reactor using the severe accident integral code ASTECV1.2 rev2. A detailed description of the reactor model is given.
Sensitivity analyses were performed in terms of break location and accumulator availability.
The break location has an impact on the carrier gas temperature and in turn on the chemical speciation of the fission products. Also retention is influenced by the different flow pathways establishing in the circuit.
The accumulator availability extends the duration of the core degradation process affecting the total production of hydrogen and the cumulated released mass of low, semi and highly volatile fission products.
In agreement with the ASTEC equilibrium chemistry model, the Mo/Cs (Rb) molar ratio has the most influence on the fraction of Iodine which can reach the containment in the gaseous or highly volatile form. Due to the surplus of Cs, the predicted dominant Iodine species to the containment are CsI and its dimmer.
A 3-4% of Iodine which reaches the break exists in gaseous (HI) and highly volatile metal-iodides (I2MoO2, SnI2, SnI4) species.

How to obtain EU publications

Our priced publications are available from EU Bookshop (http://bookshop.europa.eu), where you can place an order with the sales agent of your choice.

The Publications Office has a worldwide network of sales agents. You can obtain their contact details by sending a fax to (352) 29 29-42758.

The mission of the JRC is to provide customer-driven scientific and technical support for the conception, development, implementation and monitoring of EU policies. As a service of the European Commission, the JRC functions as a reference centre of science and technology for the Union. Close to the policy-making process, it serves the common interest of the Member States, while being independent of special interests, whether private or national.

JRC
EUROPEAN COMMISSION

AA- BB- XXXXX- LL- C

Publications Office
Publications.eu.int

Bar code